Institute of Thermoelectricity, Academy of Sciences and Ministry of Education and Science of Ukraine

Journal of THERMOELECTRICITY

International Research

Founded in December, 1993

published 6 times a year

No. 5 *2013*

Editorial Board

International Editorial Board

Founders - National Academy of Sciences, Ukraine
Institute of Thermoelectricity of National Academy of Sciences and Ministry of Education and Science of Ukraine

Certificate of state registration № КВ 15496-4068 ПР

Approved for printing by the Academic Council of Institute of Thermoelectricity of the National Academy of Sciences and Ministry of Education and Science, Ukraine

Address of editorial office:
Ukraine, 58002, Chernivtsi, General Post Office, P.O. Box 86.
Phone: +(380-3722) 7 58 60.
Fax: +(380-3722) 4 19 17.
E-mail: jt@inst.cv.ua
http:// www.jt.cv.ua

Signed for publication 25.10.13. Format 70×108/16. Offset paper №1. Offset printing.
Printer's sheet 11.1. Publisher's signature 9.2. Circulation 400 copies. Order 6.

Printed from the layout original made by "Journal of Thermoelectricity" editorial board
in the printing house of "Bukrek" publishers,
10, Radischev Str., Chernivtsi, 58000, Ukraine

CONTENTS

P.V. Gorsky, V.P. Mikhalchenko

P.V. Gorsky

Institute of Thermoelectricity of the NAS and MES
of Ukraine, 1, Nauky Str. Chernivtsi, 58029, Ukraine

ON THE ISSUE OF THE MECHANISM FOR INCREASING THE THERMOELECTRIC FIGURE OF MERIT OF THE BULK NANOSTRUCTURED MATERIALS

V.P. Mikhalchenko

Charge carrier and phonon scattering on the boundaries of spherical powder particle has been considered as the mechanism for increasing the figure of merit of the bulk nanostructured material as compared to a single crystal. In so doing, charge carrier scattering is considered in the approximation of constant mean free path, and phonon scattering – within two approaches, namely constant mean free path and with account of frequency dependence of phonon relaxation time. It is shown that with constant mean free paths of electrons and phonons the thermoelectric figure of merit of nanostructured material is considerably lower than that of a single crystal. However, with account of frequency dependence of phonon relaxation time it turns out that with a proper selection of nanopowder size, namely if its particles have the radius of the order of 30 – 40 nm, the figure of merit of Bi_2Te_3 based material can be increased by a factor of 2.1 as compared to a single crystal under oriented pressing and retained at a level of 0.87 ÷ 1.23 of its value for a single crystal under conventional pressing, when cleavage planes of individual particles are randomly oriented.

Key words: nanostructured material, thermoelectric figure of merit, phonons, electrons, scattering, relaxation time, normal processes, Umklapp processes.

Introduction

Bismuth telluride Bi_2Te_3 is thermoelectric material most commonly used for the manufacture of working elements of various thermoelectric instruments and devices [1]. Its specific feature is a pronounced electric conductivity and thermal conductivity anisotropy. Taking into account that this crystal possesses $R3m$ group symmetry and cleavage planes along which it easily splits, its thermal conductivity and electric conductivity tensors have two independent components each. In particular, in the absence of a magnetic field, electric conductivity tensor has component σ_{11} in cleavage plane and component σ_{33} in a perpendicular direction, with $\sigma_{11} > \sigma_{33}$. The same inequality is valid for thermal conductivity components: $\chi_{11} > \chi_{33}$. Therefore, thermoelectric modules of a single crystal are made so that temperature gradient and electric current are parallel to cleavage planes, owing to which the dimensionless thermoelectric figure of merit ZT at 300 K reaches 1. This direction can be also retained when passing from a single crystal to powder based materials prepared by hot pressing, extrusion or spark plasma sintering methods, if oriented pressing is used. However, non-oriented pressing, whereby cleavage planes of individual particles are randomly oriented, is much more common.

As a result, the figure of merit of material in conformity with the Odelevsky formula with regard to thermal and electric conductivity anisotropy factors should have reduced by a factor of about $\sqrt{2}-\sqrt{3}$, i.e. by 30 to 40 %, however, in practice such reduction is not observed. On the other hand, there are many theoretical works, for instance, [2-4], where it is shown that transition from a single

crystal to the bulk nanostructured material should increase the thermoelectric figure of merit. As the mechanisms for such increase, on the one hand, phonon scattering on the boundaries of nanoparticles [2], leading to lattice thermal conductivity reduction is considered, on the other hand – quantum tunneling of charge carriers through vacuum or dielectric gaps between particles, leading to increase in electric conductivity and thermoEMF, hence, in power factor [3, 4]. In these papers it is shown that the best values of dimensionless thermoelectric figure of merit of bismuth telluride based bulk nanostructured material should have achieved 3.5 ÷ 3.6, but in practice no such increase is observed. The discrepancy between theory and experiment is generally related to stronger restrictions on thermoEMF and electric conductivity when passing from a single crystal to bulk nanostructured material than it is predicted by theory. This factor forces the experimenters to employ combined materials based on powders, consisting of a nanocomponent with particle size 5 ÷ 20 nm, and a microcomponent with particle size 40 ÷ 70 μm [5]. The function of microcomponent is to retain power factor typical of a single crystal, the function of a nanocomponent is to reduce lattice thermal conductivity due to additional phonon scattering on the boundaries of nanoparticles. Mass ratio between nano- and microcomponents is selected so as to assure the maximum value of the dimensionless thermoelectric figure of merit.

Among the weak points of [2-4] and some other theoretical papers covering this problem, is a modeling character of tunneling effects calculations caused by the absence of valid knowledge on the shape and height of potential barriers between nanoparticles, as well as ignoring the frequency dependence of phonon relaxation time when considering their scattering on nanoparticle boundaries.

With regard to the foregoing, our purpose in this paper is to consider the mechanism of thermoelectric figure of merit variation when passing from a single crystal to bulk nanostructured material due to charge carrier and phonon scattering on the boundaries of spherical nanoparticles in the drift approximation.

Consideration of the problem in the approximation of constant electron and phonon mean free paths

Consider this problem in the approximation of constant electron and phonon mean free paths. It can be shown that in the framework of this approximation thermoEMF is not changed, as long as both thermal diffusion flux and electric current are proportional to relaxation time. Therefore, a change in thermoelectric figure of merit in this case is completely determined by a change in electric conductivity to thermal conductivity ratio. If electron and phonon mean free paths are l_e and l_{ph}, respectively, then the ratio of figure of merit Z_n of bulk nanostructured material consisting of equal particles of radius r to figure of merit Z_m of a single crystal in conformity with the rule of summation of the inverse mean free paths will make by analogy with [6]:

$$Z_n \Big/ Z_m = \left[\int_0^1\int_{-1}^1 \frac{(r/l_e)\sqrt{y^2+2zy+1}\,y^2\,\mathrm{d}z\mathrm{d}y}{(r/l_e)\sqrt{y^2+2zy+1}+1}\right]\left[\int_0^1\int_{-1}^1 \frac{(r/l_{ph})\sqrt{y^2+2zy+1}\,y^2\,\mathrm{d}z\mathrm{d}y}{(r/l_{ph})\sqrt{y^2+2zy+1}+1}\right]^{-1}. \quad (1)$$

Double integrals in this formula appear due to averaging of expressions for thermal conductivity and electric conductivity over the mean free paths inside the sphere.

Problem consideration with regard to frequency dependence of phonon relaxation time

We now consider this problem with regard to frequency dependence of phonon relaxation time. For this purpose we first write a general expression for the larger component of lattice thermal

conductivity, taking into account that in the temperature region relevant for thermoelectric applications it is determined by Umklapp processes, as well as by normal processes, capable of modifying scattering on sample boundaries by virtue of scattering probabilities redistribution according to frequencies [7, 8]. This expression is of the form [9]:

$$\chi_{l\|} = \frac{3\hbar\rho v_{\|}^4 k_B}{32\gamma^2 \left(k_B T_D\right)^2 \theta^3 \pi} \int_0^1 \frac{x^4 \exp\left(x/\theta\right)}{\left[\exp\left(x/\theta\right)-1\right]^2} \left(\frac{1}{Q_{l\|}(x)} + \frac{2}{Q_{t\|}(x)} \right) \mathrm{d}x. \tag{2}$$

In this formula, index || refers to lattice thermal conductivity in the direction parallel to layers (cleavage planes), ρ is crystal density, ν is sound velocity in it, k_B is the Boltzmann constant; γ is the Gruneisen parameter, T_D is the Debye temperature, $\theta = T/T_D$, $Q_{l\|}(x)$ and $Q_{t\|}(x)$ are frequency polynomials determined by the mechanisms of scattering longitudinal and transverse phonons, respectively, and having in this case the form:

$$Q_{l\|}\left(x\right) = x^4 + \mu_{\|} x, \tag{3}$$

$$Q_{t\|} = \left(\mu_{\|} + 3.125\theta^3\right) x. \tag{4}$$

In these formulae, $\mu_{\|}$ is certain coefficient depending in the simplest case of cubic lattice on its geometry.

With regard to thermal conductivity dependence on material density, we note that formula (2) in this respect is precise for a simple cubic lattice with one atom in a unit cell. The real Bi_2Te_3 lattice is not of that kind, but we have to replace it by such, provided the real material density is maintained. Coefficient μ was approximately calculated for a simple cubic lattice by Leibfried and Shleman [7], but, according to experimental data given in [6], even for materials with such lattice it is not universal. Therefore, we will "derive" coefficient $\mu_{\|}$ from the real value of the respective component of Bi_2Te_3 thermal conductivity tensor [1], assuming that the latter coincides with the theoretical value (2) with regard to (3) and (4). At $\chi_{l\|} = 1.45$ W/m·K, $\rho = 7859$ kg/m^3, $\gamma = 1.5$, $v_{\|} = 2952$ m/s, $T_D = 155$ K and $T = 300$ K we obtain $\mu_{\|} = 0.022$.

The ratio of nanoparticle thermal conductivity to single crystal thermal conductivity in this case is [9]:

$$\chi_l^{(nano)} \Big/ \chi_{l\|m} = 1.5 \int_0^1 \int_0^1 \int_{-1}^1 \frac{z^2 x^4 \exp\left(x/\theta\right)}{\left[\exp\left(x/\theta\right)-1\right]^2} \left(\frac{\left(r/L^*\right)\sqrt{z^2-2zy+1}}{1+\left(r/L^*\right)Q_{l\|}(x)\sqrt{z^2-2zy+1}} + \right.$$
$$\left. + \frac{2\left(r/L^*\right)\sqrt{z^2-2zy+1}}{1+\left(r/L^*\right)Q_{t\|}(x)\sqrt{z^2-2zy+1}} \right) \mathrm{d}y\mathrm{d}z\mathrm{d}x \left\{ \int_0^1 \frac{x^4 \exp\left(x/\theta\right)}{\left[\exp\left(x/\theta\right)-1\right]^2} \left(\frac{1}{Q_{l\|}(x)} + \frac{2}{Q_{t\|}(x)} \right) \mathrm{d}x \right\}^{-1}. \tag{5}$$

In formula (5), $L^* = \rho\hbar^4 v_{\|}^6 \Big/ \gamma^2 \left(k_B T_D\right)^5$.

In this case the ratio of bulk nanostructured material figure of merit to single crystal figure of merit is determined as:

$$Z_n \Big/ Z_m = 1.5 \left[\int_0^1 \int_{-1}^1 \frac{\left(r/l_e\right)\sqrt{y^2+2zy+1}\, y^2 \mathrm{d}z\mathrm{d}y}{\left(r/l_e\right)\sqrt{y^2+2zy+1}+1} \right] \left[\chi_l^{(nano)} \Big/ \chi_{\|lm} \right]^{-1}. \tag{6}$$

Dependence of a relative thermoelectric figure of merit of Bi_2Te_3 based bulk nanostructured material on the radius of nanoparticles is shown in Fig. 1.

In the construction of curve 2 in this figure, based on the reference data [1] it was assumed that $l_{ph} = 4.16$ nm, $l_e = 38.6$ nm at a temperature of 300 K. In connection with this figure a question may arise as to the validity of transferring the properties of an individual nanoparticle to the properties of material as a whole. Therefore, we note that if pores in material structure are vacuum, there is no tunneling of charge carriers, and the pores are not communicating, then material porosity, both in the framework of percolation theory, and within the approach set forth, for instance, in [4], enters into the expressions for thermal conductivity and electric conductivity through the same multiplier, hence, it does not produce a direct effect on the thermoelectric figure of merit. Thus, abstracting from the size distribution of nanoparticles, the thermoelectric figure of merit of bulk nanostructured material as a whole is completely determined by the kinetic coefficients of an individual particle.

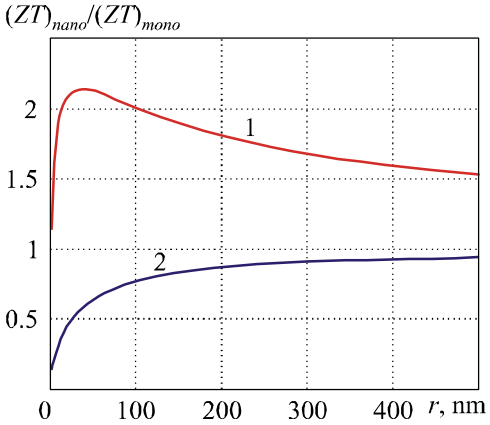

Fig. 1. Dependence of a relative thermoelectric figure of merit of bulk nanostructured material on nanoparticle radius: 1) – with regard to frequency dependence of phonon relaxation time; 2) – in the approximation of constant mean free paths of electrons and phonons.

From the figure it is evident that with regard to frequency dependence of phonon relaxation time the relative thermoelectric figure of merit has a maximum 2.14 which is achieved in the range of nanoparticle radii 35 ÷ 40 nm. However, it is possible only with oriented pressing. Whereas with a random orientation of cleavage planes, the relative thermoelectric figure of merit of Bi_2Te_3 based bulk nanostructured material will be a factor of $\sqrt{3}$ lower, i.e. it will remain at a level of about 23 % higher than the thermoelectric figure of merit of a single crystal. Even with nanoparticle radius of the order of 5nm with correction for random orientation of cleavage planes, the thermoelectric figure of merit of bulk nanostructured material should remain at a level of at least 97 % of the thermoelectric figure of merit of a single crystal. These results are in qualitative, as well as quantitative agreement with the results of experimental works [10, 11], but contradict to the results of paper [5] according to which the thermoelectric figure of merit of Bi_2Te_3 based bulk nanostructured material of nanoparticles with the radius 5 ÷ 20 nm at 300 K is as low as 82 % of the thermoelectric figure of merit of a single crystal. Thus, when passing from a single crystal to bulk nanostructured material, power factor is scarcely ever retained, which permits calling in question the presence of energy filtration of current carriers that should have resulted in thermoEMF increase. Even if such filtration occurs, then, apparently, it does not always contribute to power factor retention, since the electric conductivity is decreased stronger than squared thermoEMF is increased. However, in the approximation of constant mean free paths of electrons and phonons, with increase in nanoparticle radius, the thermoelectric figure of merit monotonously increases from a low value to 1. Therefore, in such approximation the thermoelectric figure of merit values of the bulk nanostructured material exceeding unity with regard to a single crystal are mainly attributable to tunneling effects.

Conclusions and recommendations

1. In the approximation of constant mean free paths of charge carriers and phonons the thermoelectric figure of merit of Bi_2Te_3 based bulk nanostructured material, calculated without regard to possible

increase of power factor due to tunnelling effects, in the range of nanoparticle radii 5 ÷ 500 nm at 300 K does not exceed 1, even if cleavage planes of individual crystallites are oriented parallel to temperature gradient and electric current directions.

2. With regard to frequency dependence of phonon-phonon relaxation time, even in the drift approximation it turns out that in the range of nanoparticle radii 40 ÷ 500 nm the thermoelectric figure of merit of Bi_2Te_3 based bulk nanostructured material can reach 1.5 ÷ 2.1 with regard to a single crystal, if cleavage planes of individual crystallites are oriented parallel to temperature gradient and electric current directions. If, however, cleavage planes are randomly oriented, then the thermoelectric figure of merit of such nanostructured material is retained at a level of 0.88 ÷ 1.23 of single crystal thermoelectric figure of merit.
3. The experimentally observed in a number of cases lower values of thermoelectric figure of merit of bulk nanostructured material are attributable to a drop in power factor as a result of incomplete recovery of thermoEMF and electric conductivity in these materials with respect to single crystals.

References

1. B.M. Goltsman, V.A. Kudinov, and I.A. Smirnov, *Semiconductor Thermoelectric Materials Based on Bi_2Te_3* (Moscow: Nauka, 1972), 320 p.
2. L.P. Bulat, I.A. Drabkin, V.V. Karatayev, V.B. Osvensky and D.A. Pshenai-Severin, The Effect of Boundary Scattering on the Thermal Conductivity of Nanostructured $Bi_xSb_{2-x}Te_3$ Semiconductor Material, *Physics of the Solid State* **52**, 1712 (2010).
3. L.P. Bulat, V.V. Osvensky, Yu.N. Parkhomenko, and D.A. Pshenai-Severin, Study on the Possibilities of Thermoelectric Figure of Merit Improvement in Nanostructured Materials Based on Bi_2Te_3-Sb_2Te_3, *Physics of the Solid State* **54**, 20 – 26 (2012).
4. A.A. Snarskii, A.K. Sarychev, I.V. Bezsudnov, and A.N. Lagarkov, Thermoelectric Figure of Merit of the Bulk Nanostructured Composites with Distributed Parameters, *Semiconductors* **46**, 677 – 683 (2012).
5. S. Fan, J. Zhao, J. Guo, Q. Yan, J. Ma, H.H. Hang, Influence of Nanoinclusions on Thermoelectric Properties of *n*-type Bi_2Te_3 Nanocomposites, *J. Electronic Materials* **40** (5), 1018 – 1023 (2011).
6. P.V. Gorsky, V.P. Mikhalchenko, On the Electric Conductivity of Contacting Particles of Thermoelectric Material, *J. Thermoelectricity* **2**, 12 – 18 (2013).
7. P.G. Klemens, Lattice thermal conductivity. In: *Solid State Physics. Advances in Research and Applications.* Vol. 7, pp. 1 – 98 (New York: Academic Press. Inc. Publishers, 1958), 526 p.
8. P. Klemens, Effect of Thermal and Phonon Processes on Ultrasound Attenuation, In: Physical Acoustics, V. 3, Part B, Lattice Dynamics, Ed. by W. Mason, P. 244 – 284 (Moscow: Mir, 1968), 526 p.
9. P.V. Gorsky, V.P. Mikhalchenko, Reduction of Thermoelectric Material Lattice Thermal Conductivity Using Shape-Forming Element Optimization, *J. Thermoelectricity* **1**, 18 – 25 (2013).
10. V.T. Bublik, I.A. Drabkin, V.V. Karatayev, et al., Bulk Nanostructured Thermoelectric Material Based on $(Bi, Sb)_2Te_3$ Prepared by Spark Plasma Sintering Method (SPS), *Thermoelectrics and Their Applications: XIII Interstate Workshop* (Saint-Petersburg, 2012).
11. I.A. Drabkin, V.B. Osvensky, A.I. Sorokin, et.al., Anisotropy of Thermoelectric Properties of the Bulk Nanostructured Material Based on $(Bi, Sb)_2Te_3$ Prepared by Spark Plasma Sintering Method (SPS), Thermoelectrics and their Applications: XIII Interstate Workshop (Saint-Petersburg, 2012).

Submitted 18.03.2013.

M.A. Korzhuev

A.A. Baikov Institute of Metallurgy and Material Science of RAS,
49, Leninskiy Ave., Moscow, 119991, Russian Federation

M.A. Korzhuev

THERMOELECTRIC NANOSTRUCTURES: PROS AND CONS

The limits for increase in the figure of merit Z and power W of thermoelectric materials (TEM) at nanostructurization are determined. It is shown that parameters Z and W of nanostructures (NS) vary due to the transitions $\lambda_{ph} \rightarrow$ and $\lambda_e \rightarrow a$ in TEM. (Here, a is interatomic distance, λ_{ph} and λ_e are average mean free paths of phonons and electrons in the samples). It is found out that in the range $1 \sim \lambda_{ph}/a < \lambda_e/a < 2 – 3$ the transition $\lambda_e \rightarrow a$ can be used for a simultaneous increase in the Z and W of TEM. It is established that NS TEM with the simultaneously increased parameters Z and W can effectively work in maximum power mode in thermoelectric power converters. Some negative characteristics of NS TEM are also revealed. It is optimal carrier concentration mismatch of TEM parameters Z and W, increase in the electrical and thermal contact resistances, as well as development of diffusion instability of samples at high temperatures $T > T_T \sim 0.5\ T_m \sim 400 – 500$ K. (Here, T_T is the Tammann temperature and T_m is material melting temperature).

Key words: thermoelectricity, figure of merit *Z* and power *W*, nanostructures (NS).

Introduction

At the present time many researchers study the properties of nanosized material particles ($x \sim 10^{-9}$ m), as well as the bulk heterogeneous nanostructures (NS) formed on their basis with a small identity period $x = 1 – 100$ nm [1]. It was found that the properties of such NS can differ considerably from the properties of homogeneous crystalline materials, which is generally related to the impact of surface and (or) quantum-size effects [2]. Thus, for a series of NS thermoelectric materials (TEM) there was a considerable increase in the thermoelectric figure of merit $Z = W/\kappa$ (up to 5 times and more) and power $W = \alpha^2\sigma$ (up to 1.5 – 2 times) at room temperature (Table 1). (Here α is the Seebeck coefficient, σ and $\kappa = \kappa_L + \kappa_e$ are the electric conductivity and thermal conductivity, κ_L and κ_e are the lattice and electron components of thermal conductivity) [3-4]. The maximum figure of merit values

$$Z_{\max} \sim W_{\max}\kappa_p^{-1} \sim Nm_d^{3/2}\mu T^{3/2}e^r\kappa_p^{-1}, \quad (1)$$

are known to be achieved in TEM at temperatures $T_{\max} = E_g/bk_0$ that are determined by the onset of intrinsic conductivity development in the samples. (Here N is the number of equivalent extremums in conduction band (valence), m_d is the effective mass of the density of states in a separate extremum, $\mu = \sigma/(en(p))$ is mobility, e is elementary charge, $n(p)$ is electron (hole) concentration in the samples, T is absolute temperature, r is scattering parameter, E_g is energy gap width, k_0 is the Boltzmann constant, $b = 5 – 10$ is the coefficient that varies depending on the ratio between electron and hole mobilities $a = \mu_e/\mu_p$ in the samples) [3-4]. It is generally assumed that at the transition "crystal → NS" the band structure of TEM is not changed (N, $m_d \sim$ const) [1]. In so doing, increase in $Z_{\max}$ of NS TEM is

attributable to a decrease in κ_L and increase in r due to additional scattering of phonons and electrons (holes) on the inhomogeneities with $x = 1 – 100$ nm (Table 1) [1, 2]. Research on NS TEM is a new promising direction of modern material science. Here, alongside with the evident advantages of NS TEM, some of their essential shortcomings were revealed. Thus, increase in Z of samples is, as a rule, accompanied by a reduction of σ and W, which complicates the use of NS TEM in power thermoelectric converters (TEC) (generators (TEG), coolers (TEC), heaters (TEH)), operated in maximum power mode [1]. Moreover, NS TEM are also characterized by complexity and high cost of fabrication, toxicity and reduced reproducibility of characteristics [5]. The major fault of NS is their instability (morphological, diffusion, chemical), which becomes apparent in the process of manufacture, storage and operation of samples [1, 2]. Finally, installation of NS into TEC entails additional problems related to optimization of materials and connection of legs [1-6]. The purpose of this work was all-round analysis of the strong and weak points of NS TEM, as well as determination of the immediate prospects of their use in TEC.

1. Preparation and properties of NS TEM

1.1. Formation of PGEC phase

The bulk NS TEM were obtained by different methods that can be conventionally classified as "artificial" and "natural" (Table 1) [5-14]. In the former case the necessary identity periods x in the samples were assigned by means of additional technological operations (grinding with subsequent sintering, evaporation and epitaxial growth of nanolayers, introduction of "quantum dots", irradiation, etc.) (Table 1) [5, 7-9]. In the latter case (less expensive and promising one) the nano-like TEM structures were obtained "spontaneously" as a result of "self-organization" of initially homogeneous, nonequilibrium samples, with various phase transitions (decomposition of oversaturated solid solutions, superstructural transitions, doping and self-doping of disordered phases, etc.) (Table 1) [6, 10-14]. In all cases the researchers' immediate objective was to obtain from TEM the "phonon glass-electron crystal" phase (PGEC) (Table 1) [2]. The PGEC is a partially disordered phase of TEM which is characterized by low thermal conductivity κ_L inherent in amorphous materials, and high electric conductivity σ, typical of crystals [1, 2]. As a result, at the transition "crystal → PGEC" considerable growth of TEM parameter Z can be observed [1]. The possibility of PGEC phase formation in TEM is related to the difference in average mean free paths of phonons and electrons in crystals:

$$\lambda_{ph} = 3\kappa_{ph} / CV \tag{2}$$

and

$$\lambda_e = v\tau = \left(2E_F / m_d\right)^{1/2} m_c\mu / e = \hbar(3\pi^2 n / N^2)^{1/3}\mu / e, \tag{3}$$

where $C = C_{mol}\, d/M$ is heat capacity of volume unit, C_{mol} is molar heat capacity, d is density, M is molecular mass, V is sound velocity, v and $\tau = \tau_0 E^{r-½}$ is velocity and average in energy E relaxation time of electrons or holes, r is scattering parameter, τ_0 is energy-independent factor, E_F is the Fermi energy, e is the unit cell, μ is current carrier mobility, $N = m_d/m_c$ is the number of extremums in the band, m_c and m_d are the effective masses of conductivity and density of states of electrons (holes) in the samples [15, 16]. As a rule, for crystalline semiconductors we have: $a << \lambda_{ph} << \lambda_e$ (here $a \sim 0.3$ nm is interatomic distance) (3, Fig. 1) [16]. However, crystalline TEM were selected from semiconductor materials by Z_{max} criterion (1). Therefore, they are noted for low κ_p values and high N, which according to (1) and (2), determines low λ_{ph} and λ_e values in the samples (Fig. 1) [15-19]. Thus, TEM turn to be closer to the transitions $\lambda_{ph} \to a$ and $\lambda_e \to a$ than conventional semiconductor materials, which facilitates formation of PGEC phase in the samples [16].

Table 1

Change in the properties of crystalline samples at "artificial" and "natural" nanostructurization of TEM by different methods

NS preparation technique	"Artificial"				"Natural"			
	Introduction of "quantum dots" [7]	Evaporation of superlattices [8]	Grinding and pressing [5]	Super fast cooling and pressing [9]	Spinodal decomposition of *PbS* particle (3 – 5 nm) [10] [a]	Paraelectric phase doping (T_c > 630 – 700 K) [6] [a]		Transition into superionic phase (T> 413 K) [11-13]	Crystallization of superlattices [14]
						GeTe<5%*Bi*>	TAGS-90 [c]		
Sample	*PbTe/PbSeTe*	Bi_2Te_3/ Sb_2Te_3	$Bi_{0.3}Sb_{1.7}Te_3$	$Bi_{0.52}Sb_{1.48}Te_3$	$(PbTe)_{0.92}(PbS)_{0.08}$			$Cu_{1.99}Se$	$GeBi_4Te_7$
x, nm	10	16	10/(100-300)*	$10^4/10^3$ *	10-20	~ 1.2 [d]	~ 0.9 [d]	~ 0.6 [e]	2.4
T, K	300	300	300	300	650	800→750	800→750	700	300
$\bar{\lambda}_e/a$	9.2→8.6**	8.8→6.4**	8.8→6.2**	9.2→6.0**	10→7.5**	3→2**	3→2**	0.9**	14**
λ_{ph}/a	6.0→1.2**	3.3→1.03**	1.5→1.7**	2.5→1.7**	4.0→1.8**	3→1.1**	3→1**	1**	~1.4**
α, μV/K	-300→-330**	-250→-261**	196→213	230→250	-200→(-200)**	140→200	140→200	240	-160
σ, S/cm	300→290**	810→590**	810→580	850→550	400→(300)**	2000→750	2000→1000	190	500
κ, W/(m·K)	2.5→0.6	1.45→0.6	0.94→0.82	1.36→0.9	1.1→0.5	4..5→1.8	4..5→~2.3	1.0	0.8
W, W/(cm·K)	28→32	51→40	31→26	45→34	16→12	39→27	39→40	1.1	12.8**
$Z{\cdot}10^3$, 1/K	~1.1→5.3	~3.5→6.7	~3.1→3.2	~3.3→3.7	1.4→2.3	0.9→1.7	0.9→1.7	1.1	1.6**
PGEC phase	+	+	–	–	–	+	+	Glass	–

* – before/after pressing; ** – estimates of this work; [a] – comparison to *PbTe*; [b] – comparison to *GeTe*; [c] – $(AgSbTe_2)_{0.1}(GeTe)_{0/9}$; [d] – average distance between impurity atoms; [e] – average distance between copper atoms of melted sublattice.

As long as the transition $\lambda_{ph} \rightarrow a$ in TEM is generally terminated sooner than the transition $\lambda_e \rightarrow a$, in the range

$$a = \lambda_{ph} < \lambda_e \tag{4}$$

formation of PGEC phase appears to be possible (5, 6, Fig. 1) [16].

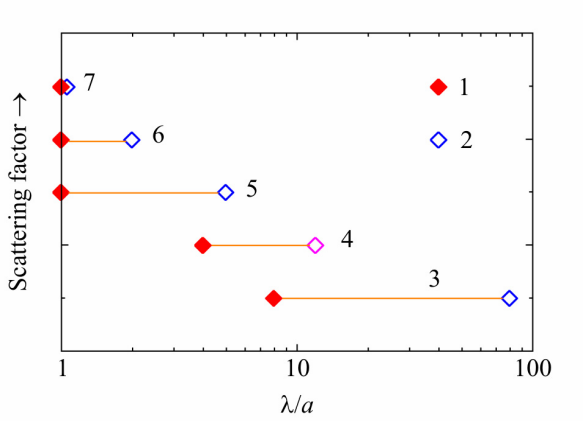

Fig. 1. Dependence of mean free path of phonons λ_{ph}/a and electrons λ_e/a (2) on scattering factor (3 – 7). Samples: 3 – solid semiconductors; 4 – 7 – TEM; 5 – 6 – PGEC phase; 7 – amorphous bodies. Materials: 4 – PbTe [1, 6]; 5 – PbTe/PbSeTe ($1 \sim \lambda_{ph}/a < \lambda_e/a$) [7]; 6 – TAGS ($1 \sim \lambda_{ph}/a < \lambda_e/a < 2 – 3$) [6, 10]; 7 – $Cu_{1.99}Se$ ($1 \sim \lambda_{ph}/a \sim \lambda_e/a$) [11-13]. Temperature, T, K: 5 – 300; 4 – 600; 6, 7 – 700.

1.2. λ-diagnostics of NS TEM

To determine belonging of samples (Table 1) to PGEC phase (3), we used the method of λ-diagnostics of TEM based on the estimation of values λ_{ph} and λ_e by the formulae (1) and (2) [16]. In the estimates, the data of original works as well as the reference data was employed [20, 21]. For *GeTe<Bi>* alloys and TAGS-90 the x parameters were calculated in the approximation of uniform distribution of dopants in the sample, and for $Cu_{1.99}Se$ alloys – of mobile interstitial copper ($T > T_c = 700$ K) (Table 1). From Table 1 it is seen that for *PbTe/PbSeTe* [7] and Bi_2Te_3/Sb_2Te_3 [8] samples the PGEC phase (3) is formed already at room temperature, as confirmed by a drastic increase in Z by a factor of 2 – 5.[1] Formation of PGEC phase (3) was also observed in doped alloys *GeTe <Bi>* and TAGS-90 [6] at a temperature of $T = 750 – 800$ K, which is accompanied by Z increase by a factor of ~ 2 as compared to *GeTe* (Table 1). The samples of $(PbTe)_{0.92}(PbS)_{0.08}$ [10] were also close to formation of PGEC phase ($Z^{650\,K}$ increase by a factor of ~ 1.6 as compared to *PbTe*) and $GeBi_4Te_7$ [14] ($Z^{300\,K}$ increase by a factor of ~ 1.6 as compared to *GeTe*) (Table 1). However, in $Bi_{0.3}Sb_{1.7}Te_3$ [5] and $Bi_{0.52}Sb_{1.48}Te_3$ [9] samples the transition $\lambda_{ph} \rightarrow a$ proved to be incomplete, PGEC phase was not obtained and, as a result, Z value increased only slightly (Table 1). The incompleteness of the transition $\lambda_{ph} \rightarrow a$ in the sample $Bi_{0.52}Sb_{1.48}Te_3$ [9] (Table 1) is due to insufficient material dispersion ($x \sim 10^3$ nm). At the same time, the sample $Bi_{0.3}Sb_{1.7}Te_3$ [5] (Table 1) obtained from nanoparticles of the necessary size ($x \sim 10$ nm, in the course of hot pressing was recrystallized with grain increase (effect of "knockout" from nanoregion) ($x = 10 \rightarrow 300$ nm) [16]. Moreover, in all NS TEM (Table 1) there was also the transition $\lambda_e \rightarrow a$ related to increased electrons (holes) scattering with dispersion of samples. In the superionic $Cu_{1.99}Se$ the two transitions $\lambda_{ph} \rightarrow a$ and $\lambda_e \rightarrow a$ were completed ($T = 700$ K), and the sample became quasi-amorphous

[1] According to [5], the results of [7, 8] have not been reproduced to this date in any other laboratory of the world, NS based devices have not been created either.

($\lambda_e \sim \lambda_{ph} \sim a$) (7, Fig. 1) [11-13]. The results of λ-diagnostics of NS TEM (Table 1) allow determination of the basic mechanisms responsible for a change in Z and W. From Table 1 it is seen that formation of PGEC phase and Z increase of NS TEM is due to a decrease in $\kappa_L \sim \lambda_{ph}$ with the transition $\lambda_{ph} \rightarrow a$. In so doing, the attendant $\lambda_e \rightarrow a$ transition, as a rule, reduces W of TEM due to reduction of $\sigma \sim \lambda_e$ (Table 1). The exception is provided by the samples of *PbTe*/*PbSeTe* [7] and TAGS-90 [6] (Table 1) where a slight growth of W was observed due to increased α of the samples. In case of NS [7] the growth of α was accounted for by additional current carrier scattering on "quantum dots" ($x = 10 – 16$ nm) [1], and for the sample [6] – by peculiarities of TEM band structure in the transient region $1 < \lambda_e/a \sim 3$ [16].

1.3. Two-channel band model of TEM

According to [15, 16], the band structure of TEM in the transient region $1 < \lambda_e/a \sim 2 – 3$ is varied considerably. With the transition $\lambda_e \rightarrow a$ in TEM in addition to a "band" conduction channel ($\lambda_e / a > 1$) (1, Fig. 2), a diffusion conduction channel is formed in conduction (valence) band (2), related to the appearance of a group of current carriers with a low mobility, moving in the sites of crystal lattice ($\lambda_e/a = 1$) [15]. With further scattering increase, the "band" current carriers disappear, and the "diffusion" ones cover the entire band (arrow, Fig. 2). The model (Fig. 2) corresponds to p-type conductivity and acoustic scattering mechanism ($r = 0$). With increase in $r > ½$, the situation is changed, namely the "diffusion" conduction channel (2, Fig. 2) is formed near the band edge, and then it is distributed in the band toward larger energies [16].

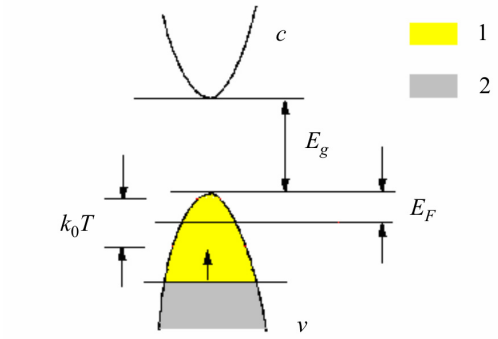

Fig. 2. Two-channel band model of TEM. Bands: v – valence; c – conduction. Channels: 1 – "band" ($\lambda_e > a$), 2 – "diffusion" ($\lambda_e = a$). The arrow shows a direction of channel boundary displacement in the energy scale with scattering increase in the samples (p-type conductivity, r = 0) [15, 16].

In the two-channel model (Fig. 2) the kinetic coefficients of samples with constant total carrier concentration ($p = p_1 + p_2 = \text{const}$) are given by the expressions $\sigma = \sigma_1 + \sigma_2$, and $\alpha = \alpha_1 \cdot t_1 + \alpha_2 \cdot t_2$ (Here, $t_i = \sigma_i/\sigma$ is transport ratio, α_i and σ_i are partial thermoEMF and electric conductivity, $i = 1, 2$ are numbers of channels with "band" ($\lambda_e > a$) and "diffusion" ($\lambda_e = a$) conduction, respectively) [16]. Fig. 3 shows the results of calculations of a relative change in thermoelectric figure of merit Z (curve 1), power W (curve 2) and thermal conductivity κ (curve 3) of TEM samples in the region of PGEC phase existence. In the calculations, use was made of the band parameters $\mu_1/\mu_2 \sim \kappa_L/\kappa_e \sim 10$ and $\kappa_L^{cryst}/\kappa_L^{PGEC} = 3$ (here, $\mu_{1,2}$ are partial mobilities, κ_L and κ_e are the lattice and electron components of thermal conductivity), as well as scattering parameters $r = 0$ (acoustic scattering) and $r = ½$ (scattering on neutral centres) for the "band" (1) and "diffusion" (2) conduction channels, respectively (Fig. 2) [16].

From Fig. 3 it follows that in the range of $1 < \lambda_e/a < 2 – 3$ the values of Z and W in TEM can increase simultaneously (curves 1 and 2). At $t_1 \sim 0.8$ maximum increase in Z by a factor of ~ 2.5 – 3 and W by a factor of 1.3 – 1.4 (curves 1 and 2, Fig. 3) is possible due to a combined effect of the transitions

$\lambda_{ph} \rightarrow a$ and $\lambda_e \rightarrow a$. The possibility of α and W growth (3, Fig. 3) in the model (Fig. 2) is related to energy selection of the "band" and "diffusion" current carriers taking part in conductivity [16]. Earlier the model (Fig. 2) was used to account for the anomalous growth of Z and W in $GeTe$ and $Cu_{1.99}Se$ alloys at a high temperature [15]. According to estimates (Fig. 3), two-channel conductivity can be also responsible for the simultaneous growth of Z and W at a high temperature ($T = 700 – 800$ K) in the nano-like structures of the type p-TAGS $((AgSbTe_2)_{1-x}(GeTe)_x)$ ($\lambda_e/a \sim 2$) (Table 1) [6, 10], as well as p-LAST-m ($AgPb_mSbTe_{2+m}$, $m = 18 – 22$) ($ZT = 1.6 – 2.2$) [10].

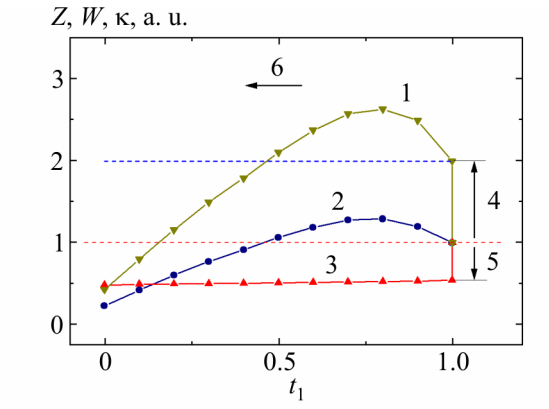

Fig. 3. Relative change in the figure of merit Z (1), power W (2) and thermal conductivity κ (3) with the transitions $\lambda_{ph} \rightarrow a$ (4, 5) and $\lambda_e \rightarrow a$ (6) in TEM depending on the transport ratio of band charge carriers t_1 (T = const).

2. Comparison of NS TEM and crystalline TEM

2.1. λ-diagnostics of crystalline TEM

The results of λ-diagnostics of crystalline TEM are given in Fig. 4 ($a – f$). Figs. 4 a and 4 b show polyterms λ_{ph}/a (a), λ_e/a (b) ($T = T_{max}$) (curves 3 and 4) depending on E_g of the best low-, medium- and high-temperature TEM [1, 6, 10-13, 21, 22]. Figs. 4 c and 4 d show the respective polyterms T_{max} (curves 5 – 8), as well as optimal charge carrier concentration $n^{opt}(p^{opt})$ (curve 9) and the Fermi energy E_F of TEM (curve 11). From Fig. 4 a and 4 b it is seen that with increase in E_g and T_{max}, the transitions $\lambda_{ph} \rightarrow a$ and $\lambda_e \rightarrow a$ occur in crystalline TEM that change the characteristics of samples. Fig. 4 c shows the impact of the transition $\lambda_e \rightarrow a$ on the T_{max} value of TEM (curves 7 and 8). According to Fig. 4 c, far from the transition $\lambda_e \rightarrow a$ ($\lambda_e/a > 10$, $E_g < 0.4$ eV) TEM behave as conventional semiconductors with high mobility μ, the values of T_{max} being in the range of $5 < b < 10$ (5 – 8, Fig. 4 c). However, at $E_g > 0.5 – 0.7$ eV and $\lambda_e / a < 2 – 3$ the values of T_{max} go beyond the range of $5 < b < 10$ (curves 7 and 8, Fig. 4 c). The effect is attributable to the appearance in the samples of "diffusion" charge carriers with a low mobility ($\lambda_e = a$), which increases the relative contribution of minor carriers to development of intrinsic conductivity in the samples ($r = 0$) [15, 16]. Here we have $T_{max}(p) < T_{max}(n)$ (curves 7 and 8, Fig. 4 c), since generally $a = \mu_e/\mu_p > 1$ [11]. The transition $\lambda_e \rightarrow a$ also affects the polyterms $n^{opt}(p)^{opt}$, $E_F = f(E_g)$ in TEM (Fig. 4 d), where one can see a reduction in growth rate $n^{opt}(p)^{opt}$ (curve 9) and even slight reduction of $E_F \sim ½\, k_0 T_{max}$ (curve 11) related to T_{max} reduction in the region of $\lambda_e \sim a$ (curve 10). Figs. 4 e and 4 f show polyterms of the figure of merit $(ZT)_{max}$ (curve 12) and power $W = f(E_g)$ (curve 15) in crystalline TEM ($T = T_{max}$). Curve 12 (Fig. 4 e) has an extended maximum $(ZT)_{max} \sim 1$ in the range of 0.1 eV $< E_g <$ 1.0 eV and drops in the area of low and high E_g. According to Figs. 4 a and 4 f, condition $(ZT)_{max} \sim 1$ in the range of

0.1 eV < E_g < 0.6 eV (curve 12, Fig. 4 *e*) is maintained due to a compensating effect of the transitions $\lambda_{ph} \rightarrow a$ and $\lambda_e \rightarrow a$ leading to a simultaneous reduction of κ_L and W of the samples.

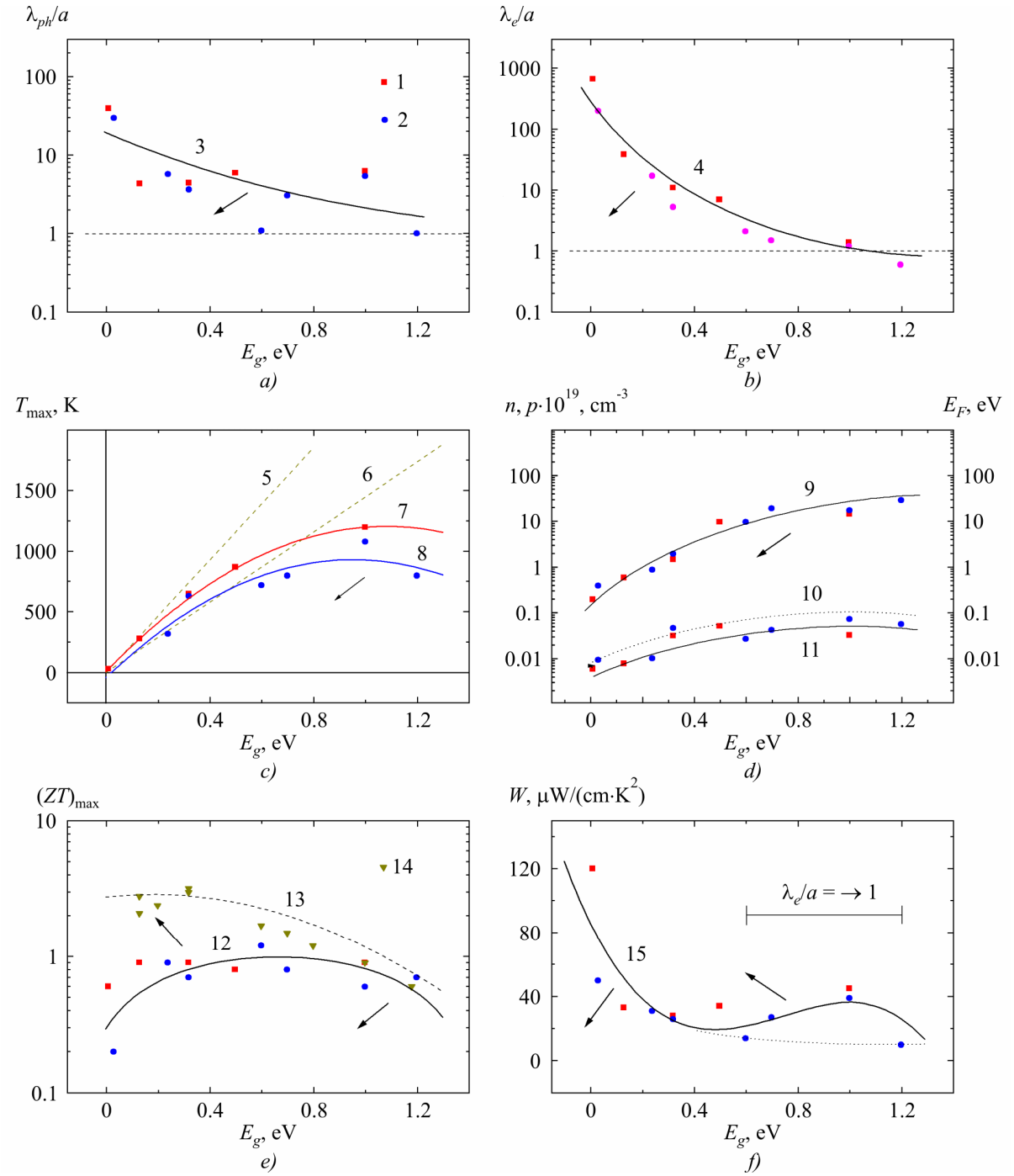

Fig. 4. Polyterms λ_{ph}/a (a), λ_e/a (b), T_{max} (c), n^{opt} (p^{opt}) and E_F (d) $(ZT)_{max}$ (e) and W (T_{max}) (f) depending on the energy gap E_g of TEM ($T = T_{max}$). Samples: 1 – 12 – crystals [1, 6, 10-13, 20-22]; 13, 14 – NS [7, 8, 10, 22]. Materials (in order of increasing E_g): 1 – n-type (BiSb, Bi_2Te_3, PbTe, $CoSb_3$, SiGe); 2 – p-type (BiSb <Sn>, Sb_2Te_3, PbTe, TAGS, GeTe, SiGe, $Cu_{1.99}Se$). 1, 2, 14-experiment; 5, 6, 10, 13 – calculation. Design formulae: 5, 6 – $E_g = bk_0T$ (b: 5 – 5; 6 – 10); 10 – $E = k_0T_{max}$; 13 – $y = (ZT_{max}$ (curve 12)) (λ_{ph}/a). Directions of possible changes in TEM characteristics at formation of NS are shown with arrows.*

In so doing, the decay in curve 12, Fig. 4 *e* at $E_g > 1.0$ eV is related to completion of the transition $\lambda_e \rightarrow a$ ($\lambda_e/a = 1$), and the decay at $E_g < 0.1$ eV – to requirements of thermodynamics – α,

$W \to 0$, at $T \to 0$, [1, 4, 6]. The results obtained (Fig. 4) show that the mechanisms of Z and W increase in NS and crystalline TEM at a high temperature are of the same physical nature. In so doing, the difference in the characteristics of NS TEM and crystalline TEM at T = const is due to different stages of the transitions $\lambda_{ph} \to a$ and $\lambda_e \to a$ in the samples. Hence it follows that the expected characteristics of NS TEM can be estimated based on the properties of crystalline TEM by extrapolation $\lambda_{ph} \to a$ and $\lambda_e \to a$. Directions of possible changes in the characteristics of TEM at the transition "crystal → PGEC" are shown by arrows in Fig. 4.

2.2. The "crystal-PGEC" transition

According to Fig. 4, on condition of E_g = const, the "crystal → PGEC" transition in TEM results in the reduction of λ_{ph} and λ_e, T_{max}, n^{opt} (p^{opt}), E_F, as well as W (at $E_g < 0.4$ eV). In so doing, for any values of E_g the value of ZT is increased due to a reduction of NS κ_L (curves 12 → 13, Fig. 4 *e*). Curve 13, Fig. 4 *e* gives the upper limit of ZT increase in samples when passing to PGEC phase. Curve 13, Fig. 4 *e* was calculated for NS by formula (1) based on curve 12 for crystals on condition of $\lambda_{ph}/a = 1$ (Fig. 4 *e)*. From Fig. 4 *e* it is seen that the greatest ZT increase when passing to PGEC phase (up to ~ 10) can be expected only at $T_{max} < 600$ K and $E_g < 0.4$ eV (curve 12 → 13). With $T_{max} > 600$ K and $E_g > 0.4$ eV the possibilities of ZT increase for NS in PGEC phase are reduced considerably (up to~ 1.5) (Fig. 4 *e)*.[2] By and large, the above conclusion is confirmed by the experimental observations of $(ZT)_{max}$ for NS TEM (14, Fig. 4 *e*). Further increase in $(ZT)_{max}$ of NS TEM can be promoted by increase in power parameter W with the transition $\lambda_e/a \to 1$ related to a displacement of W features in the range of $1 < \lambda_e/a < 3$ toward low E_g (Fig. 4 *e*).

2.3. Simultaneous increase in *Z* and *W* of TEM

The main problem of using NS TEM in TEC is a reduction in the majority of cases of power parameter W of NS as compared to crystalline materials (Table 1) [1, 2]. As is known, the Z value of TEM determines maximum temperature difference of TEC and TEH, namely $\Delta T_{max} = ½\, ZT_1^2 = ½\, Z((1 + 2T_0Z)^{½} - 1)/Z)^2$ and TEC efficiency – $\eta = \eta_c\ (M_0 - 1)/(M_0 + T_c/T_h)$ (maximum efficiency mode), or $\eta = \eta_c/(2 + 4/ZT_h - \eta_c/2)$ (maximum power mode) (Here, $\eta_c = (T_0 + T_1)/T_1$ is the Carnot factor, $M = R/r$ is the relative electric load of TEG; R is the electric resistance of load; $M_0 = (1 + Z\,\overline{T})^{1/2}$; $\overline{T} = ½\ (T_0 + T_1)$ is the average temperature) [1]. On the other hand, the W of TEM determines maximum cooling capacity of TEC and TEH, namely $Q_{max} = \Delta T_{max}\kappa S/l \sim ½ W\, T_1^2$, as well as maximum net power of TEG $W_{max} = W\Delta T^2/4 = WS/4l$ [1, 6]. As an example, Fig. 5 shows a relative change in the temperature difference $\Delta T/\Delta T_0$ of TEC with different Z and W as a function of cooling capacity Q/Q_0. From Fig. 5 it is evident that using NS TEM with increased Z (curves

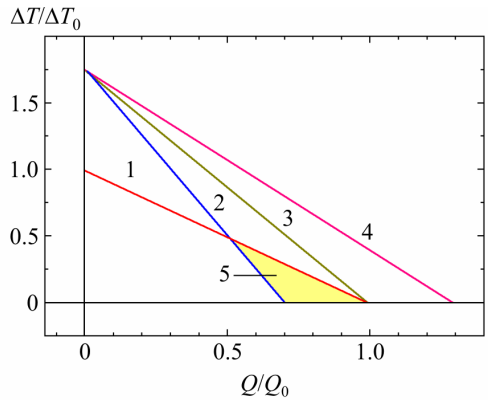

Fig. 5. Relative change in temperature difference $\Delta T/\Delta T_0$ (1 – 4) versus cooling capacity Q/Q_0 of TEC. Materials: 1 – crystals ($\Delta T/\Delta T_0 = Q/Q_0 = 1$); 2 – 4 – NS. $Z_{HS}/Z_{CR} = 3$; W_{HS}/W_{CR} : 2 – 0.7; 3 – 1; 4 – 1.3. 5 – region where NS (2) are inferior in characteristics to crystals (1).

[2] This conclusion refers to averaged Z values of TEM. For instance, in *SiGe* alloys, where $\lambda_{ph}/a \sim 8$ (Fig. 4 *a*), there are considerable additional reserves for Z growth [1].

2 – 4), in the mode of zero thermal load ($Q = 0$) one can always expect ΔT_{max} growth as compared to crystals (curve 1). However, when passing to maximum power mode, with increase in Q in Fig. 5 appears a region (5), with NS characteristics inferior to crystals. Hence it follows that for an adequate use of NS TEM in TEC a simultaneous increase in parameters Z and W is needed (1 → 3, 4, Fig. 5) [1, 10, 20]. For a simultaneous increase of Z and W in TEM the most efficient method was optimization of the band parameters of materials (N, E_F and energy gap E_g). It is also possible to use quantum-size effects (superlattices, quantum wells, wires and dots, etc.), to create in the permitted band close to E_F the "resonance" states, to use grain boundary scattering providing carriers "filtration" according to energies (growth of r and α) [1, 4, 6, 8, 10]. According to Fig. 3 – 4, for a simultaneous increase of Z and W in NS TEM one can also use the effect of "two-channel" conduction acting in TEM in the range of $1 \sim \lambda_{ph}/a < \lambda_e/a < 2 – 3$. If necessary, further increase of Z and W in TEM is possible due to the use of quantum effects in NS [1, 10, 20].

3. Other problems of using NS TEM

3.1. NS TEM instability

Different types of NS TEM instability are directly related to the instability of nanoparticles that form them and possess increased surface energy [1, 2, 23]. Therefore, in the process of compaction of such nanoparticles when preparing the bulk materials there is recrystallization of grains accompanied by increase in their size by several orders (effect of "knockout" from the nanoregion) (Table 1) [5]. However, in some cases the "knockout" effect can be conquered, for instance, by using plasma sintering of particles accompanied by formation of secondary grain substructure [1, 10, 22]. The main type of NS TEM instability is their diffusion instability manifested in the rise of temperature $T > T_T \sim 0.4 – 0.6\ T_m \sim 400 – 700$ K (Here, T_T and T_m are the Tammann and material melting temperatures, respectively) [22]. Fig.6 shows melting temperature T_m (1), T_{max} (2) and the Tammann temperature $T_T = 0.6\ T_m$ (3) of crystalline TEM depending on E_g of samples.

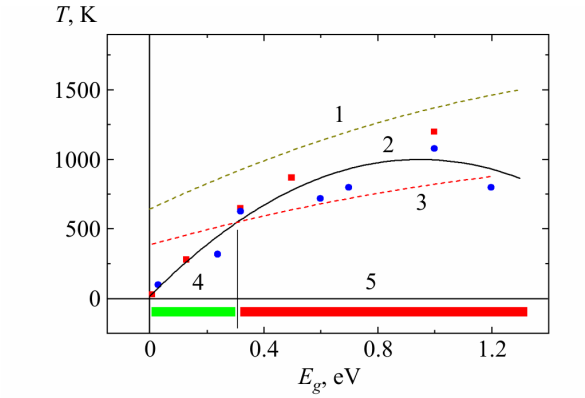

Fig. 6. Melting temperature T_m (1), T_{max} (2) and the Tammann temperature $T_T = 0.6\ T_m$ (3) of crystalline TEM versus the energy gap E_g. 4 and 5 are NS stability and instability ranges at $T = T_{max}$. Samples: see caption to Fig. 4.

From Fig. 6 it is seen that at $T_{max} > 500 – 600$ K and $E_g > 0.3$ eV NS TEM are instable at temperature $T \sim T_{max}$ (range 5). At temperature T_{max} only the alloys with $T_{max} < 500$ K and $E_g < 0.3$ remain stable (range 4), which restricts considerably the prospects of using NS in high-temperature region. To the full extent this conclusion refers to "artificial" NS TEM and to a lesser degree to NS TEM obtained at decomposition of oversaturated solid solutions (Table 1). Even to a lesser extent this conclusion is related to natural superlattices of TEM obtained by crystallization from the melt [1], as

well as strongly disordered nano-like structures of the type $Ge_{1-x}Te$, TAGS, LAST and $Cu_{2-x}Se$ (Table 1). Diffusion instability of NS TEM directly accounts for their chemical instability determined by high rate of reagents diffusion along the grain boundaries. Various technical methods for combatting chemical instability of NS TEM are applied with profit [1, 22].

3.2. Change in material optimization parameters

The transition "crystal → NS" reduces the values of T_{max}, n^{opt} (p^{opt}), and in some cases E_F of the samples (Fig. 4). This necessitates a change in optimization rules of NS TEM as compared to crystals. Fig. 7 demonstrates the Bergholz diagrams qualitatively explaining the differences in the optimal concentration of current carriers in crystal and NS [3]. From Fig. 7 it is seen that on condition of $\alpha \sim \alpha$ (crystal) $\sim \alpha$ (HS) $\sim$ const (Table 1), the optimal concentration of current carriers n_{opt} of NS will be reduced, and the known mismatch between n_{opt} for Z and W will increase ($\Delta_1 > \Delta_2$).

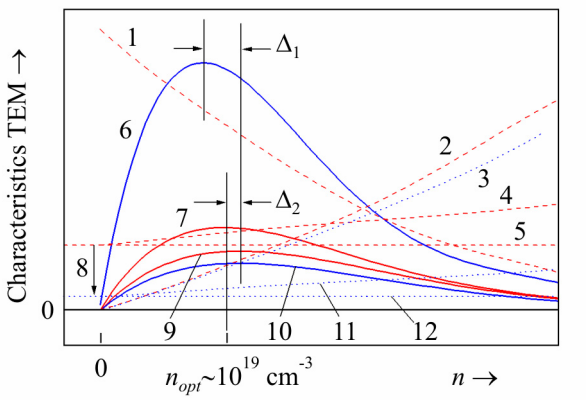

Fig. 7. The Bergholz diagrams of TEM. 1, 2, 4, 5, 7, 9 – crystals; 1, 3, 6, 10, 11, 12 – NS (T = 300 K). Characteristics: 1 – α ~ α (crystal) ~ α (HS) ~ const; 2, 3 – σ; 4, 11 – κ = κ_L + κ_e; 5, 12 – κ_L; 6, 7 – Z; 9, 10 – W. Mismatch in n_{opt} between Z and W: Δ_1 are NS; Δ_2 are crystals. 8 is transition λ_{ph}→a.

The mismatch $\Delta_1 > \Delta_2$ can result in the necessity of developing NS TEM with different parameters as applied to maximum efficiency and maximum power modes of TEC.

3.3. Contact effects and material saving

The transition "crystal → NS" is accompanied by increase in thermal ($r^T = \kappa^{-1}$) and electrical resistance ($\rho = \sigma^{-1}$) of the samples. As a result, the use of NS TEM in TEC is accompanied by increase in transient contact thermal and electrical resistances of thermocouples, which can generate a need for longer legs and reduced device efficiency [1, 6]. However, in [23] it was shown that for the case of automobile thermoelectric generators (ATEG) using gas heat carriers [6] the contribution of contact resistances of NS TEM can be assumed to be inessential as compared to parasitic resistances of heat exchangers. In this case, the use of NS TEM can lead to a simultaneous increase in TEC efficiency and considerable saving of costly TEM (up 3 times and more) [24]. However, in the case of TEC using liquid and solid heat carriers, the contribution of NS contact resistances to TEC efficiency can prove to be essential, and it should be taken into account in the development of devices [6].

Conclusion

Research on NS TEM is a new upcoming trend of modern material science [1, 2]. In this paper, a thorough analysis of NS TEM characteristics is made and mechanisms for improving their

thermoelectric figure of merit Z and power W are determined. Transition of TEM into "phonon glass-electron crystal" (PGEC) phase underlies the growth of NS parameter Z. The possibility of PGEC phase formation in the samples ($a = \lambda_{ph} < \lambda_e$) is related to the proximity of TEM to the transitions $\lambda_{ph} \rightarrow a$ and $\lambda_e \rightarrow a$. (Here a is interatomic distance, λ_{ph} and λ_e is the average mean free path of phonons and electrons). To determine the degree of proximity to PGEC phase, the method of λ-diagnostics of TEM based on the estimation of λ_{ph} and λ_e values in the samples is developed in [16]. The use of λ-diagnostics allowed to establish that increase of Z and W in NS TEM, as well as TEM crystals at high temperature are determined by the same mechanisms. Owing to this result, the theoretical limits of increase in Z and W parameters in NS TEM were estimated in various temperature ranges. According to estimates, the greatest growth of Z in NS TEM is possible at room and lower temperatures; with a rise in temperature, the possibilities of Z growth in NS TEM are reduced. The use of λ-diagnostics also allowed establishing the mechanisms responsible for growth of Z and W in NS TEM. It is shown that formation of PGEC phase and growth of Z in NS TEM is due to reduction of $\kappa_L \sim \lambda_{ph}$ at the transition $\lambda_{ph} \rightarrow a$. In so doing, the attendant transition $\lambda_e \rightarrow a$, as a rule, reduces W of TEM due to reduction of $\sigma \sim \lambda_e$. As long as reduction of W complicates the use of NS TEM in power TEC, it is necessary to further increase α and W of NS TEM by various methods. With this aim in view, in the present paper it is proposed to use the effect of two-channel conduction assuring simultaneous growth of Z and W in the range of $1 \sim \lambda_{ph}/a < \lambda_e/a < 2 - 3$. This paper also covers some negative characteristics of NS TEM preventing their wide use in TEC. In particular, the ranges of diffusion instability of NS at high temperatures are determined. It is shown that at present the "safe" range of using "artificial" NS TEM is probably restricted to near-room and lower temperatures. One is inclined to think that the above disadvantages of NS TEM can be overcome, and the stability of samples at high temperatures can be increased using various technical methods. However, since the above problems have not been solved up to now, only the "natural" NS such as naturally-occurring superlattices based on multicomponent systems seem to be the most promising so far for high-temperature use[3]. Also of great interest are "natural" nano-like structures of the type *GeTe*, TAGS and LAST based on strongly disordered phases, that have already proved their reliability by failure-free operation on space objects for 10 and more years [1, 6, 10].

References

1. G.S. Nolas, J. Sharp, and H.J. Goldsmid, *Thermoelectrics. Basic Principles and New Materials Developments* (Berlin: Springer, 2001), 293 p.
2. G. Slack, *New Materials and Performance Limits for Thermoelectric Cooling*, CRC Handbook of Thermoelectrics, Ed.: D.M. Rowe (N.Y.: Boca Raton, 1995), P. 407 – 440.
3. U. Birkholz, Thermoelectric Elements, In: *Amorphous and Polycrystalline Semiconductors*. Ed. by W. Heywang. Transl from German (Moscow, Mir, 1987), P. 47 – 74.
4. L.I. Anatychuk, *Thermoelements and Thermoelectric Devices* (Kyiv: Naukova Dumka, 1979), 768 p.
5. L.P. Bulat, D.A. Pshenai-Severin, I.A. Drabkin, et al., Mechanisms for Thermoelectric Figure of Merit Improvement in the Bulk Nanotructured Polycrystals, *J. Thermoelectricity* **1**, 13 – 18 (2011).
6. A.S. Okhotin, A.A. Yefremov, V.S. Okhotin, and A.S. Pushkarsky, *Thermoelectric Generators* (Moscow: Atomizdat, 1976), 320 p.

[3] The "natural" NS also include layered crystals of the type Bi_2Te_3 whose identity period $x \sim 3$ nm appears somewhat lower than that optimal for TEM ($x \sim 10 - 40$ nm) [1, 2].

7. T.C. Harman, P.J. Taylor, M.P. Walsh, and B.E. LaForge, Quantum Dot Superlattice Thermoelectric Materials and Devices, *Science* **297**, 2229 (2002).
8. R. Ventkatasubramanian, E. Siivola, T. Colpitts, and B. O'Quinn, Thin-Film Thermoelectric Devices with High Room-Temperature Figures of Merit, *Nature* **413** (6856), 597 – 602 (2001).
9. L.D. Ivanova, L.I. Petrova, Yu.V. Granatkina, V.S. Zemskov, S.A. Varlamov, A.S. Ivanov, Yu.P. Prilepo, A.M. Sychev, A.G. Chuiko, Materials Based bon $Bi_{0.5}Sb_{1.5}Te_3$ Solid Solution Prepared with the Use of Spinning Method, Thermoelectrics and Their Applications. Ed. by M.V. Vedernikov, L.N. Lukyanova (The Petersburg Nuclear Physics Institute RAS, 2010), P. 88 – 93.
10. J. Sootsman, D.Y. Chung, and M.G. Kanatzidis, New and Old Concept in Thermoelectric Materials *Angew. Chem. Int. Ed.* **48**, 8616 – 8639 (2009).
11. A.A. Voskanyan, P.N. Inglizyan, Ya.M. Shevchenko, and T.B. Shmakova, Thermal Field Effect on the Electric Properties of Copper Selenide, *Semiconductors* **14** (4), 804 – 806 (1980).
12. M.A. Korzhuev, V.F. Bankina, B.F. Gruzinov, and G.S. Bushmarina, Electrophysical Properties of Superionic $Cu_{2-x}Se$, *Semiconductors* **23** (9), 1545 – 1551 (1989).
13. M.A. Korzhuev, V.F. Bankina, B.A. Yefimova, and N.N. Filipovich, Electrophysical Properties of $Cu_{2-x}Se$ Alloys Doped with Electroactive Dopants, *Semiconductors* **24** (5), 805 – 812 (1990).
14. V.S. Zemskov, L.E. Shelimova, O.G. Karpinsky et al., Thermoelectric Materials Based on Layered Compounds in Chalcogenide Systems with Homologous Series, *J. Thermoelectricity* **1**, 15 – 29 (2010).
15. M.A. Korzhuev, A.V. Laptev, and V.F. Degtyarev, The Use of Two-Channel Conductivity Model for the Description of Kinetic Coefficients of $Ge_{1-x}Te$ и $Cu_{2-x}Se$ Type Crystals in High Temperature Region, *Thermoelectrics and Their Applications* (The Petersburg Nuclear Physics Institute, 2002), P. 133 – 138.
16. M.A. Korzhuev, Effect of Average Mean Free Path of Phonons and Electrons on the Parameters of Figure of Merit Z and Power W of Thermoelectric Nanostructures, *Thermoelectrics and Their Applications*, Ed. by M.I. Fedorov, L.N. Lukyanova (The Petersburg Nuclear Physics Institute, 2002), P. 99 – 105.
17. M.A. Korzhuev, Concomitant Effects in High-Performance Thermoelectric Materials, *Vysokochistye Veschestva* **2**, 74 – 89 (1996).
18. M.A. Korzhuev, Symmetry Analysis of Thermoelectric Energy Converters with Inhomogeneous Legs, *JEMS* **39** (9), 1381 – 1385 (2010).
19. M.A. Korzhuev, The Hall Effect in Thermoelectric Materials of the Type $Ge_{1-x}Te$ and $Cu_{2-x}Se$ in the Region $\lambda \rightarrow a$, *Physics of the Solid State* **35** (11), 3043 – 3052 (1993).
20. *Physicochemical Properties of Semiconductor Substances*. Handbook. Ed. by A.V. Novoselova (Moscow: Nauka, 1979), 340 p.
21. N.N. Kiseleva, V.A. Dudarev, and M.A. Korzhuev, The Bandgap of Solids (Semiconductors, Dielectrics, Semimetals). Determination of the Bandgap of Inorganic Substances-Semiconductors, *Datebase «Bandgap» b.g.imet-db.ru/ about database.asp. 2007.*
22. T. Kajikawa, Advances in Thermoelectric Power Generation Technology in Japan, *J. Thermoelectricity* **3**, 5 – 18 (2011).
23. K. Meyer, *Physicochemical Crystallography*. Transl. from German. (Noscow: Metallurgiya, 1972), 480 p.
24. M.A. Korzhuev, Yu.V. Granatkina, Some Bottlenecks in the Vehicular Thermoelectric Generators and a Search for New Materials to Eliminate Them, *J. Thermoelectricity* **1**, 74 – 86 (2012).

Submitted 22.04.2013.

S.I. Olkhovskaya, E.I. Rogacheva

S.I. Olkhovskaya

National Technical University
"Kharkiv Polytechnic Institute", 21, Frunze Str.,
Kharkiv, 61002, Ukraine

E.I. Rogacheva

SIZE EFFECTS IN LEAD TELLURIDE THIN FILMS AND THERMOELECTRIC PROPERTIES

The influence of thickness d on thermoelectric properties (the Seebeck coefficient S, electric conductivity σ, the Hall coefficient R_H, charge carrier mobility μ_H) of films d = 8 – 170 nm in thickness, prepared by vacuum evaporation of PbTe crystals with lead excess onto (001) KCl substrates coated with Al_2O_3 layer has been studied. It has been established that films with d < 75 nm possess hole conductivity, and at d > 75 nm carrier transport is determined by n-type charge carriers. The inversion of conductivity sign close to d ≈ 75 nm is attributed to a change in thermodynamic equilibrium conditions in the films as compared to crystal, as well as to material evaporation and condensation features. Oscillations on the d-dependences of the kinetic coefficients of films with p-type conductivity are attributable to quantization of the hole gas of carriers. Calculation of oscillation period Δd using a model of infinitely deep rectangular potential well is in good agreement with the experimentally determined Δd value. For n-type conductivity films the values of kinetic coefficients increase with increase in d, which points to manifestation of a classical size effect.

Key words: thin film, classical and quantum size effect, thickness.

Introduction

The IV-VI semiconductor compounds are widely used in thermoelectricity, optoelectronics, infrared technology and other fields of science and engineering [1-4]. Lead telluride (*PbTe*) is well known as one of the best materials for thermoelectric (TE) generators operated in medium temperature range [2, 3].

Considerable improvement of TE figure of merit in superlattices based on IV-VI semiconductors [5-8] earlier predicted theoretically [5], arouses interest in studying thermoelectric properties of *PbTe* in the thin-film state.

One of the main tasks of nanophysics and nanotechnologies is development of methods for preparation and study of material properties in the low-dimensional state (quantum wells, quantum wires, quantum dots). In the thin-film state the size of a sample in one direction is considerably smaller than in the other two directions. Considerable impact on the transport properties of 2*D*-structures can be produced by size effects, namely classical (ClSE) which can be observed in the case when the mean free path of charge carriers is comparable to film thickness *d*, and quantum (QSE), which is manifested when film thickness becomes comparable to de Broglie wavelength value [9].

In a number of works (see, for instance, [10-16]) for lead chalcogenide films (*PbS*, *PbSe*, *PbTe*) prepared by vacuum evaporation of a blend with different concentration of charge carriers of both *n*- and *p*-type (from $\sim 10^{18}$ to 10^{20} cm^{-3}) the authors observed the oscillatory behaviour of the dependences of TE properties (the Seebeck coefficient *S*, electric conductivity σ, Hall charge carrier mobility μ_H and TE power $P = S^2\sigma$) on the film thickness *d*, attributing this phenomenon to

manifestation of QSE. The increase in monotonic components of σ and μ_H versus thickness, discovered in *PbSe* films prepared from crystals of stoichiometric *p-PbSe*, was attributed by the authors of [17] to manifestation of ClSE due to increased contribution of diffused carriers scattering on interfaces with a reduced *d*. The results obtained in [16, 17] have demonstrated that varying film thickness in small steps according to the value of *d* in a wide thickness range, one can study QSE and ClSE on the same objects simultaneously.

The purpose of this work is to study size effects in the films prepared by vacuum evaporation onto (001) *KCl* substrates of *n-PbTe* crystals with lead excess (2 at.% *Pb*) and coated with Al_2O_3 layer. In [15], on the films prepared in a similar way, protected from interaction with air oxygen by *EuS* layer ~ 30 nm thick and having *n*-type conductivity, there were revealed thickness oscillations of the kinetic properties with the period $\Delta d \sim 100$ nm, though the theoretical calculation of Δd, with the use of a model of a rectangular well with infinitely high walls yielded much lower value, namely $\Delta d = 20$ nm. The observed discrepancy was attributed by the authors of [15] to a great deal of simplifications used in the model, as well as to insufficient number of thin-film samples with different values of *d*. The latter factor predetermined the arrangement of the present work.

As a result of research performed in this work, we have managed to establish the presence of *p*-type conductivity region in small thickness range, to discover the oscillatory behaviour of *d*-dependences of kinetic properties in this region, to determine the oscillation period practically corresponding to theoretically calculated one, as well as to observe manifestation of ClSE in the thickness range with n-type conductivity.

Experimental procedure

Epitaxial films *PbTe* of thickness $d = 8 – 170$ nm were prepared by vacuum evaporation ($\sim 10^{-5} – 10^{-6}$ Pa) of *PbTe<Pb>* crystals with lead excess (2 at.% *Pb*) with subsequent condensation onto fresh cleavages of (001) *KCl* at a temperature of (520 ± 10) K. The rate of material condensation was 0.5 – 1.0 nm/s. Film thickness *d* was controlled by means of a quartz resonator preliminarily calibrated with the aid of interferometer (for $d > 100$ nm) and small-angle *X*-ray diffraction method (for $d < 100$ nm). Electron-beam technique was used to deposit Al_2O_3 layer ~ 10 – 15 nm thick on top of the film. The wide-gap Al_2O_3 semiconductor, on the one hand, protected *PbTe<Pb>* films from oxidation and mechanical damages, and, on the other hand, served as a barrier layer whose contribution to conductivity was small. The electrical conductivity σ and the Hall coefficient R_H were measured by standard *dc* method with an error not exceeding ± 5 %. Indium was used for contacts. The Hall mobility of charge carriers μ_H was calculated by the formula $\mu_H = R_H \cdot \sigma$, and charge carrier concentration was determined on the assumption of one sort of charge carriers as $n = r/(e \cdot R_H)$, where the Hall factor $r = 1$. The measurements of *S* were done by compensation method with respect to copper in the plane of films to an accuracy of ± 3 %. The type of charge carriers was determined by the sign of R_H and *S*. The measurements were conducted on as-prepared samples at room temperature.

Results

The measurements have shown that *PbTe<Pb>* crystal, used as blend for preparation of films, possessed *n*-type conductivity (which is in agreement with the reported data [1]) and had the following electrophysical parameters: $n = 7 \cdot 10^{18}$ cm^{-3}, $S = -180$ μV/K, $\sigma = 140$ Ω^{-1}·cm^{-1}, $\mu_H = 125$ cm^2/V·s. In passing to the thin-film state, *n*-type conductivity was observed only in the films of thickness $d \geq 75$ nm, and at lower thicknesses the conductivity sign changed for the opposite.

One of possible reasons for the appearance of *p*-type conductivity at $d \leq 75$ nm in *PbTe<Pb>* films can be a change in thermodynamic equilibrium conditions in the thin-film state as compared to the bulk crystal and, as a consequence, a change in equilibrium concentration of defects in the film. It can be also supposed that a change in conductivity type with a change in film thickness is determined by the specific features of crystals evaporation. In the course of heating *PbTe* is mainly evaporated in the form of *PbTe* molecules (dissociation energy of *PbTe* molecule 229.2 J/mole is much in excess of sublimation heat 224.6 J/mole), though apart from *PbTe* molecules, small amounts of lead or tellurium atoms can be present in the vapours [18]. Though the content of free *Te* in the vapours is small, during condensation this *Te* excess can be accumulated in the bulk of the deposited film and result in *p*-type conductivity. The impact of this factor will be the greatest with small film thicknesses. One should also take into account the possibility of partial reevaporation of lead excess during deposition on the substrates. In [15], with the use of the same blend material as in the present work, *p*-region was not observed. It is apparently due to the fact that the thickness (30 nm) and material (*EuS*) of protective coating on *PbTe* film differed from these values in the present work and better protected the film from oxidation. In [15, 19] it was established that the type of conductivity can be controlled by changing film thickness *d* and protective layer thickness d_{EuS}, namely the presence of *EuS* with $d_{EuS} > 30$ nm completely protects lead chalcogenide films from oxidation and retains *n*-type conductivity, and with $d_{EuS} < 30$ nm the inversion point of conductivity type is displaced toward the region of smaller thicknesses.

Fig. 1 gives *d*-dependences of *S*, σ, R_H and μ_H of *PbTe<Pb>* thin films obtained in the present work.

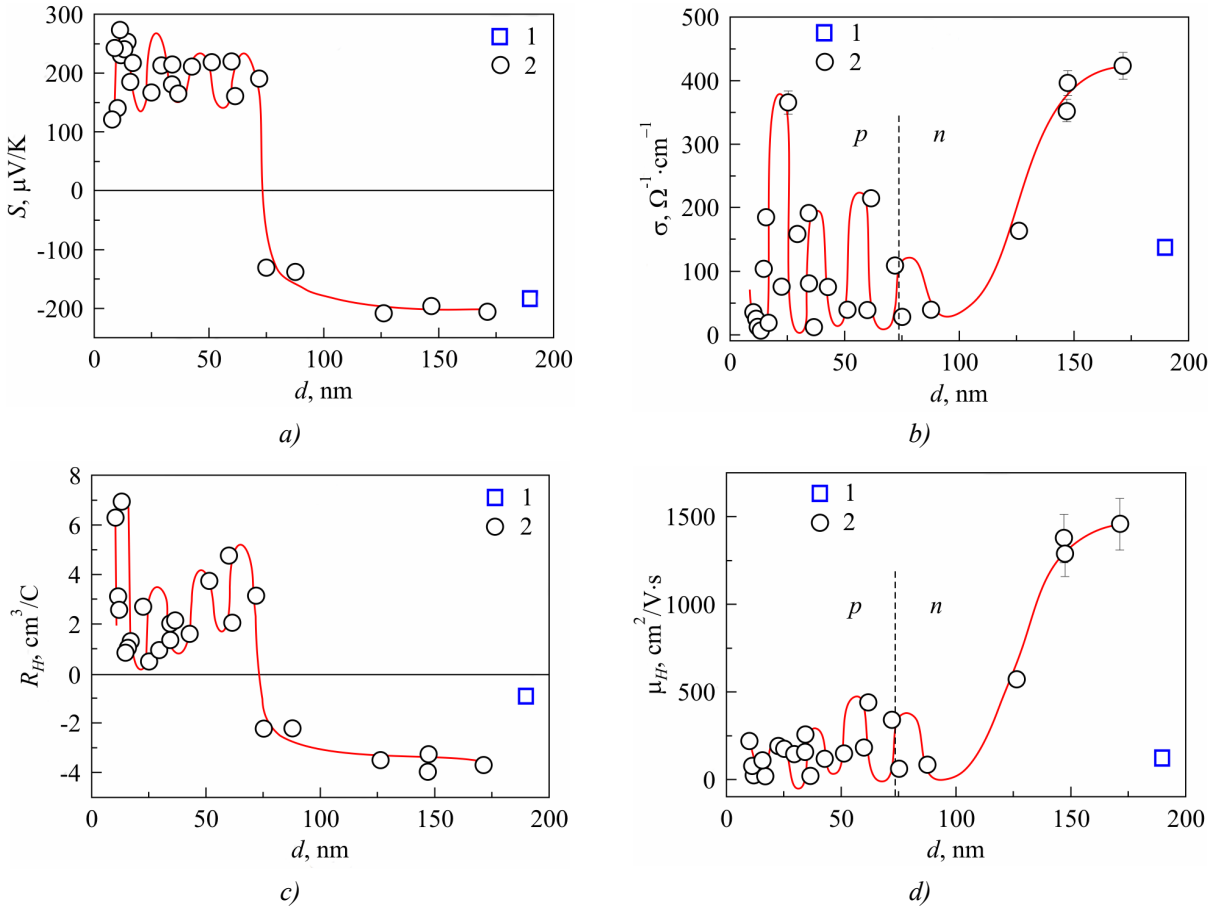

Fig. 1. Thickness dependences of the Seebeck coefficient S (a), electric conductivity σ (b), the Hall coefficient R_H (c) and the Hall mobility μ_H (d): 1 – crystal PbTe<Pb>; 2 – films (001)KCl/PbTe<Pb>/Al_2O_3.

From Fig. 1 it is seen that in the range of thicknesses corresponding to *p*-type conductivity in *PbTe<Pb>* films, there is a non-monotonous behaviour of S, σ, R_H and μ_H versus the thickness, namely the kinetic coefficients oscillate with increase in d. Note that positions of peaks on the dependences $S(d)$ and $R_H(d)$ coincide and correspond to the minima on the curves $\sigma(d)$ and $\mu_H(d)$ (Fig. 1). This, as well as the fact that σ, S and R_H were measured independently, confirms the reality of oscillations existence. The average distance between the peaks or minima (oscillation period) is $\Delta d = (16 \pm 2)$ nm. It should be noted that oscillation amplitudes on the dependences $S(d)$, $\sigma(d)$, $R_H(d)$ and $\mu_H(d)$ are rather large and reach 25 %, 100 %, 80 % and 80 %, respectively. With the increase in film thickness, the amplitude of d-oscillations of the kinetic coefficients is decreased.

We attribute the presence of oscillations on d-dependences of the kinetic properties of *p-PbTe<Pb>* films to the manifestation of QSE. Taking into account that *PbTe<Pb>* film is located between two isolators, namely the substrate (001) *KCl* and Al_2O_3 protective layer, the motion of charge carriers (here holes) in the direction normal to the plane of thin film, is restricted, which results in the quantization of the transverse component of hole quasi-pulse in this direction and the formation of transverse energy subbands. Carrier motion in the plane of a film is not quantized. Therefore, the structure (001) *KCl*/*PbTe<Pb>*/Al_2O_3 can be approximately represented as a rectangular potential quantum well with infinitely high walls. In this case in the effective mass approximation the energy levels are written as [9]:

$$E = \frac{\hbar^2}{2m_z^*}\frac{\pi^2}{d^2}N^2 + \frac{\hbar^2 k_x^2}{2m_x^*} + \frac{\hbar^2 k_y^2}{2m_y^*}, \tag{1}$$

where m_z^* is the effective mass along the direction normal to quantum well, k_x, k_y and m_x^*, m_y^* are the wave vector and effective mass components, respectively, with charge carrier motion parallel to quantum well. With a change of d by the value equal to half de Broglie wavelength, $\lambda_F/2$ (λ_F is de Broglie wavelength on the Fermi level), N subbands will consecutively cross the Fermi level ε_F, which will involve a stepwise change in the density of states. Density of states oscillations lead to transport properties oscillations. The oscillation period values Δd and N can be determined using the following expressions [9]:

$$\Delta d = \frac{\lambda_F}{2} = \frac{h}{\sqrt{8m_z^*\varepsilon_F}}, \tag{2}$$

$$N = \frac{k_F d}{\pi} = \frac{d}{\lambda_F/2} = \frac{d\sqrt{8m_z^*\varepsilon_F}}{h}. \tag{3}$$

It can be readily shown [14] that the thickness d_1 whereby the first subband crosses the Fermi level ($E_1 = \varepsilon_F$) is equal to $d_1 = h\Big/\sqrt{8m_z^*\varepsilon_F} = \Delta d$, i.e. is nothing but oscillation period. So, to determine Δd, there is no need to measure transport properties of films in a wide thickness range, it is enough to determine experimentally the first extremum on d-dependences of properties which will yield the most precise value of Δd.

For the investigated structures (001) *KCl*/*PbTe<Pb>*/Al_2O_3 with regard to known values of the effective mass of holes in *p-PbTe* (the transverse and longitudinal components of the effective mass $m_t^* = 0.022\, m_0$, $m_l^* = 0.31\, m_0$, respectively) [1] and the value ε_F determined by the average concentration of holes ($p = 3.8 \cdot 10^{18}$ cm^{-3}) in the area with *p*-type conductivity ($d < 75$ nm), the oscillation period was calculated from formula (2) that made $\Delta d = (17 \pm 2)$ nm. The resulting value of Δd is in very good agreement with the experimentally determined average distance between the

adjacent maxima on d-dependences of S, R_H, σ and μ_H, as well as with the position of the first extremum in p-region ($d_1 = 14 \pm 1$ nm) (Fig. 1).

Quantum thickness oscillations of the kinetic properties become pronounced at room temperature, though according to theoretical models the oscillations can be distinctly pronounced only at low temperatures [20]. The fact of observation of quantum size effect can point to sufficiently high degree of structural perfection of films and/or the impact of other factor.

In *n-PbTe<Pb>* films (with $d > 75$ nm) higher values of σ and μ_H were obtained than in *PbTe<Pb>* crystal from which the films were prepared, which can testify to a higher structural perfection of films as compared to crystal.

When analyzing the kinetic coefficients behaviour versus the thickness of films with n-type conductivity ($d > 75$ nm) it is seen (Fig. 1) that, with increase in d, the monotonous component of S, σ and μ_H is increased and gradually reaches saturation. Such behaviour of S, σ and μ_H with thickness points to the existence of classical size effect (ClSE).

Conclusions

Vacuum evaporation technique of *PbTe* crystals with lead excess and subsequent condensation on (001) *KCl* substrates was used to prepare *PbTe<Pb>* thin films of thickness $d = 8 – 170$ nm. A change of p-type conductivity for n-type with *PbTe* layer thickness $d \approx 75$ nm was established. It is supposed that conductivity sign inversion can be due to a change in thermodynamic equilibrium conditions in 2D-state as compared to the bulk crystal, peculiarities of evaporation and condensation processes or to insufficient thickness of Al_2O_3 protective coating.

It is shown that in the range of thickness $d \leq 75$ nm there are thickness oscillations of the Seebeck coefficient, the Hall coefficient, electric conductivity and mobility of holes with the period $\Delta d = (16 \pm 2)$ nm, which is related to quantization of hole energy spectrum and manifestation of quantum size effect. Theoretical calculation of quantum oscillation period with the use of a model of infinitely deep rectangular potential well is in good agreement with the experimentally determined Δd value.

Analysis of the monotonous components of transport coefficient dependences on the thickness of films with n-type conductivity ($d \geq 75$ nm) has shown that the values of the Seebeck coefficient, electric conductivity and electron mobility are increased with thickness increase and gradually reach saturation, which is related to manifestation of a classical size effect.

The work was performed with support from the State Foundation for Basic Research (Ukraine) (Grant No. UU 42/006) and US Civilian Research and Development Foundation (CRDF Global, Grant No. UKP-7074-KK-12).

References

1. Yu.I. Ravich, B.A. Yefimova, and I.A. Smirnov, Methods of Research on Semiconductors as Applied to Lead Chalcogenides and *PbS* (Moscow: Nauka, 1968), 384 p.
2. C. Sorrell, S. Sugihara, and J. Nowotny, *Materials for Energy Conversion Devices* (Woodhead Pub. Limited, 2005), 416 p.
3. A.D. LaLonde, Y. Pei, H. Wang, and G.J. Snyder, Lead Telluride Alloy Thermoelectrics, *Materials Today* **14**, 526 – 532 (2011).
4. Y. Pei, H. Wang, and G.J. Snyder, Band Engineering of Thermoelectric Materials, *Advanced Materials* **24**, 6125 – 6135 (2012).

5. M.S. Dresselhaus, Y.-M. Lin, S.B. Cronin, O. Rabin, M.R. Black, and G. Dresselhaus, *Semiconductors and Semimetals: Recent Trends in Thermoelectric Materials Research* (San Diego, CA: Academic Press, 2001), 121 p.
6. L.D. Hicks, T.C. Harman, X. Sun, M.S. Dresselhaus, Experimental Study of the Effect of Quantum-Well Structures on the Thermoelectric Figure of Merit, *Phys. Rev. B* **53**, R10493 – R10496 (1996).
7. T.C. Harman, D.L. Spears, and M.J.J. Manfra, High Thermoelectric Figures of Merit in *PbTe* Quantum Wells, *J. Electron. Mater*. **25**, 1121 – 1127 (1996).
8. T.C. Harman, D.L. Spears, and M.P. Walsh, *PbTe/Te* Superlattice Structures with Enhanced Thermoelectric Figures of Merit, *J. Electron. Mater*. **28,** L1 – L5 (1999).
9. Yu.F. Komnik, *Physics of Metal Films* (Moscow: Atomizdat, 1979), 264 p.
10. E.I. Rogacheva, T.V. Tavrina, O.N. Nashchekina, S.N. Grigorov, K.A. Nasedkin, M.S. Dresselhaus, S.B. Cronin, Quantum Size Effects in *PbSe* Quantum Wells, *Appl. Phys. Lett*. **80**, 2690 – 2693 (2002).
11. E.I. Rogacheva, O.N. Nashchekina, T.V. Tavrina, M. Us, M.S. Dresselhaus, S.B. Cronin, and O. Rabin, Quantum Size Effects in IV-VI Quantum Wells, *Physica E* **17**, 313 – 315 (2003).
12. E.I. Rogacheva, O.N. Nashchekina, Y.O. Vekhov, M.S. Dresselhaus, S.B. Cronin, Effect of Thickness on the Thermoelectric Properties of *PbS* Thin Films, *Thin Solid Films* **423**, 115 – 118 (2002).
13. E.I. Rogacheva, O.S. Vodorez, O.N. Nashchekina, A.Yu. Sipatov, A.G. Fedorov, S.I. Olkhovskaya, and M.S. Dresselhaus, Oscillatory Behavior of Thermoelectric Properties in *p-PbTe* Quantum Wells, *J. Electronic Materials* **39** (9), 2085 – 2091 (2010).
14. E.I. Rogacheva and M.S. Dresselhaus, Quantum Size Effects and Thermoelectric Transport in IV-VI-Based 2*D*-Structures, *Proc. ECT (Odessa, Ukraine, 2007)*, P. 29 – 34.
15. E.I. Rogacheva, O.N. Nashchekina, S.N. Grigorov, M.A. Us, M.S. Dresselhaus, and S.B. Cronin, Oscillatory Behaviour of the Transport Properties in *PbTe* Quantum Wells, *Nanotechnology* **14**, 53 – 59 (2003).
16. E.I. Rogacheva, O.N. Nashchekina, S.I. Olkhovskaya, and M.S. Dresselhaus, Size Effects in *PbSe* Thin Films, *J. Thermoelectricity* **4**, 25 – 32 (2012).
17. E.I. Rogacheva, S.I. Olkhovskaya, A.Yu. Sipatov, and A.G. Fedorov, Size Effect in Lead Selenide Thin Films, *Bulletin of Kharkiv National University, Physics* **914** (13), 115 – 118 (2010).
18. D.M. Freik, Preparation of Films of $A^{IV}B^{VI}$ Compounds (Review), *Instruments and Experimental Techniques* **5**, 7 – 17 (1976).
19. E.I. Rogacheva, I.M. Krivulkin, O.N. Nashchekina, A.Yu. Sipatov, V.V. Volobuev, and M.S. Dresselhaus, Effect of Oxidation on the Thermoelectric Properties of *PbTe* and *PbS* Epitaxial Films, *Applied Physics Letters* **78**, 1661 – 1663 (2001).
20. B.A. Tavger, V.Ya. Demikhovsky, Quantum Size Effects in Semiconductor and Semimetal Films, *Advances in Physical Sciences* **96**, 61 – 86 (1968).

Submitted 20.09.2013.

V.V. Shchennikov, I.V. Korobeynikov, G.V. Vorontsov

Institute of Metal Physics of RAS, Urals Division,
18, S. Kovalevskaya Str., Yekaterinburg, 620990, Russia

ENHANCEMENT OF POWER FACTOR OF THERMOELECTRIC ELEMENT UNDER PRESSURE

The objective of creating a thermoelectric element with improved characteristics using high-pressure impact is considered. The search for p- and n-type thermoelectrics whose thermoelectric parameters are improved under pressure has been performed. The measurements have been carried out using an automated set-up with both diamond and hard alloy anvils. The results obtained for some compounds indicate the possibility of creating a thermoelectric element containing both n- and p-type legs with enhanced characteristics within the same pressure range. The power factor of the element has been estimated for specific values of applied pressure with respect to normal conditions. Various variants of using high pressure in thermoelectric devices have been discussed. The work is partly supported by the Program of the RAS Presidium.
Key words: thermoelement, high pressures, Bi_2Te_3 based compounds, thermoelectric power.

Introduction

The improvement of thermoelectric (TE) parameters, namely, the power factor æ = S^2/ρ and the figure of merit $Z = S^2/(\rho\lambda)$, where S is the thermopower, ρ is the electrical resistivity, λ is the thermal conductivity, is still the primary objective in the research of thermoelectric materials [1, 2]. Bismuth telluride compounds are the most promising among the basic materials for high-performance low-temperature thermoelements. Along with traditional *n*-type Bi_2Te_3-based TE compounds, *p*-type materials of similar structure are also much-in-demand for TE industry [3-6]. The TE parameters of Bi_2Te_3 are usually optimized by "technological factors" such as (I) doping and ions substitution [5-8], (II) variation in mesostructure (nanostructures, superlattices, quantum dots and wires) [3, 9-15], and (III) variation in synthesis conditions [15-18]. A permanent search for alternative medium-temperature TE materials is under way [19]. High pressure-related enhancement of TE properties of *p*-Bi_2Te_3 has been found recently [20, 21].

In the present paper, measurements of thermopower S and electrical resistance R of the ternary and quaternary chalcogenides based on $Bi_2(Sb_2)Te_3$ crystals possessing high initial TE parameters under normal conditions have been performed. The purpose of the work is searching for the possibility to enhance zero-pressure TE parameters (æ, Z) of both *n*- and *p*-type crystals for creation of high-performance thermoelement.

Details of experiment

The $S(P)$ and $R(P)$ dependences were measured by an automated high-pressure setup allowing simultaneous registration of several properties of a microsample at high pressure [22]. Two different anvil cells were employed for pressure generation: one of the Bridgman type, made of synthetic diamonds with

a working diameter $d \sim 0.6$ mm, and another one of toroidal shape, made of tungsten-carbide hard alloy with a working diameter of the central semispherically concave anvils $d \sim 1$ mm [23, 24].

Table 1

TE parameters of samples under normal conditions

No.	Compound	Thermopower S, $\mu V \cdot K^{-1}$	Conductivity σ, $\Omega^{-1} \cdot cm^{-1}$	Power æ, 10^{-5} $W \cdot cm^{-1} \cdot K^{-2}$
2	$Bi_2Te_{2.73}Se_{0.27}$	–227	938	4.83
3	$Bi_2Te_{2.7}Se_{0.3}$	–225	882	4.47
4	$Bi_2Te_{2.82}Se_{0.09}S_{0.09}$	–216	987	4.60
6	$Bi_{0.4}Sb_{1.6}Te_3$	205	1216	5.11
7	$Bi_{0.6}Sb_{1.4}Te_3$	209	998	4.36
8	$Bi_{0.5}Sb_{1.5}Te_3$	220	1037	5.02

A sample of $\sim 200 \times 200 \times 30$ and $200 \times 200 \times 250$ μm^3 was placed into a hole of a container made of the lithographic stone in the Bridgman and toroidal cells, respectively [23, 24]. The pressure values were determined to an accuracy of ~ 10 % from a calibration "force-pressure" curve based on the registration of phase transitions in *Bi*, *PbS*, *PbSe*, *CdSe*, etc. [25]. Applied force was measured by a digital dynamometer with resistive-strain sensors [23]. The anvils were characterized by a high electrical conductivity, and, therefore, were used as electrical contacts to a sample. In the thermopower measurements the upper anvil was heated. The temperature difference along the sample ΔT was determined at the fixed points of the anvils using copper-constantan thermocouples. Calculations of temperature distribution inside the "anvils-container-sample" system were performed in [22, 25]. Several measurement cycles (up to 5) were performed for each sample with pressure increase/decrease.

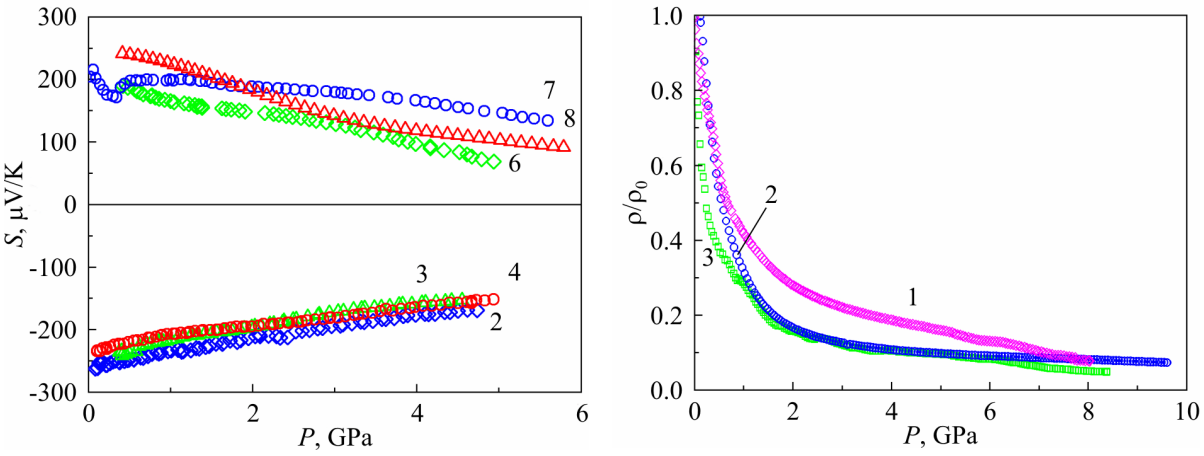

a) *b)*

Fig. 1. Pressure P dependences of the thermoelectric power S (a) and normalized resistance ρ/ρ0 (b) for samples listed in Table 1. Curve numbers correspond to sample numbers [26].

Results of thermoelectric testing and discussion

The ternary and quaternary $Bi_2(Sb_2)Te_3$-based crystals of both *p*- and *n*-type possessing high TE parameters under normal conditions (see Table 1) were taken for investigation. The characteristics of the samples are shown in Table 1. As Bi_2Te_3 and compounds on its basis are known to suffer structural transition at a pressure above 6 – 8 GPa [27, 28], the upper limit of applied pressure was restricted to ~ 5 – 6 GPa for checking the reversibility of TE properties at pressure variation.

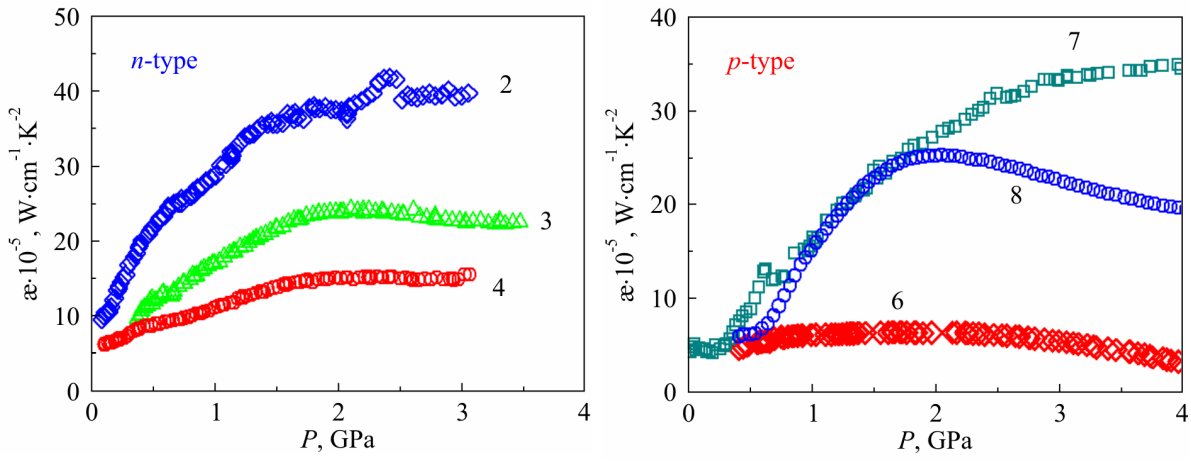

a) *b)*

Fig. 2. Pressure P dependencies of the power factor æ for samples 2, 3, 4 (a) and 6, 7, 8 (b) listed in Table 1. Curve numbers correspond to sample numbers [26].

The gradual decrease in thermopower *S* (in absolute values) with pressure increase was observed both for *n*- and *p*-type samples (Fig. 1). The electrical resistance also drops with pressure increase, as in the case of a binary compound Bi_2Te_3 (Fig. 1) [20]. The calculated values of power factor obtained using the experimental *S*(*P*) and *R*(*P*) data for *p*-type compounds have a non-monotonic dependence on *P* with a maximum in the region of ~ 2 to 4 GPa (Fig. 2), whereas for *n*-type compounds they reach maximal values at ~ 2 GPa and then remain unchanged with pressure increase (see Fig. 2). The non-monotonic dependence of æ on *P* is obviously due to pressure-driven electron structure variation [20, 27-29]. With regard to experimental results, it seems possible to choose the pairs of *n*- and *p*-type compounds having maximal values of æ at the same pressure range, e.g. samples No. 2 – 4 (*n*-type) and sample No. 7 (*p*-type) at ~ 3 – 5 GPa, or samples No. 2 – 4 (*n*-type) and sample No. 8 (*p*-type) at ~ 2 GPa, and samples No. 2 – 4 (*n*-type) and sample No. 6 (*p*-type) at ~ 2 – 3.5 GPa. The highest values of æ are achieved for the pair "sample 3 or 4 (*n*-type) – sample 7 (*p*-type)" near *P* ~ 4 GPa (see Fig. 2). Decompression cycles showed the reversibility of pressure-induced æ-enhancement effect. Thus, manufacture of high-performance TE element containing both *p*- and *n*-type legs seems to be feasible due to retention of pressure ~ 2 to 4 GPa in small devices or strained films. A variant of autonomous synthetic diamond chamber used in magnetic field measurements [21] may be a suitable device, as synthetic diamonds possess both excellent thermal conductivity and high electrical conductivity, to provide the input/output of thermal flows as well as electrical connection in TE-element.

The observed enhancement of power factor under pressure is related to a moderate decrease in the absolute value of *S* and a more rapid drop of electrical resistance. In a binary compound Bi_2Te_3 the semiconductor gap E_g = 0.17 eV decreases with pressure increase which explains the behavior of *S* and

R. In the ternary and quaternary $Bi_2(Sb_2)Te_3$-based chalcogenides the value of E_g is somewhat modified by chemical substitution in the lattice, so the "optimal" semiconductor gap [21], hence the highest TE parameters, are achieved at different values of *P* (Fig. 2).

From the general expression for the electrical conductivity σ, and thermoEMF S:$\sigma = \int\sigma(E)(-\partial f/\partial E)dE$ and $S = (k/|e|)\int[(E - E_F)/(kT)][\sigma(E)/\sigma](-\partial f/\partial E)dE$ (where f is the distribution function, E_F is the Fermi energy, E is the electron energy, k is Boltzmann's constant, and e is the electron charge), the equation for the Seebeck coefficient of a semiconductor with one additional hole band may be obtained as follows [20]:

$$\frac{S}{k/|e|} = \left\{ \sum_i \frac{\sigma_{pi} - \sigma_{ni}}{\sigma} \times (r+2) + \sum_i \frac{(\sigma_{pi} - \sigma_{ni})}{\sigma} \frac{E_g}{2kT} + \frac{3}{4} \ln \frac{m_p^*}{m_n^*} + \frac{\Delta E_v}{kT} \frac{\sigma_{p2}}{\sigma} \right\}, \quad (1)$$

where $\sigma = \Sigma(\sigma_{ni} + \sigma_{pi})$ is the total conductivity and *r* is the scattering parameter of carriers. The index *i* corresponds to the electron and the hole bands and to the additional hole band ($i = 2$). According to recent calculations [30], the topmost valence band in Bi_2Te_3 lies along the $Z - U$ direction in the Brillouin zone and exceeds the second band in energy by $\Delta E_v \approx 3.8$ meV ($\Delta E_v \approx 40$ meV in [31]). The second valence band is important in achieving high values of TE properties both in a binary Bi_2Te_3 compound [20, 29] and in Bi_2Te_3-based ternary and quaternary chalcogenides. The energy gap between the hole bands ΔE_v increases with pressure ($dE_v/dP \sim +30$ meV/GPa [32]), whereas the forbidden gap is reduced at a rate of 20/60 meV/GPa below/above $P \sim 3$ GPa [28]. Since pressure application leads to narrowing of the forbidden gap, and therefore, to the increase in the carrier concentration, it eventually brings about the intrinsic conductivity increase. The above equation makes it possible to explain the complex behavior of *S* versus *P* for these compounds.

It is also interesting to evaluate the behavior of figure of merit *ZT* under pressure (where *T* is temperature). Under normal conditions for *n*- and *p*-type materials the figure of merit *ZT* is ~ 0.9. The experimental data of [33-35] on thermal conductivity variation at high pressures 1.6 – 10 GPa for Bi_2Te_3 and Sb_2Te_3 compounds show the maximal increase of thermal conductivity λ by a factor of 2 under a pressure of 4 GPa. Thus, the attainable figure of merit values for the samples under study may be roughly estimated to be $ZT \approx 3$. This value is close to that of the advanced bulk $Bi_2(Sb_2)Te_3$ based thermoelectrics [1-3]. This value may be overestimated to a certain extent due to unknown contribution of electron component of thermal conductivity in the samples under study, which ought to rise due to a strong decrease in resistivity.

High-pressure thermoelement testing

In the framework of this work the high-pressure thermoelement has been created and tested. The schematic of this device represents a miniature high-pressure chamber with insulating boron nitride anvils of the Bridgman type (Fig. 3). *p*-type and *n*-type pellets (legs) of the element made of samples No. 8 and No. 2 (Table 1) were placed into a container similar to the above described experimental setups (Fig. 3). The diameter of working tips of the anvils was 2.0 mm. Thin bronze tapes were used to provide the electrical contacts to each thermoelement leg and to electrical outputs of the entire thermoelement. According to experimental data represented in Fig. 2 the highest TE power factor for this thermoelement is achieved at a pressure of ~ 2 – 3 GPa. The device has a hold-down-nut which permits high pressure retention after thermoelement unloading.

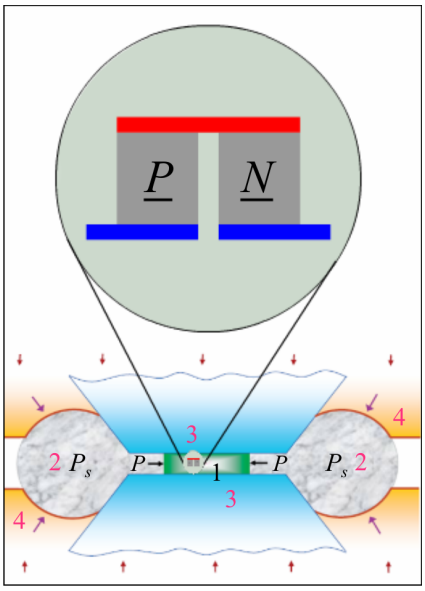

Fig. 3. Schematic of the high-pressure thermoelement: 1 – thermoelement, 2 – container, 3 – anvils, 4 – plungers.

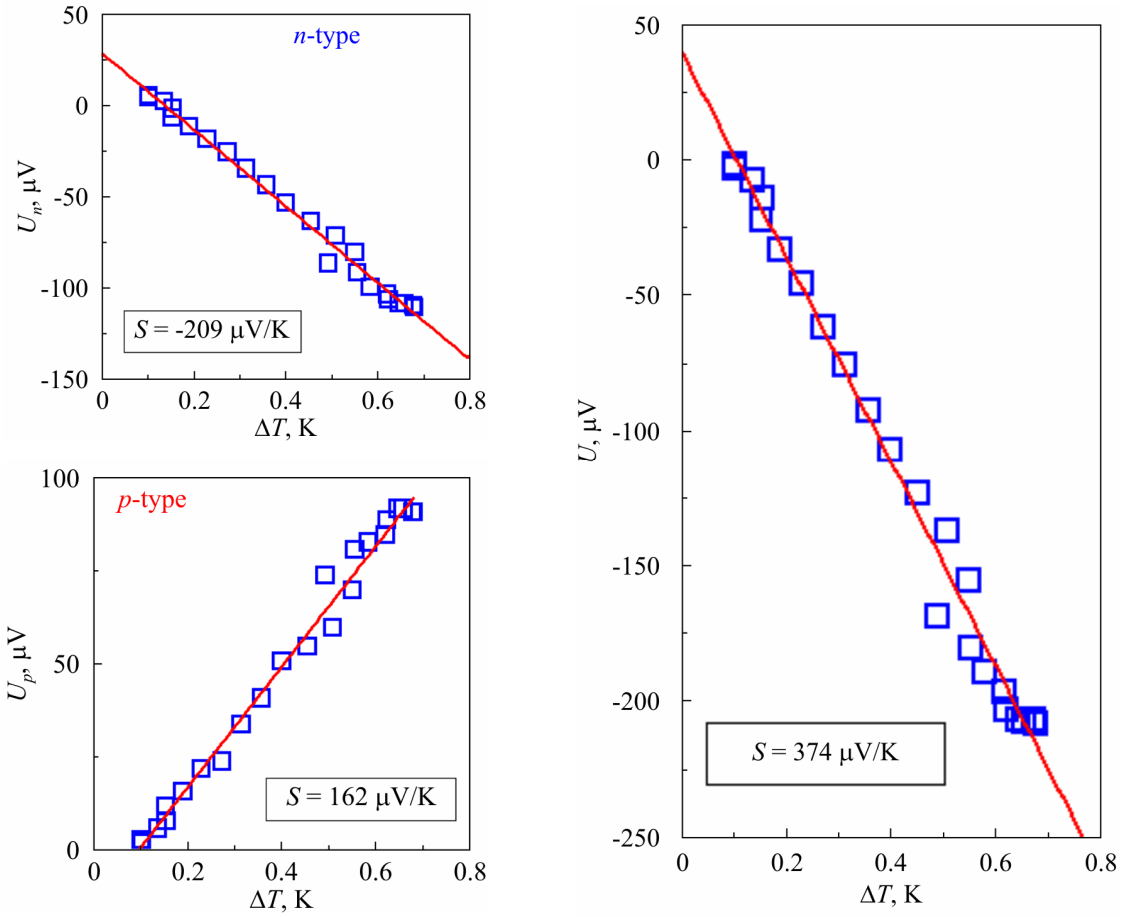

a) *b)*

Fig. 4. Experimental data of the thermoelectric measurements for each leg (a) and for the entire thermoelement (b) at a pressure of ~ 2.5 GPa. The plots represent experimental dependences of TE signal on the temperature difference (marked as squares). The Seebeck coefficient S was determined from the linear slope of the dependences (straight lines).

High pressure ~ 2.5 GPa was generated in the TE device by using a hydraulic press, following which the pressure was fixed for TE measurements. Results of TE measurements allowed estimating the TE power factor of high-pressure thermoelement (Fig. 4). Using the data on the pressure dependences of electrical resistance (not shown) and thermoelectric power (Fig. 4), the $\sim 3.4 \pm 0.9$-fold increase in thermoelectric power factor was observed for each leg and for the entire thermoelement. To the authors' knowledge, this is the first testing of the entire thermoelement at high pressures up to ~ 2.5 GPa.

Conclusion

To summarize, pressure application was established to lead to a significant improvement in the TE figure of merit of *p*- and *n*-samples of the ternary and quaternary $Bi_2(Sb_2)Te_3$-based chalcogenides possessing high initial TE parameters under normal conditions. The effect exceeds the values reported previously [36].

The working model of thermoelement has been created and tested at a pressure of ~ 2.5 GPa. The $\sim 3.4 \pm 0.9$-fold increase in thermoelectric power has been achieved for each leg and for the entire thermoelement. There are several ways for high pressure retention under normal conditions, including: I) miniature synthetic diamond (boron nitride) anvils; II) retention of pressure in strained films; III) generation of pressure due to creation of thermal gradient by using materials with high temperature expansion coefficient (water at low temperatures, some polymers, etc.).

It should be noted that a search for high TE parameters is usually restricted to normal pressure. However, the best parameters obtained at present for the known thermoelectrics are by no means related to normal temperature. Thus, for some Bi_2Te_3-based compounds the optimal temperature range lies below room temperatures, whereas for *PbTe*-based compounds and *SiGe* alloys the optimal values of TE parameters are achieved at much higher temperatures, namely ~ 600 – 1000 K. The variation of chemical composition of these materials does not cause a shift of the optimal temperature range to normal temperature. Using this analogy, one may suggest that at least for the above mentioned materials the optimal pressure range for the highest TE parameters may also lie far from the normal conditions (at atmospheric *P*), and so, from this point of view the sufficient increase in power factor under pressure obtained in the present work for a thermoelement comes as no surprise.

Acknowledgments. The work was done within RAS Program (Project no. 01.2.006 13394), by UD RAS as part of Program ''Matter at high energy densities'' of the Presidium of RAS (project 12-P-2-1004), by the Ministry of Education and Science of the Russian Federation (Contract 14.518.11.7020), and by the Oriented Basic Research Project of the Ural Branch of the Russian Academy of Sciences.

References

1. F.J. DiSalvo, Thermoelectric Cooling and Power Generation, *Science* **285**, 703 – 706(1999).
2. T.M. Tritt, Holey and Unholey Semiconductors, *Science* **283**, 804 – 805(1999).
3. R. Venkatasubramanian, E. Siivola, T. Colpitts, and B. O'Quinn, Thin-Film Thermoelectric Devices with High Room-Temperature Figures of Merit, *Nature* **413**, 597 – 602 (2001).
4. X.F. Tang, W.J. Xie, H. Li, W.Y. Zhao, Q.J. Zhang, and M. Niino, Preparation and Thermoelectric Transport Properties of High-Performance *p*-type Bi_2Te_3 with Layered Nanostructure, *Appl. Phys. Lett*. **90**, 012102 (2007).
5. D.-Y. Chung, T. Hogan, P. Brazis, M. Rocci-Lane, C. Kannewurf, M. Bastea, C. Uher, and

M.G. Kanatzidis, $CsBi_4Te_6$: A High-Performance Thermoelectric Material for Low-Temperature Applications, *Science* **287**, 1024 – 1027 (2000).

6. D.A. Polvani, J.F. Meng, N.V.C. Shekar, J. Sharp, J.V. Badding, Large Improvement in Thermoelectric Properties in Pressure-Tuned *p*-type $Sb_{1.5}Bi_{0.5}Te_3$, *Chem. Mater*. **13**, 2068 – 2071 (2001).
7. G.F. Wang, T. Cagin, Investigation of Effective Mass of Carriers in $Bi_2Te_3Sb_2Te_3$ Superlattices via Electronic Structure Studies on its Component Crystals, *Appl. Phys. Lett*. **89**, 152101 (2006).
8. V.A. Kutasov, L.N. Luk'yanova, and P.P. Konstantinov, An Analysis of the Thermoelectric Efficiency of *n*-$(Bi, Sb)_2(Te, Se, S)_3$ Solid Solutions within an Isotropic Scattering Model, Phys. Solid State **42**, 2039 – 2046 (2000).
9. M.P. Singh, C.M. Bhandari, Thermoelectric Properties of Bismuth Telluride Quantum Wires, *Solid State Commun*. **127**, 649 – 654 (2003).
10. X.B. Zhao, X.H. Ji, Y.H. Zhang, T.J. Zhu, J.P. Tu, and X.B. Zhang, Bismuth Telluride Nanotubes and the Effects on the Thermoelectric Properties of Nanotube-Containing Nanocomposites, *Appl. Phys. Lett.* **86**, 062111 (2005).
11. J.H. Zhou, C.J. Jin, J.H. Seol, X.G. Li, and L. Shi, Thermoelectric Properties of Individual Electrodeposited Bismuth Telluride Nanowires, *Appl. Phys. Lett*. **87**, 133109 (2005).
12. S. Lee, P. Allmen, Tight-Binding Modeling of Thermoelectric Properties of Bismuth Telluride, *Appl. Phys. Lett*. **88**, 022107 (2006).
13. G.E. Bulman, E. Siivola, B. Shen, and R. Venkatasubramanian, Large External ΔT and Cooling Power Densities in Thin-Film Bi_2Te_3-Superlattice Thermoelectric Cooling Devices, *Appl. Phys. Lett.* **89**, 122117 (2006).
14. B. Yang, Z.H. Han, Temperature-Dependent Thermal Conductivity of Nanorod-Based Nanofluids, *Appl. Phys. Lett*. **89**, 083111 (2006).
15. H.L. Ni, X.B. Zhao, T.J. Zhu, X.H. J, and J.P. Tu, Synthesis and Thermoelectric Properties of Bi_2Te_3 Based Nanocomposites, *J. Alloys Compd*. **397**, 317 – 321 (2005).
16. O. Yamashita, S. Tomiyoshi, and K.J. Makita, Bismuth Telluride Compounds with High Thermoelectric Figures of Merit, *Appl. Phys*. **93**, 368 – 374 (2003).
17. J. Walachova, R. Zeipl, J. Zelinka, V. Malina, M. Pavelka, M. Jelinek, V. Studnicka, and P. Lostak, High Room-Temperature Figure of Merit of Thin Layers Prepared by Laser Ablation from Bi_2Te_3 Target, *Appl. Phys. Lett*. **87**, 081902 (2005).
18. T.C. Su, P.W. Zhu, H.A. Ma, G.Z. Ren, L.X. Chen, W.L. Guo, Y. Iami, and X.P. Jia, Electrical Transport and High Thermoelectric Properties of *PbTe* Doped with Bi_2Te_3 Prepared by HPHT, *Solid State Commun*. **138**, 580 – 584 (2006).
19. N.D. Lowhorn, T.M. Tritt, E.E. Abbott, and J.W. Kolis, Enhancement of the Power Factor of the Transition Metal Pentatelluride $HfTe_5$ by Rare-Earth Doping, *Appl. Phys. Lett.* **88**, 022101 (2006).
20. S.V. Ovsyannikov, V.V. Shchennikov, G.V. Vorontsov, A.Y. Manakov, A.Y. Likhacheva, and V.A. Kulbachinskii, Giant Improvement of Thermoelectric Power Factor of Bi_2Te_3 under Pressure, *J. Appl. Phys*. **104**, 53713 (2008).
21. S.V. Ovsyannikov, V.V. Shchennikov, High-Pressure Routes in the Thermoelectricity or How one Can Improve a Performance of Thermoelectrics., *Chem Mater* **22**, 635 – 647 (2010).
22. V.V. Shchennikov, S.V. Ovsyannikov, A.Y. Derevskov, and V.V. Shchennikov Jr, Automated Portable High-Pressure Setup for Study of Phase Transitions in Solids, *J. Phys. Chem. Solids* **67**, 2203 – 2209 (2006).
23. S.V. Ovsyannikov, V.V. Shchennikov, Observation of a New High-Pressure Semimetal Phase of *GaAs* from Pressure Dependence of the Thermopower, *J. Phys.: Condens. Matter* **18**, L551 (2006).

24. S.V. Ovsyannikov, V.V. Shchennikov, Pressure-Tuned Colossal Improvement of Thermoelectric Efficiency of *PbTe*, *Appl. Phys. Lett*. **90**, 122103 (2007).
25. V.V. Shchennikov, S.V. Ovsyannikov, and A.V. Bazhenov, A Composite High-Pressure Cell with Sintered Diamond Insets for Study of Thermoelectric and Thermomagnetic Properties in a Range up to 30 GPa: Application to *Pr* and *PbTe*, *J. Phys. Chem. Solids* **69**, 2315 – 324 (2008).
26. V.V. Shchennikov, I.V. Korobeynikov, G.V. Vorontsov, L.N. Luk'yanova, and V.A. Kutasov, Thermoelectric Properties of Ternary and Quaternary Bi_2Te_3-Based Crystals under High Pressure, Proceedings of XIII International Workshop "Thermoelectrics and Their Applications" (Russia, Saint-Petersburg, Ioffe Institute, November 13 – 14, 2013), 162 – 167.
27. S.V. Ovsyannikov, Yu.A. Grigor'eva, G.V. Vorontsov, L.N. Luk'yanova, V.A. Kutasov, and V.V. Shchennikov, Thermoelectric Properties of p-$Bi_{2-x}Sb_xTe_3$ Solid Solutions under Pressure, *Phys. Solid State* **54**, 261 – 266 (2012).
28. B.M. Goltsman, B.A. Kudinov, and I.A. Smirnov, *Thermoelectric Semiconductor Materials Based on* Bi_2Te_3 (Moscow, Nauka, 1972), 320 p.
29. B.M. Askerov, *Electron Transport Phenomena in Semiconductors* (Singapore, World Scientific, 1994), 416 p.
30. S.J. Youn, A.J. Freeman, First-Principles Electronic Structure and its Relation to Thermoelectric Properties of Bi_2Te_3, *Phys. Rev. B* **63**, 085112 (2001).
31. T.J. Scheidemantel, C. Ambrosch-Draxl, T. Thonhauser, J.V. Badding, and J.O. Sofo, Transport Coefficients from First-Principles Calculations, *Phys. Rev. B* **68**, 125210 (2003).
32. V.A. Kulbachinskii, N.E. Klokova, J. Gorak, P. Lostjak, S.A. Azou, and G.A. Mironova, Influence of Pressure on the Energy Spectrum of p-type Bi_2Te_3, *Fiz. Tverd. Tela* **31**, 205 – 208 (1989).
33. A.A. Averkin, Z.Z. Zhaparov, and L.S. Stilbans, Influence of Hydrostatic Pressure on Thermal Conductivity of Semiconducting Materials, *Sov. Phys. Semicond*. **5**, 1954 – 1956 (1972).
34. N. Sakai, T. Kajiwara, K. Takemura, S. Minomura, and Y. Fujii, Pressure-Induced Phase Transition in Sb_2Te_3, *Solid State Commun*. **40**, 1045 – 1047 (1981).
35. M.K. Jacobsen, S.V. Sinogeikin, R.S. Kumar, and A.L. Cornelius, High Pressure Transport Characteristics of Bi_2Te_3, Sb_2Te_3, and $BiSbTe_3$, *J. Phys. Chem. Solids* **73**, 1154 – 1158 (2010).
36. L.G. Khvostantsev, A.I. Orlov, N.K. Abrikosov, T.E. Svechnikova, and S.N. Chizhevskaya, Thermoelectric Properties and Phase Transitions in Bi_2Te_3 Under Hydrostatic Pressure up to 9 GPa and Temperature up to 300 °C, *Phys. Status Solidi A* **71**, 49 – 53 (1982).

Submitted 18.05.2013.

L.I. Anatychuk[1], Jenn-Dong Hwang[2], V.V. Lysko[1], A.V. Prybyla[1]

[1]Institute of Thermoelectricity of the NAS and MES of Ukraine,
1, Nauky Str., Chernivtsi, 58029, Ukraine;
[2]Industrial Technology Research Institute, MCL/ITRI,
Bldg. 77, No. 195 Sec. 4 Chung Hsing Rd., Chutung, Hsinchu, Taiwan

THERMOELECTRIC HEAT RECUPERATORS FOR CEMENT KILNS

In the present work the results of the research aimed at the studies of the possibility of use of thermoelectric energy conversion for recuperation of the heat radiated by the preheated rotating surfaces of the cement kilns are presented. The temperature specifications of the kilns functioning remain unchanged, though. To reach this, the degree of emissivity of the kiln surface should be changed. The dependences were obtained of the maximum efficiency and temperature of the thermoelectric generator hot heat exchanger on the emissivity of the cement kiln surface. Both maximum efficiency of a thermoelectric generator and its designed capacity were estimated.
Key words: recuperation, cement kiln, thermoelectric module.

Introduction

General characterization of the problem. Nearly all equipment for the industrial technological processes, such as heat engines (turbines, combustion engines etc.) scatter huge amounts of waste heat during their operation, the said waste heat being a part and parcel of heat pollution of the environment [1]. Therefore, the elimination of waste heat as well as its utilization in order to obtain electric energy is a problem of the exceptional significance. The temperatures of such waste heat differ considerably and lie approximately in the range from 50 to 700 °C. For most cases within this range of temperatures, especially for those below 400 °C, it is unreasonable to apply heat engines. As the analysis has shown, the most favourable for heat recuperation at such temperatures is the thermoelectric method of direct thermal into electric energy conversion [2-4]. Moreover, the characteristics of heat sources (their dimensions, operation modes, heat carriers) are rather various. Of particular interest is here the problem of recuperation of the heat radiated from the cement kilns rotating surfaces. For conditions like those the most suitable is the thermoelectric method of energy conversion as thermoelectric converters are easy to adapt to various thermal energy sources [5]. The fact that such converters (modules) have been designed recently whose specific cost equals to 0.5 – 2 $/W thus ensuring the profitability of thermoelectric heat recuperators is also of great importance.

Analysis of the literature. Thermoelectric devices for combustion engines waste heat recuperation [6], gas rolling mill furnaces [7] and gas-pumping aggregate turbines [8]. For all cases considered a thermoelectric generator (its hot heat exchanging surface) is in contact with the heated heat-release surface. Such a construction, though, is inappropriate when the heat from the rotating cement kiln is used. Effective in this case is the utilization of heat radiation off these heated surfaces [9]. The fact that the presence of a thermoelectric generator causes changes in the temperature mode of the kiln itself, which is but undesirable for the technological process of cement production, is an

obstacle to the said thermoelectric generators being used for cement kilns heat recuperation.

The purpose of the present work is the analysis of the possibility of employment of the thermoelectric energy conversion for recuperation of heat radiated by the rotating surfaces of cement kilns without changing temperature specifications of the said kilns operation.

Problem definition

The cement kiln appearance and diagrammatic view are presented in Figs. 1 and 2.

Fig. 1. A cement kiln appearance [10].

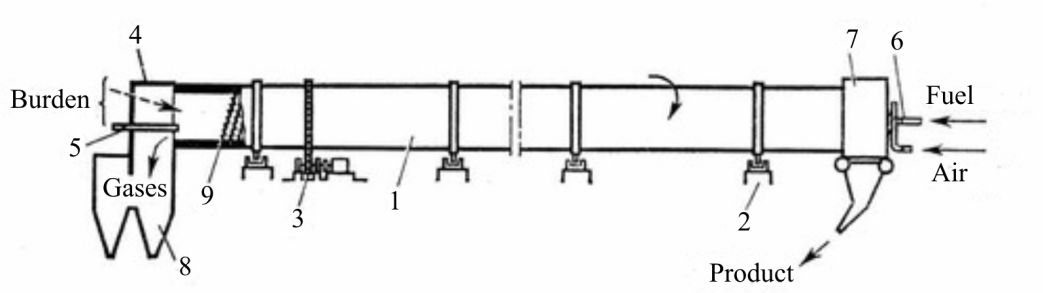

Fig. 2. A cement kiln diagrammatic view [11]. 1 – metallic cylinder, 2 – bearing rollers, 3 – electric motor with the reducer and gear, 4 – burden load cap, 5 – burden load injector, 6 – fuel input injectors, 7 – hot cap, 8 –dusting system, 9 – heat exchangers.

To reach the purpose of the present work, two physical models of the cement kiln heat exchange were used. The first one considers the kiln heat exchange without a thermoelectric generator (Fig.3). It was necessary for heat irradiation estimation in the absence of an external heat consumer. In the second model the thermoelectric generator was taken into account that introduces changes into both temperature and thermal modes of the cement kiln. The estimation was also performed for the increase in emissivity of the kiln surface required to preserve the unchanged heat irradiation from the kiln.

A cement kiln heat exchange without a thermoelectric generator

The cement kiln model under study is a cylinder 1 with the diameter of d = 4.8 m and the length of L = 76 m, the temperature of which is constant and equals T_1 = 300 °C (Fig. 3).

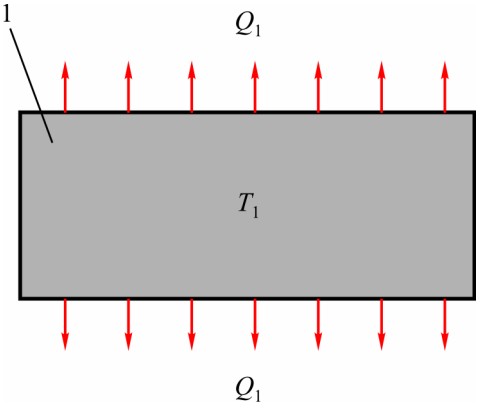

Fig. 3. A cement kiln model without a thermoelectric generator.

The kiln temperature is set due to the balance of heat released inside it and heat transfer into the environment. At the same time heat transfer into the environment takes place by way of free convection and radiation. The total heat flux off the lateral surface of such cylinder can be written in the form of

$$Q_1 = Q_{conv} + Q_{rad}, \tag{1}$$

where: Q_{conv} is the convections heat flux, Q_{rad} heat flux radiated from kiln surface.

The heat flux radiated from kiln surface can be determined proceeding from the Stefan-Boltzmann law

$$Q_{rad} = \varepsilon_1 \sigma S\left(T_1^4 - T_0^4\right), \tag{2}$$

where: ε_1 is the surface emissivity, $\sigma = 5.67 \cdot 10^{-8}$ W·m^{-2}·K^{-4} is the Stefan-Boltzmann constant, $S = \pi dL$ is the kiln lateral surface area, T_0 is the ambient temperature.

To estimate a convection component, it is necessary to define the Nusselt number which is a function of the Prandtl and Grashof numbers under free convection and depends but slightly on the shape of the body [12, 13].

$$\frac{\alpha l}{\kappa} = f\left(\frac{\nu}{a};\ \frac{gl^3}{\nu^2}\beta\Delta t;\ \text{shape of body}\right). \tag{3}$$

Here β [1/degree] is the medium expansiveness; Δt is thermal head;

$$\frac{\nu}{a} = Pr,\ \frac{gl^3}{\nu^2}\beta\Delta t = Gr. \tag{4}$$

Thermal resistance in gases is concentrated in the narrow wall layer where molecular friction prevails. The system of equations will thus contain only four independent variables instead of five (a, $g\rho\beta\Delta t$, μ, l) ρ – density, μ – dynamic viscosity, and give only one key criterion:

$$Pr\ Gr = \frac{gl^3}{a\nu}\beta\Delta t. \tag{5}$$

The diameter of the horizontal pipe is taken to be its linear dimension l. Calculation formulae have the form of:

a) at $10^{-3} < Pr\,Gr < 5\cdot10^{2}$

$$\alpha = A_1\left(\frac{\Delta t}{l^5}\right)^{1/3}. \tag{6}$$

b) at $5\cdot10^{2} < Pr\,Gr < 2\cdot10^{7}$

$$\alpha = A_2\left(\frac{\Delta t}{l}\right)^{1/4}. \tag{7}$$

c) $Pr\,Gr > 2\cdot10^{7}$

$$\alpha = A_3\Delta t^{1/3}. \tag{8}$$

For the air at the average temperature being $T_{av} = \frac{1}{2}(T_1 + T_0)$ the values of coefficients $A_{1\text{-}3}$ are the following: $A_1 = 0.28$, $A_2 = 1.07$, $A_3 = 1.05$.

For the case considered here $Pr\,Gr = 1.3\cdot10^{12}$ and, correspondingly, $\alpha = 6.8$ W/(m^2·K). Therefore, the total heat flux Q_1 from the kiln lateral surface will be equal to 5.07 MW, 2.1 MW due to convection and 2.97 MW due to radiation included.

A cement kiln heat exchange with a thermoelectric generator placed around its lateral surface

When a set of thermoelectric generators is placed around the lateral surface of the kiln (Fig. 2) whose hot side temperature should be higher than that of the environment, the heat flux off the kiln surface will decrease which is impermissible. Therefore, to ensure the initial heat removal, it is necessary to increase the kiln emissivity.

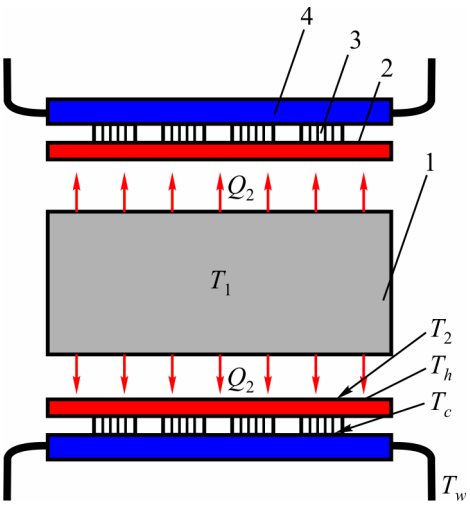

Fig. 4. A cement kiln model with a thermoelectric generator. 1 – a part of the kiln surface, 2 –a hot heat exchanger, 3 –thermoelectric modules, 4 – a cold water heat exchanger.

The total heat flux off the lateral surface of the kiln can be written in the form of

$$Q_2 = \varepsilon_1'\varepsilon_2\sigma S\left(T_1^4 - T_2^4\right) + Q'_{conv}, \tag{9}$$

Heat transfer due to convection Q'_{conv} can here be considered according to the formulae for thermal conductivity for a solid wall by way of introducing the equivalent air space heat conductivity factor.

The equivalent air space heat conductivity factor when heat emission due to radiation from one wall to another is neglected can be determined from the formula

$$\kappa_{eq} = \varepsilon_{conv}\kappa. \tag{10}$$

where κ is heat conductivity factor of the medium filling the air space (κ = 0.0355 W/(m·K) for the air average temperature of 150 °C); $\varepsilon_{conv} = f\,(Pr\,Gr)$ is the factor considering convection impact.

Calculation formulae for the convection factor are:

a) at $10^4 < Pr\,Gr\left(\frac{L_1}{L_2}\right)^k\left(\frac{d}{\delta}\right)^n < 10^7$

$$\varepsilon_{conv}=0.062\left[Pr\,Gr\left(\frac{L_1}{L_2}\right)^k\left(\frac{d}{\delta}\right)^n\right]^{1/3} \tag{11}$$

b) at $10^7 < Pr\,Gr\left(\frac{L_1}{L_2}\right)^k\left(\frac{d}{\delta}\right)^n < 10^{10}$

$$\varepsilon_{conv}=0.22\left[Pr\,Gr\left(\frac{L_1}{L_2}\right)^k\left(\frac{d}{\delta}\right)^n\right]^{1/4} \tag{12}$$

where: δ is the layer thickness, L_1/L_2 is the relation between the convection flux path length from the lower boundary of the heater to the cooler and the height of this path, d to the heater diameter. For the inclined cylindrical layer $L_1/L_2 = 1$, $k = 3$, $n = 0$. For the horizontal cylindrical layer $\frac{L_1}{L_2}=\frac{\pi r+\delta}{d+\delta}$, $k = 3$, $n = 0$.

At the value of the combination $Pr\,Gr\left(\frac{L_1}{L_2}\right)^k\left(\frac{d}{\delta}\right)^n < 10^3$ the impact of convection inside the gap is actually absent and only thermal conductivity is considered in calculations.

While defining the criteria the average temperature is taken as the determinant one

$$T_{av} = \frac{1}{2}\left(T_1 + T_0\right), \tag{13}$$

and the layer thickness δ (5 cm) is taken as the determinant, respectively.

For this case the value of $Pr\,Gr\left(\frac{L_1}{L_2}\right)^k\left(\frac{d}{\delta}\right)^n = 7.6\cdot 10^5$, and $\varepsilon_{conv} = 2.62$. Correspondingly, κ_{eq} = 0.093 W/(m·K), whereas the heat flux due to convection from the kiln lateral surface to the hot heat exchanger of the thermoelectric generator will surely depend on the temperature T_2 thus set.

The effect of the internal cylinder rotation on the heat emission in the problems like this, the Couette-Taylor problems, is considered via dimensionless parameters, namely, the Reynolds number Re_h which characterizes the forced circular flow, or the Taylor number. A modified Taylor number is highly convenient to use for these purposes [14].

$$Ta_m = \frac{\Omega^2 d^2\delta^3}{2\nu\left(d+\delta\right)}\left(\frac{1697}{\pi^4}C\right), \tag{14}$$

$$C = 0.0571\left(1-0.652\frac{2\delta}{d}\right)+0.00056\left(1-0.652\frac{2\delta}{d}\right)^{-1} \tag{15}$$

where Ω is the angular rotational velocity.

Before the secondary flows appear ($Ta_m < 1700$), the Nusselt number Nu^* is defined by the equation

$$Nu^* = 2 \tag{16}$$

and does not depend on either gas properties or the size and rotation velocity of the cylinder.

At the emergence of macro eddy secondary flows the Taylor number should be considered. Within the range of $Ta_m \approx 1700 \ldots 1 \cdot 10^5$ the heat transfer factor for the air is described by the empiric formula

$$Nu^* = 0.128 Ta_m^{0.367} \tag{17}$$

Within the range of $Ta_m \approx 10^4 \ldots 2 \cdot 10^8$

$$Nu^* = 0.42 Ta_m^{0.25} Pr^{0.25} \tag{18}$$

Within the range of $Ta_m \approx 10^7 \ldots 2 \cdot 10^9$

$$Nu^* = 0.28 Ta_m^{0.285}. \tag{19}$$

Therefore, when the kiln rotation is taken into consideration, the heat emission due to convection increases up to 2.2 times.

To find a new emissivity value for the kiln lateral surface ε'_1, required for the preset heat sink, it is necessary to obtain the balance between Q_1 and Q_2. In so doing, the temperature of the hot heat exchanger becomes the function of ε'_1. According to calculations, the value of hot heat exchanger temperature T_2 when the surface of the kiln is covered with a special paint with the emissivity from 0.80 to 0.99 is in the range from 80 to 172 °C (Fig. 5.).

The dependence of the thermopile efficiency on ε'_1 derived from the experimental dependences of η on the temperature difference $(T_h - T_c)$ is presented in Fig. 6.

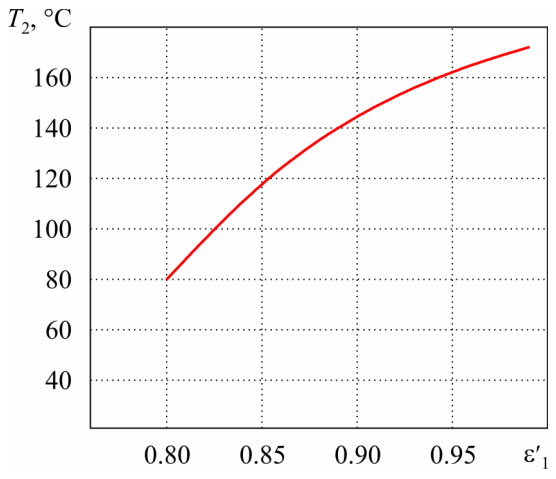

Fig. 5. Temperature of the hot heat exchanger as a function of kiln emissivity.

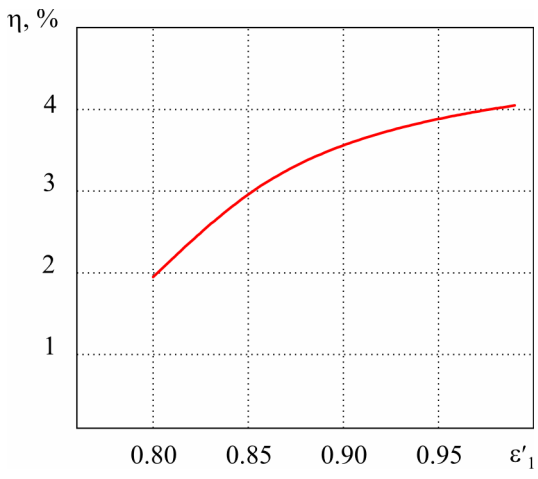

Fig. 6. Maximum efficiency of a thermopile as a function of kiln emissivity.

Thus, the maximum efficiency of dedicated thermoelectric modules of "Altec-M" company (Ukraine) will be 4.05 % taking into consideration that with the use of water cooling their cold side temperature $T_c \approx 30$ °C. In this case, the generator design capacity with account of the expenditures on the power supply of thermoelectric modules cooling system will be 130 W/m^2.

Conclusions

1. Mathematical modeling was obtained that allows estimating the impact of a thermoelectric generator on the cement kiln heat exchange, its rotation considered. The possibility of such impact elimination by way of changing the surface emissivity was determined.
2. The dependences were obtained of the maximum efficiency and temperature of the thermoelectric generator hot heat exchanger on the emissivity of the cement kiln surface.
3. The thermoelectric generator maximum efficiency was computed for the design of the cement kiln under discussion, the said efficiency being 4.05 %.
4. The generator designed capacity where the expenditures on the power supply of the thermoelectric modules cooling system are taken into account will equal to 130 W/m^2.

References

1. V. Panyakiv, Co-Generation: How it Works, *Seti i Business* **4**, (2010).
2. L.I. Anatychuk, Reasonable Areas of Research into and Application of Thermoelectricity, *J. Thermoelectricity* **1**, 3 – 14 (2001).
3. L.I. Anatychuk, State-of-the-Art and Some Prospects of Thermoelectricity, *J. Thermoelectricity* **2**, 7 – 20 (2007).
4. A.S. Bernstein, *Thermoelectric Generators* (Moscow: *Gosenergoizdat*, 1956), 47 p.
5. L.I. Anatychuk, *Thermoelements and Thermoelectric Devices: Handbook* (Kyiv: Naukova Dumka, 1979), 768 p.
6. L.I. Anatychuk, O.J. Luste, and R.V. Kuz, Theoretical and Experimental Studies of the Thermoelectric Generator for Vehicles, *Journal of Electronic Materials* **40** (5), 2011.
7. L.I. Anatychuk, Jenn-Dong Hwang, and A.V. Prybyla, Thermoelectric Generator for Conversion of Heat from Gas Rolling Furnaces, *Proc. of 29-th International Conference on Thermoelectrics (*China, Shanghai, 2010).
8. L.I. Anatychuk, A.V. Prybyla, Thermoelectric Heat Recuperator for Gas Turbines, *Proc. of XIII Intergovernmental Workshop "Thermoelectrics and their Applications"* (St.-Petersburg, Russia, November 13 – 14, 2012*)*.
9. T. Kajikawa, State-of-the-Art in the Technology of Power Thermoelectric Generation in Japan, *J. Thermoelectricity* **2***,* 21 – 31 (2007).
10. http://www.innovaterussia.ru/project/gallery/current/16325
11. Ye.I. Khodorov, *Cement Industry Kilns* (Leningrad, 1968), 456 p.
12. S.S. Kutateladze, V.M. Borishansky, *Handbook on Heat Transfer* (Leningrad, Moscow: Gosenergoizdat, 1958), 414 p.
13. F.F. Tsvetkov, B.A. Grigoriev, *Heat-Mass Exchange* (Moscow: MEI Publishers, 2005), 550 p.
14. Ye.V. Mochalin, S.A. Yuriev, Heat Exchange and Hydraulic Losses in the Spacing between Rotating Cylinders, *Technology Audit and Production Reserves* **3** (11), 45 – 49 (2013).

Submitted 12.09.2013.

S.O. Filin, B. Jasinska

S.O. Filin

West Pomeranian University of Technology,
17, Aleja Piastów, Szczecin, 70310, Poland

B. Jasinska

EXPERIMENTAL INVESTIGATIONS OF TWO-LEVEL TEMPERATURE CONTROLLERS FOR TRANSPORT THERMOELECTRIC REFRIGERATORS

This paper presents the problems of energy saving in transport thermoelectric refrigerators equipped with temperature controller, and describes the results of testing the selected object, namely embedded into furniture section thermoelectric refrigerator with compartment volume 27.7 dm^3 with different supply circuits from on-board mains, allowing practical implementation of the idea of two-level temperature control. The possibility and expedience of using this type of control with indication of concrete most efficient technical solutions is proved experimentally. The specific power consumption of tested refrigerator as compared to ON-OFF control has been reduced, on the average, by a factor of 3.

Key words: thermoelectric refrigerator, temperature control, electrical power, energy saving.

Introduction

In our everyday life we use increasingly often the concept of "energy security" integrating technical, organizational and political problems. The former can be solved on different levels and in different aspects, starting from replacement of incandescent lamps in apartments and offices by energy-saving lamps and ending in diversification of energy supply in certain country or region. Cooling equipment and air conditioners used in industry, transport and everyday life account for 20 to 80 % in the structure of nationwide energy consumption [1-6].

As had been shown in the previous works of the members of Air Conditioning and Refrigerated Transport Department of West Pomeranian University of Technology in Szczecin [7, 8], the use of two-level temperature control in compartments of various-purpose thermoelectric refrigerators (hereinafter TER) is the most efficient and at the same time accessible method for reduction of their energy consumption. For the first time this method whereby thermostat switches power of thermoelectric refrigerator cooling unit from a higher to lower voltage level was used in the design of TER-40 "Chaika" of the volume of 40 dm^3 [9]. However, the above refrigerator was not designed for continuous operation in energy saving working mode referred to by the authors as "pause current" mode. Moreover, prior art solution, as well as its later modifications, prevented from implementing the idea of two-level control when powering the refrigerator from on-board vehicle mains with a nominal voltage 12 or 24 V DC.

The object, purpose and results of preliminary test stage

As the object of test, a thermoelectric cooler with compartment volume 27.7 dm^3 embedded into furniture section was taken. This refrigerator type is used in ship and yacht cabins, trailers, auto shops,

railway carriages, planes and other transport means. The internal dimensions of thermoelectric refrigerator compartment: width – 440 mm, depth – 240 mm, height – 262 mm. The compartment is made of lumber- core board 18 mm thick and heat insulation layer of polystyrene foam plate 30 mm thick. The refrigerator cooling unit comprises two thermoelectric modules of the type T-2-1.6-127 ([10], appendix 1), two heat sinks of the same type made of aluminum shapes (one on the cold and one on the hot side of the unit) and two axial fans[1] of the type VD 9225 HS, installed on each heat sink and powered by nominal voltage 12 V DC.

The refrigerator also comprises a manometric thermostat of the type Danfoss 077B7008 and electromagnetic relay of the type R8 powered by nominal voltage 12 V DC. The thermostat sensor is in a direct contact with the cold heat sink surface.

The test bench comprises several supply sources (hereinafter SS), i.e. alternating to direct current converters with output voltage and/or current stabilization. Some of their characteristics are represented in Table 1. In the test, the source PowerLab RXN3010D was predominantly used.

Table 1

Main specifications of supply sources (SS)

SS type	Control range	Resolution	Voltage/current stabilization
BP-20 (custom-made)	12…22 V up to 5 A	0.01 V* 0.01 A*	–/–
M10-DP two-channel	2 × 0…30 V 2 × 0…5 A	0.1 V, 0.01 V* 0.1 A, 0.01 A*	+/+
PowerLab RXN3010D	0…30 V 0…10 A	0.1 V, 0.01 V* 0.1 A, 0.01 A*	+/+

* – when using external devices of M838 type.

The measuring part of the test bench consists of 8-channel data recorder AR205 with J type thermocouples connected to its inputs. In temperature measurement mode the device resolution was 0.1 K. In the test, the following temperatures were measured: ambient air, the cold and hot heat sink surface, chamber air at three points at various heights according to appropriate standard requirements. Verification of temperature measurements was carried out using digital temperature meters: 10-channel CR7701-02 with thermocouples of *L* type and single-channel CR7702 with a thermistor of resistance 50 Ω. Both meters have class 0.05 accuracy with a resolution of 0.1 K. The general view of the test bench and refrigerator is represented in Fig. 1.

Fig. 1. Transport thermoelectric cooler (as seen from thermoelectric unit) during the test.

Daily electric energy consumption is measured using Energy Logger electron meters (models 3000 and 3500) with 1 W·h of resolution, which is extremely important for testing devices with low power consumption. In addition to high measurement

[1] It means that technical solution with forced compartment air convection typical of modern thermoelectric refrigerator models has been selected.

precision, several-fold reduction of test time is achieved. Apart from electric energy consumption, Energy Logger meters assure measurement of the following parameters: current values of AC voltage and current strength, mains current frequency, power factor (cos φ), effective and apparent current values of power consumption (see Fig. 2), and, on introduction of proper electricity tariffs, the cost of energy consumption is calculated with regard to the difference in day and night tariffs. Parameter measurement frequency is 1 second. The Energy Logger 3500 model offers the opportunity of on-line recording and transfer of data to a computer. Verification of electric energy consumption measurement was done with the aid of electromechanical energy meter of the type SO-I446. Time was registered by a timer with 1 second of resolution.

Fig. 2. Work moment of electric parameter recording.

Selected were 5 variants of electrical supply circuit of thermoelectric refrigerator cooling unit which are represented in Table 2 and in Fig. 3. All variants provide for power switching for a group of two thermoelectric modules when passing from a parallel to series connection, whereby each module voltage is reduced from 12 V to 6 V DC. The variants differ from each other in the way of connection and switching of fans M1 and M2. In variant I (circuit *a*) the voltage of fans in both operating modes is not varied and makes 12 V. In variant II (circuit *b*) only the internal fan M2 is switched over to lower voltage. In variant III (circuit *c*) both fans are switched over to voltage 6 V. In variant IV (circuit *d*) the fans are constantly powered by voltage 6 V. In variant V (circuit *e*) in working mode fan M1 is powered by voltage 12 V, and fan M2 is idle, while in "pause current" mode both fans are powered by voltage 6 V.

Table 2

Plan of experiment with a change in supply circuits of thermoelectric refrigerator

Unit working mode	Connection			
	Modules	external fan M1	internal fan M2	Variant number /circuits
"operation"	Parallel (12)	12	12	I, II, III (Fig. 3 *a*)
		6	6	IV (Fig. 3 *d*)
		12	0	V (Fig. 3 *e*)
"pause"	Series (6)	12	12	I (Fig. 3 *a*)
		12	6	II (Fig. 3 *b*) V (Fig. 3 *e*)
		6	6	III (Fig. 3 *c*) IV (Fig. 3 *d*)

*0, 6, 12 – supply voltage of this element

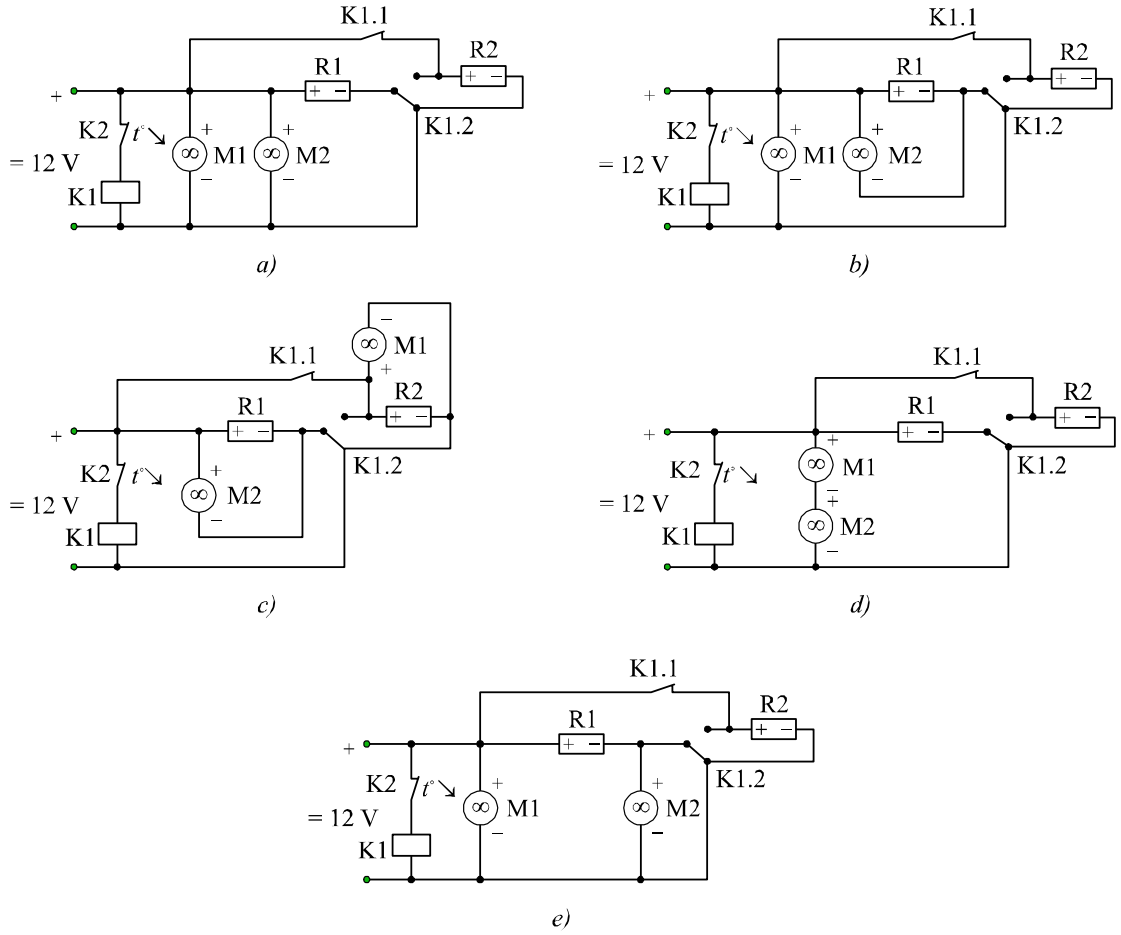

Fig. 3. Selected variants of electrical supply circuits of cooling unit of refrigerator under test.

Operating mode without temperature control at constant voltage 12 V and operating mode ON-OFF type control were assumed as a basis for comparison. Study of these two modes was the essence of preliminary test stage, and its objective was:

- experimental validation of the functionality of chosen supply circuits with a two-level temperature control in thermoelectric refrigerator compartment;
- revealing the influence of selected parameters on electric energy consumption of object under study, i.e. transport thermoelectric refrigerator (during this stage we decided to restrict ourselves to a change in supply voltage in the range from 6 to 14 V with a step 0.5 V and a change in thermostat setting);
- comparative analysis of thermoelectric refrigerator's electric energy consumption with different methods of temperature control.

Preliminary tests were performed at the same constant ambient temperature 22 °C, at different thermostat settings, with an empty compartment and in the absence of its lighting. The temperature in test room was maintained at the constant level to an accuracy of $\pm$ 0.3 K by means of air-conditioner Sanyo, model SAP KR(CR)127EHAX. The main measured parameter was thermoelectric refrigerator's daily electric energy consumption. Additionally measured and calculated were: time from the moment of start to the moment of reaching the lowest average temperature in the compartment (at constant operation), time to first thermostat actuation, operating time, pause time, cycle time, operating time factor (with a cyclic operation). Electric energy consumption was measured from the moment of thermoelectric refrigerator start, but for comparative analysis we took into

account the consumption in the period of steady-state operation of refrigerator, the onset of which is determined in conformity with the concepts described in [7]. Other important peculiarities of test procedure are represented below when discussing particular results.

Preliminary test results are represented in Tables 3 and 4. In continuous working mode the average air temperature in refrigerator compartment has reduced to 4.3 °C. The registered temperature difference between the compartment air and the cold heat sink made 2.2 °C, which should be considered a very good result as compared to prior art constructions of thermoelectric refrigerators with a fan in the compartment described in [7], [8], [10].

Table 3

Results of refrigerator test in basic working modes

Measured and calculated characteristics	Working modes		
	Continuous operation	ON-OFF	ON-OFF
Thermostat setting	7 (min)	1 (max)	2
Temperature [^{o}C]:			
Average compartment temperature in steady-state working mode and at the instants of thermostat actuation	4.3 –	9.5 7.3/11.6	7.6 5.2/10.0
Average temperature of cold heat sink or its temperatures at the instants of thermostat actuation	2.1	5.0/10.4	2.9/8.5
Average temperature of hot heat sink or its temperatures at the instants of thermostat actuation	32.0	32.6/23.2	32.0/23.0
Temporal			
Time to achieve steady-state working mode [min]	150	30[1] 108[2]	65[1] 50[2]
Time of cycle (time of "operation" mode + time of "pause" mode) [s]	–	1270 (840 + 430)	2115 (1620 + 495)
Working time factor [–]	–	0.661	0.766
Electric and energy			
Unit supply voltage [V]	12.00	12.0/0	12.0/0
Strength of unit supply current in steady-state mode or at the instants of thermostat actuation [A]	5.14	5.46/5.22/0	5.32/5.12/0
Unit power consumption in steady-state working mode or at the instants of thermostat actuation [W]	61.7	65.5/62.6/0	63.9/61.4/0
Power consumption of supply source (from AC mains) [W]	157.2	169.1/158.2/ 27.3	169.0/156.3/27.4
Average electric efficiency of supply source [–]	0.392	0.399[3]	0.399[3]
Daily energy consumption of supply source [kWh]	3.78	2.72	3.10
Daily energy consumption of unit [kWh]	1.48	1.01	1.15
The factor of specific power consumption P_{spec} of refrigerator [W/dm^{3}K]	0.126	0.185	0.157

[1] – time to the first actuation of thermostat; [2] – time of cycle parameters stabilization; [3] – in "working" mode.

Table 4

Supply voltage dependence of thermoelectric refrigerator and supply source parameters in continuous working mode

Supply voltage of the unit U, [V]	Current strength I, [A]	Power consumption of the unit P_u, [W]	Power consumption of supply source P_{ss}, [W]	Average electric efficiency of supply source ε_{ss}, [–]	Average compartment temperature T_{comp} [°C]	Cold heat sink temperature T_c [°C]	Hot heat sink temperature T_h [°C]
5.0	2.09	10.5	60.9	0.172	9.0	6.5	26.4
6.0	2.54	15.2	68.0	0.224	7.7	5.3	27.0
7.0	2.96	20.7	75.2	0.276	6.4	4.0	27.8
8.0	3.40	27.2	114.2*	0.238*	5.5	3.0	28.4
9.0	3.84	34.6	126.0	0.274	4.8	2.5	29.2
10.0	4.28	42.8	135.8	0.315	4.7	2.4	30.6
10.5	4.50	47.3	141.2	0.335	4.6	2.3	30.9
11.0	4.72	51.9	146.2	0.355	4.5	2.2	31.2
11.5	4.93	56.7	151.8	0.374	4.4	2.2	31.6
12.0	5.14	61.7	157.2	0.392	4.3	2.1	32.0
12.5	5.35	66.9	163.9	0.408	4.4	2.1	32.5
13.0	5.55	72.1	166.4	0.433	4.5	2.2	33.1
13.5	5.75	77.6	172.1	0.451	4.5	2.2	33.5
14.0	5.95	83.3	176.8	0.471	4.6	2.3	34.1

* – stepwise change in P_{ss} (u) and ε_{ss} (u) dependences is related to supply source construction and follows from dividing voltage control range into sub-ranges, one of the boundaries between the sub-ranges being close to voltage 7.1 V.

The values of power consumption and daily energy consumption of supply source and thermoelectric refrigerator were determined. Moreover, in order to facilitate subsequent comparative analysis, the factor of specific power consumption was determined [7] whose values are represented in Table 3.

At ambient temperature 22 °C the use of chosen thermostat type in refrigerator under test allows two-level temperature control in its compartment only in setting range from ① to ②. This restriction, no doubt, narrows down possible range of temperature setting in compartment, but does not complicate comparative analysis that can be explained as follows. On the one hand, expansion of thermostat dead band upwards, i.e. above 7.3 °C[2], does not fit in the concept of general-purpose

[2] With the adopted tuning scale it would imply its change, for instance, from ① to ⑥.

refrigerator, and, on the other hand, reduction of actuation temperature below 2.1 °C (which is identical to transition from setting ② to ③) will bring about the situation when no thermostat actuation takes place and the unit will remain in continuous working mode.

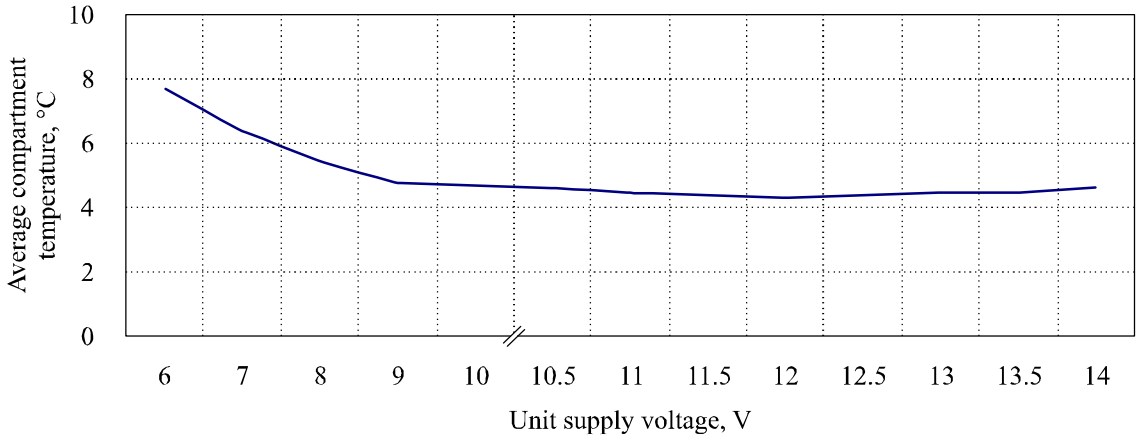

Fig. 4. Average temperature in thermoelectric refrigerator compartment versus supply voltage in continuous working mode at ambient temperature 22 °C.

Analysis of results represented in Table 4 shows that minimum average compartment temperature T_{comp} corresponds to supply voltage 12.0 V. This result testifies to correctness of underlying technical solutions for continuous working conditions. A very flat type of the dependence T_{comp} [U] in the region of voltage variation from 9 to 14 V (Fig. 4) qualitatively well coincides with the results obtained for thermoelectric refrigerators of other types [10], [11], including those without a fan in the compartment [12]. This feature of thermoelectric refrigerator should be estimated as positive, since it makes the refrigerator less sensitive to supply voltage variations and voltage changes due to switching from the battery (12 V) to the generator of on-board vehicle mains (13.5...13.8 V).

A relatively small difference in temperatures T_{comp} with different supply voltages 12 V and 6 V (4.3 °C and 7.7 °C, respectively) allows the following conclusions:

– the refrigerator remains functional in a very wide range of supply voltage variation;
– according to the results of refrigerator test in basic working modes it can be expected that, with no change in the supply circuit of the fans, switching of modules power supply from a parallel to series circuit will not raise chamber temperature so high as to cause a reverse thermostat actuation and return to working mode. That is, the unit will continue working in the energy saving mode ("pause current"), when power consumption is about 4 times less than in working mode. This implies the possibility of achieving the same effect that was obtained in thermoelectric refrigerators powered from alternating current mains with the use of supply sources specially designed for this purpose. This conclusion should be confirmed by the next test stage.

Conditions and results of principal test stage

The list of parameters measured in experiment and the measured results are presented in Table 5. Just as for the basic ON-OFF variant, all the variants were tested for two thermostat settings ① and ②. Energy consumption was measured on a permanent basis, meter readings were taken every 15 minutes, as well as at thermostat actuation moments. In determination of daily energy consumption account was taken of only the period of steady-state working conditions (at stabilized chamber temperatures) of duration at least 3 hours.

Table 5

Refrigerator test results for different variants of supply circuits

Circuit variant and thermostat setting Characteristics	I (circuit *a*)		II (circuit *b*)		III (circuit *c*)		IV (circuit *d*)		V (circuit *e*)	
	①	②	①	②	①	②	①	②	①	②
Temperature										
Average chamber temperature in steady-state working mode, [ºC]	8.0	7.7	5.3	5.6	6.3	6.2	6.8	6.3	4.2	4.6
Average ambient temperature during test, [ºC]	21.7	21.4	21.8	22.9	22.1	22.1	21.6	21.4	21.1	22.1
Temperature difference created by thermoelectric refrigerator, [K]	13.7	13.7	16.5	17.3	15.8	15.9	14.8	15.1	16.9	17.5
Cold and hot heat sink temperatures at the instant of thermostat actuation, [ºC]	4.1 33.6	2.5 33.4	4.2 32.9	2.2 32.8	4.1 34.3	2.5 32.7	4.0 38.9	2.5 39.2	0.9 32.6	–0.7 32.9
Cold and hot heat sink temperatures in steady-state mode [ºC]	6.2 26.0	6.0 25.8	2.2 26.3	3.0 28.2	3.7 27.8	3.6 27.5	4.4 27.8	3.9 27.5	1.8 25.9	2.3 25.8
Temperature nonuniformity along the compartment height (top-bottom), [ºC]	0.6	0.6	0.6	0.6	0.6	0.7	0.7	0.6	0.7	0.6
Temporal										
Time from switching to the first thermostat actuation, [min:s]	30:35	67:00	25:10	58:00	38:18	71:00	29:10	42:00	13:30	17:40
Time to stabilization of working conditions after thermostat actuation [min:s]	25:00	23:00	35:00	32:00	33:00	27:00	24:00	28:00	47:00	51:00
Energy										
Supply voltage of the unit, [V]	12.0	12.0	12.0	12.0	12.0	12.0	12.0	12.0	12.0	12.0
Supply current of the unit (at switching /at thermostat actuation / under steady-state mode), [A]	6.3/ 5.5/ 1.7	6.3/ 5.5/ 1.7	6.3/ 5.6/ 1.5	6.3/ 5.5/ 1.5	6.3/ 5.5/ 1.3	6.3/ 5.5/ 1.3	6.3/ 5.0/ 1.3	6.3/ 5.0/ 1.3	6.4/ 5.3/ 1.5	6.3/ 5.3/ 1.5
Average power consumption of the unit, [W]	20.4	20.4	18.0	18.0	15.6	15.6	15.6	15.6	18.0	18.0
Power consumption of supply source [W] (meter reading and calculated as the difference in energy consumption	73.9 73.94	73.8 74.66	69.1 69.33	68.8 68.66	64.8 64.5	64.4 65.13	64.7 64.87	64.8 65.00	69.9 70.00	69.5 69.66
Average electric efficiency of supply source [-]	0.276	0.273	0.260	0.262	0.242	0.236	0.243	0.240	0.257	0.258
Daily energy consumption of supply source [kW·h]	1.77	1.79	1.66	1.64	1.55	1.56	1.56	1.56	1.68	1.67
Daily energy consumption of the unit [kW·h]	0.49	0.49	0.432	0.432	0.375	0.375	0.375	0.375	0.432	0.432
Specific power consumption P_{spec} of the refrigerator [W/dm^3·K]	0.0538	0.0538	0.0394	0.0376	0.0354	0.0354	0.0380	0.0373	0.0384	0.0371

Analysis of results and conclusions

All five selected supply circuits (see Fig. 3 and Table 5) assure the possibility of long refrigerator operation in the energy-saving working mode, when the temperature in the compartment does not rise to the upper boundary of the employed thermostat dead band[3]. As compared to continuous working mode at operating current, when created temperature difference is maximum:ΔT_{max} = 17.7 K, the same parameter for the above circuits fits in the limits from 13.7 K (variant I) to 17.5 K (variant V), which makes from 77.4 % to 98.8 % ΔT_{max} respectively (Fig. 5). In terms of purely mathematical analysis such a result might be considered satisfactory. However, if we consider the average temperatures in the compartment, then variant I where this temperature made 7.7...8.0 °C is already of limited application bearing in mind the variety if products stored in a thermoelectric refrigerator. For instance, this temperature level according to regulatory documents is inadmissible for storage of such confectionery products as cakes and pastries[4], but is quite acceptable in the refrigerators and window displays for storage and demonstration of the majority of sorts of wines and beverages. Other variants have no such limitations, despite slight excess of the threshold 6.0 °C (variants III and IV), that can be easily avoided by minimum strengthening thermoelectric refrigerator heat insulation.

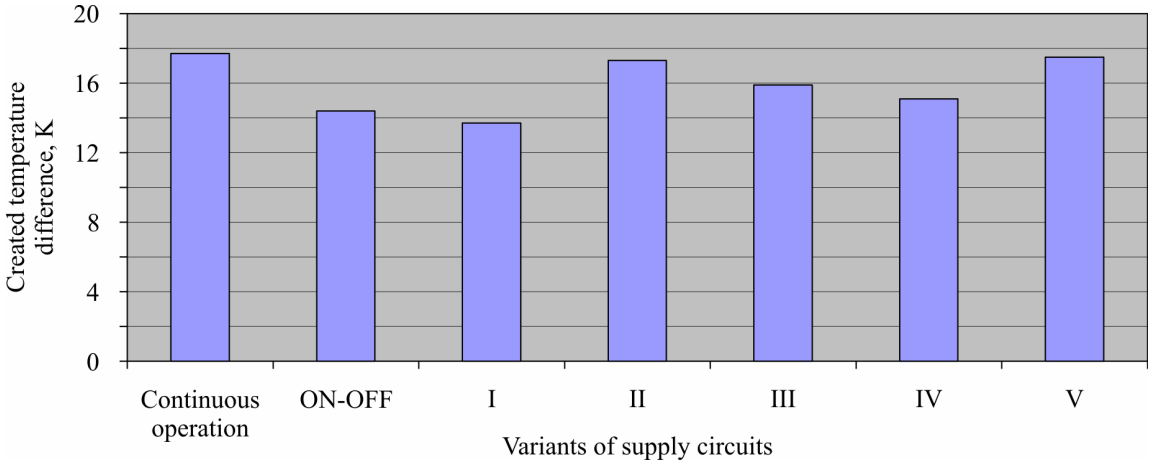

Fig. 5. Comparison of temperature differences created by the refrigerator for the investigated variants of supply circuits at thermostat setting ②.

Despite the more intensive air circulation in the compartment of variant I, the temperature in the compartment of thermoelectric refrigerator in this case is higher (see Table 5). This paradox has its own explanation. The rated capacity of a fan installed in the compartment (powered by voltage 12 V) is too high for a relatively small compartment volume. As a result, cold air "escapes" faster from the compartment through the insulation openings. Moreover, heat transfer coefficient from the internal compartment walls is rather high, leading to increase in total heat transfer coefficient K of cooling compartment and increase in heat inputs through the insulation. Hence a conclusion which agrees with the conclusions of previous research [12] that the internal fan of thermoelectric refrigerator should be powered by reduced voltage and current or a fan of at least half the power of the hot side fan should be used.

Further analysis of the refrigerator temperature characteristics shows that temperature nonuniformity along the height of its compartment does not depend on the operating mode of fan M2. Only with an idle fan, hence, the absence of forced convection in starting period for variant V the

[3] In the present thermoelectric refrigerator this temperature is 11.6 °C for setting ① and 10.0 °C for setting ②.
[4] The range of storage temperatures for confectionery products is from 0 to +6 °C. The same demands are placed on single-compartment refrigerators of general purpose.

uniformity increases to 1.0...1.3 °C[5]. With regard to the basic temperature characteristics in the energy saving operating mode of thermoelectric refrigerator, especially compartment temperature, hot heat sink temperature and created temperature difference, variant II seems to be the most balanced solution.

Measurements of temporal (dynamic) characteristics of refrigerator provide a lot of interesting information for the future more detailed analysis of refrigerator behaviour with a sudden growth of thermal load[6], leading to temporary, generally one-time transition to working mode. From the data in Fig. 6 and Table 5 it follows that advantage is offered by variant V characterized by the shortest time of operation in working mode, i.e. fast transition to energy saving mode. This results in the reduction of daily energy consumption of refrigerator. However, as follows from [8], this thesis is valid only for an empty refrigerator or in the absence of additional loading of refrigerator with warm products.

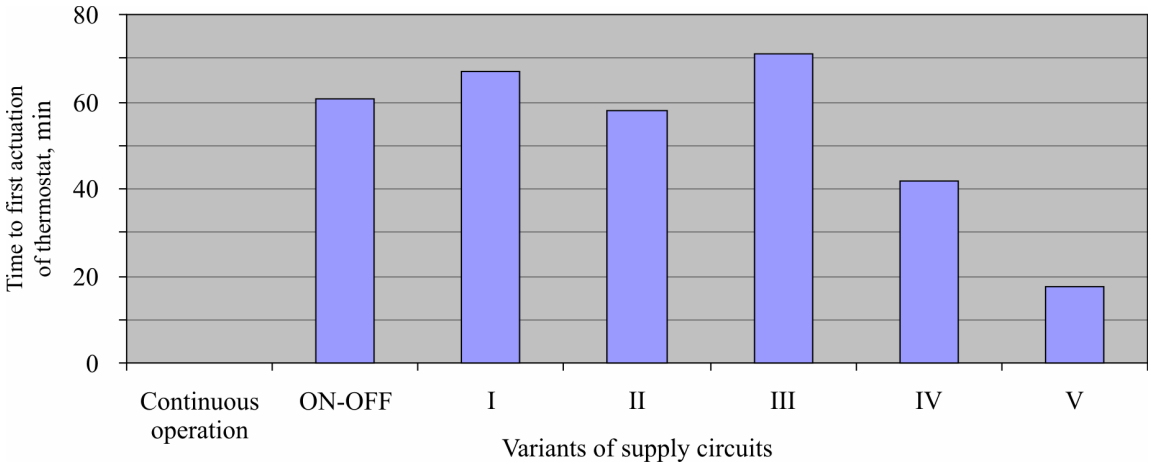

Fig. 6. Comparison of refrigerator operation time in working mode (up to the first actuation of thermostat) for the investigated variants of supply circuits at thermostat setting ②.

In general, the time to the first actuation of thermostat for setting ② varies within 1 hour, and for setting ① it is almost half as much, which depending on the manner of refrigerator employment can make from 0.5 % to 8 % of total daily time of refrigerator operation with a respective growth of its daily energy consumption. A more detailed analysis of thermoelectric refrigerator working modes with regard to thermal load variation will be the subject of further research.

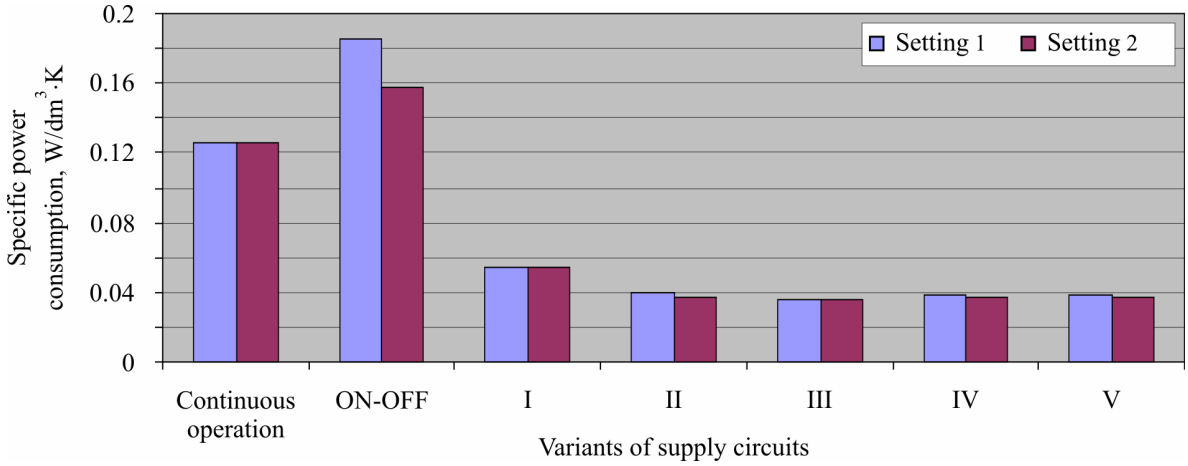

Fig. 7. Comparison of refrigerator specific power consumption for the investigated variants of supply circuits.

[5] This data is not presented in Table 5, but is available in test protocols.
[6] The most typical situation of this kind is slow opening of refrigerator door.

The most important results of the work performed are related to the energy characteristics of the investigated variants of supply circuits of thermoelectric refrigerator unit. As compared to ON-OFF working mode there is 3-4-fold reduction of power consumed from direct current mains (Table 5). This also accounts for nearly 3-fold reduction of specific power consumption (Fig. 7). From the standpoint of energy, the least-cost option is variant III (Fig. 3, circuit *c*). Its advantage over variant II can be explained by a greater share of power consumed by the fans in the total power consumption of the unit. This factor prevails over the marginal effect of reduction of temperature difference created by thermoelectric refrigerator.

The measured strength of current flowing through relay K1 was 90 mA. In terms of power consumption, the relay accounts for 1.8 % of the total unit power consumption. Taking into account that the relay consumes power only in working mode, it is of minor importance in refrigerator energy consumption, hence, the use of supply circuit with employment of electromechanical relay is reasonable.

To formulate more detailed final recommendations, one should continue research using a larger number of test objects and more precise measuring instruments, for instance, direct current energy meter. At the same time, the results obtained allow us to assert that the target goal has been achieved: the possibility and advisability of using two-level temperature control "with pause current" in transport thermoelectric refrigerators has been experimentally substantiated with indication of concrete most efficient technical solutions according to the task set (circuits *b, c* or *e*).

References

1. N. Konoplyova, *Electric Energy Consumption by a Cooler*, http://planetaklimata.com.ua/ articles/?msg =1110 15.09.2012.
2. *The Ways for Reducing the Electric Power of Supermarket Refrigerating Appliances*, http://planetaklimata.com.ua/articles/?msg=1110
3. A. Kamiński, *Optymalizacja zużycia energii elektrycznej supermarketu. Projektowanie instalacji i dobór komponentów chłodniczych*. 09.10.2012 www.chlodnictwoiklimatyzacja.pl/ index.php/ artykuly/203-wydanie-092012/2356.html
4. *Energy Saving in Shop Equipment*, http://tjet.ru/energosberezhenie
5. *Urządzenia Chłodnicze dla Sklepów – Energooszczędne Rozwiązania*. 11.09.2012 www.firmymiesne.pl /artykul/urzadzenia-chlodnicze-dla-sklepow-energooszczedne-rozwiazania, 241
6. A. Pazukhin, A. Yudina, Methods for Reduction of Power Inputs at Food Plants, *Imperia Kholoda* **10**, 36 – 37 (2011).
7. S. Filin, A.Owsicki, *Zasady Projektowania i Eksploatacji Chłodziarek Termoelektrycznych* (ZAPOL, Szczecin, 2010).
8. S.O. Filin, A.Owsicki, B.Zakrzewski, *Experimental Investigation of Stationary Thermoelectric Refrigerators* (Odessa: Astroprint, 2011).
9. V.S. Orlov, D.M.Ioffe, V.N. Lomakin et al., Domestic Thermoelectric Refrigerator, *Kholodilnaya Tekhnika* **1**, 11 – 15 (1970).
10. S.O. Filin, *Termoelektryczne Urządzenia Chłodnicze* (Gdańsk: Masta, 2002).
11. S.O. Filin, S.O. Zhurbenko, and L.N. Varyukhina, Transport Thermoelectric Refrigerator XTT-30, *Kholodilnaya Tekhnika i Tekhnologiya* **56**, 13 – 18 (1994)
12. S.O. Filin, B. Zakrzewski, and A. Owsicki, Design and Experimental Research of Glass Door Refrigeration of 100 l Volume with Thermoelectric Cooling Unit, *Proceedings of 4-th Congress CEFood (Bulgaria, Sofia, May 22-24, 2006)*.

Submitted 15.08.2013.

L.I. Anatychuk, L.N. Vikhor

Institute of Thermoelectricity of the NAS
and MES of Ukraine, 1, Nauky Str.,
Chernivtsi, 58029, Ukraine

L.I. Anatychuk

THE LIMITS OF THERMOELECTRIC COOLING FOR PHOTODETECTORS

L.N. Vikhor

The results of research on the limiting capabilities to use thermoelectric cooling for photodetectors are presented. The introduction of modern technologies for IR detectors allows shifting their operating temperature from the cryogenic region to the range of 120 – 200 K. It is shown that such temperatures can be achieved by thermoelectric cooling through use of new up-to-date approaches in the development and manufacture of stage thermoelectric modules. Such approaches are: first, using optimal functionally graded materials based on Bi-Te for the legs of cooling modules, secondly, using Bi-Sb alloys for n-type legs in low-temperature stages and arrangement of these stages in optimally homogeneous or optimally inhomogeneous magnetic field . Based on the results of computer simulation it was determined that practical introduction of these approaches in the development of modules assures the level of thermoelectric cooling of IR detectors up to 120 K with sufficient energy efficiency.

Key words: photo detector, IR detector, thermoelectric cooling.

Introduction

Semiconductor photodetectors are widely used for IR radiation recording and IR imaging in modern terrestrial and space equipment, systems for astronomical observations, automatic star tracking, in night vision devices, etc. Detectors with photoelectric conversion of IR signal possess good threshold characteristics (spectral sensitivity, detectability) and fast response. However, this requires photodetector cooling down to cryogenic temperatures [1]. Cooling is necessary to reduce thermal generation of charge carriers in a semiconductor photosensitive element. Thermal carriers transitions compete with optical ones, which results in the large value of dark noise in uncooled devices.

The operating temperature of photodetector is related to the operating range of IR detector wavelength and depends on material and technology of photosensitive element. Modern cooled IR sensors are efficient at temperatures below 200 K [1]. For cooling such devices there have been specially developed and used microcryogenic systems based on gas cryogenic Stirling machine which is combined with a cryostatted photodetector into a single design [2-6]. They assure photodetector cooling temperature 75 to 150 K. The main shortcoming of such systems is their high cost. Such mechanical cooling systems make IR sensor systems bulky, expensive and not very reliable, preventing from a wide practical use of IR devices. Medium-wave (3 – 5 μm) and long-wave (5 – 30 μm) IR sensors operated without cryocooling, are required for many important practical applications.

Scientific investigations of recent decade have demonstrated that good threshold characteristics of the sensors of medium and long-wave IR range can be assured with the operating temperatures of photodetectors considerably higher than cryogenic ones [7, 8]. These temperatures are easily achieved with the aid of thermoelectric cooling [9, 10] which in this case is more reasonable as compared to the

mechanical method for cold production.

The objective of this work is to analyze the capabilities of thermoelectricity for cooling sensor devices and to determine the reasonable operating temperature range of photodetectors with thermoelectric cooling.

The results of research

Thermoelectric cooling is widely used to assure the required operating temperature of IR detectors [1, 9, 10]. Photodetector arranged on the heat-absorbing pad of thermoelectric cooling module is, as a rule, mounted into a sealed case whose base is in a good thermal contact to heat exchanger.

Single-stage thermoelectric modules are used for shallow cooling (down to 250 K) of IR sensors and for temperature stabilization of the so-called uncooled photodetectors of visible and IR range. Cooling of IR sensors to operating temperature 230 K is provided by two-stage thermoelectric coolers (TEC), to 210 K – by three-stage TEC, to 190 K – by four-stage TEC. Characteristics of such TEC (maximum temperature difference ΔT_{max}, cooling capacity Q_{max}, voltage U_{max}, supply current I_{max}) that are stocked, for instance, for IR detectors of VIGO company, are listed in Table 1 [10].

Table 1

Characteristics of stage TEC for cooling IR detectors [10]

	2-stage TEC	3-stage TEC	4-stage TEC
$T_{detector}$, K	~ 230	~ 210	~ 195
Q_{max}, W	0.36	0.27	0.28
ΔT_{max}, K	92	114	125
U_{max}, V	1.3	3.6	8.3
I_{max}, A	1.2	0.45	0.5

Multi-stage modules are produced by various companies. Table 2 lists the characteristics of stage modules of leading companies. The modules are manufactured of conventional thermoelectric materials based on *Bi-Te* with a homogeneous distribution of impurity concentration in thermoelement legs.

Therefore, thermoelectric coolers nowadays provide cooling of IR sensors to 190 K. Such devices are small-size, mechanically stable, highly reliable with a life cycle up to 20 years. The main disadvantage of thermoelectric cooling is its low energy efficiency.

As was already mentioned, for IR detectors with the operating temperatures in the range of 70 to 150 K use is made of microcryogenic Stirling systems [3-5]. These are energy-efficient coolers. With cooling capacity in the range of 100 to 600 mW their coefficient of performance achieves the values of 10^{-2} to $3 \cdot 10^{-2}$.

At the same time, recent investigations have shown that introduction of current advanced technologies for IR detectors allows shifting the operating temperature of IR detector from the cryogenic region to the range of 150 to 200 K [8, 11-13]. In so doing, its threshold characteristics are not degraded. At the present time such temperatures can be achieved via thermoelectric cooling through use of new up-to-date approaches in the development and manufacture of stage thermoelectric modules.

One of such approaches is to use functionally graded thermoelectric materials (FGTM) for thermoelement legs [14]. These are materials with the optimal inhomogeneity of the main thermoelectric properties, namely thermoEMF α, electric conductivity σ and thermal conductivity κ.

The second approach is to use materials of improved efficiency in low-temperature region. An example of such materials can be *n*-type *Bi-Sb* alloys. These alloys have high thermoelectric figure of

merit at temperatures below 160 K, which in addition increases in a magnetic field. The use of optimally inhomogeneous magnetic field further increases the efficiency of cooling modules of such materials [15].

Table 2

Characteristics of stage modules of leading companies

Company	Module	Number of stages	Module characteristics			
			ΔT_{max}, K	Q_{max}, W	U_{max}, V	I_{max}, A
Marlow Industries USA [marlow.com]	SP402-01AB	3	111	0.5	7.5	4.5
	NL3040	3	98	0.5	4.5	6.5
Ferrotec USA [ferrotec.com]	9530/119/045B	3	111	9.7	8.6	4.5
Thermion Ukraine [thermion-company.com]	3TMCO6-070-15	3	116	0.6	5.3	0.9
	4TMB04-099-C112	4	126	0.27	6.5	0.5
	5TMB06-113-B1224	5	130	0.57	6.4	1.2
	5TMB10-164-X1224	5	136	1.8	10.2	3.7
Komatsu Japan [kelk.co.jp]	K3MC011	3	114	6.2	7.5	5.1
	K4MB005	4	134	3.6	15.3	5.1
	K5MB002	5	145	1.5	14.7	4.8
RMT.ltd Russia [rmtltd.ru]	3MDS04	3	116	0.27	5.7	0.4
Laird Technologies USA [lairdtech.com]	MS3	3	118	3.6	6.5	6.5
	MS4	4	122	2.7	7.6	3.5
	MS5	5	123	2	14.5	1.6
Tellurex USA [tellurex.com]	M3	3	98	6.6	7.8	3.6
	M4	4	112	3.4	15	3
OJSC “OSTERM SPB” Russia [osterm.ru]	PE3	3	117	3	6.5	6.5
	PE4	4	125	3.75	7.8	5.4
	PE5	5	133	8	16	7.1

Table 3 lists the results of estimated characteristics of low-temperature stage thermoelectric modules assuring cooling to temperature below 200 K at a tempertaure of heat-releasing surface 300 K. Maximum coefficient of performance was calculated with regard to the above-mentioned approaches. The calculations employed computer methods developed on the basis of optimal control theory [14].

It was determined that to achieve the temperatures of 160 to 200 K it is sufficient to use three-four-stage modules whose thermoelements are made of *Bi-Te* FGTM. Such FGTM can be created by forming a respective inhomogeneous distribution of impurities in material or changing its composition.

For cooling down to temperatures of 150 to 120 K a four-stage module of *Bi-Te* FGTM should be supplemented with low-temperature stages. In these stages it is reasonable to use for *n*-type legs the alloys based on *Bi-Sb*. At room temperature the figure of merit Z in *n-BiSb* is about $0.8 \cdot 10^{-3}$ K^{-1}, at low temperatures Z increases, reaching $5 \cdot 10^{-3}$ K^{-1} at 100 K. Magnetic field further increases this value to $8 - 9 \cdot 10^{-3}$ K^{-1} [15]. In this case *n*-type *Bi-Sb* FGTM, i.e. material with the varying main thermoelectric parameters α, σ, κ, can be obtained by optimally changing the induction of a magnetic field where this

material is placed. For further increase in the coefficient of performance one can use a combination of optimal inhomogeneity function of the field and optimal inhomogeneity of *Bi-Sb* material obtained by varying its composition [15]. Unfortunately, up to now in the arsenal of thermoelectricity there are no *p*-type materials with a similar magnetic field dependence of the figure of merit. Therefore, for *p*-type legs it is necessary to use FGTM based on traditional *Bi-Te* composition.

Table 3

Estimated values of low-temperature TEC characteristics

Cooling temperature T_c, K	Number of stages	Coefficient of performance, ε_{max}	Power at thermal load Q_0 = 10 mW, W, W	TEC material
200	3	$4\cdot10^{-2}$	0.25	*Bi-Te* FGTM
190	3	$2.5\cdot10^{-2}$	0.4	*Bi-Te* FGTM
180	4	$1.2\cdot10^{-2}$	0.83	*Bi-Te* FGTM
170	4	$5\cdot10^{-3}$	2.0	*Bi-Te* FGTM
160	4	$2\cdot10^{-3}$	5.0	*Bi-Te* FGTM
150	5	$8\cdot10^{-4}$	12.0	4 stages – *Bi-Te* FGTM, 1 upper stage – *n-BiSb* in the inhomogeneous magnetic field, *p-BiTe* FGTM
140	6	$3\cdot10^{-4}$	33.5	4 stages – *Bi-Te* FGTM, 2 upper stages – *n-BiSb* in the inhomogeneous magnetic field, *p-BiTe* FGTM
130	7	$1.8\cdot10^{-4}$	50.0	4 stages – *Bi-Te* FGTM, 3 upper stages – *n-BiSb* of nonuniform composition, in the inhomogeneous magnetic field, *p-BiTe* FGTM
120	7	$6\cdot10^{-5}$	170.0	4 stages – *Bi-Te* FGTM, 3 upper stages – *n-BiSb* of nonuniform composition, in the inhomogeneous magnetic field, *p-BiTe* FGTM
110	8	$1.4\cdot10^{-5}$	710.0	4 stages – *Bi-Te* FGTM, 4 upper stages – *n-BiSb* of nonuniform composition, in the inhomogeneous magnetic field, *p-BiTe* FGTM
100	9	$2.4\cdot10^{-6}$	4160	4 stages – *Bi-Te* FGTM, 5 upper stages – *n-BiSb* of nonuniform composition, in the inhomogeneous magnetic field, *p-BiTe* FGTM

Conclusions

The results of this research testify that practical use of modern technologies in the manufacture of modules allows expanding the temperature range of thermoelectric method of cooling IR sensors and can assure the operating temperatures of IR detectors up to 120 K with sufficient energy efficiency.

References

1. A. Rogalski, Progress in Focal Plane Arrays Technologies, *Progress in Quantum Electronics* **36** (2-3), 342 – 473 (2012).
2. M.V. Lipin, A.V. Gromov, Results of Development of a Series of Modular MCS Split-Stirling for Cryostatting Photodetectors of the 1-st and 2-nd Generations, *Applied Physics* **2**, 110 – 119 (2007).
3. M.V. Lipin, A.V. Gromov, State-of-the-Art and Prospects of Development of MCS Split-Stirling for Cooled Photodetectors, *Report to XXI International Scientific and Technical Conference on Photoelectronics and Night Vision Devices* (Moscow, May 25 – 28, 2010).
4. A. Veprik, S. Zehtzer, H. Vilenchik, and N. Pundak, Micro-Miniature Split Stirling Linear Crycooler, *AIP Conf. Proc*. **1218**, 363 – 370 (2010).
5. M.V. Lipin, A.V. Gromov, State-of-the-Art and Prospects of Development of MCS Split-Stirling for Cooled Photodetectors, Report to *XX International Scientific and Technical Conference on Photoelectronics and Night Vision Devices* (Moscow, May 27 – 30, 2008), www.cryontk.ru.
6. M.V. Lipin, A.V. Smirnov, E.A. Lohman, and E.V. Zabenkova, Results of Modernization of Cooling Module for 2nd Class Photodetectors of the Type MCS NSMG-3V-1/80 KVO.0733.000. *Report to XXI International Scientific and Technical Conference on Photoelectronics and Night Vision Devices* (Moscow, May 25 – 28, 2010).
7. M.A. Kinch, Fundamental Physics of Infrared Detector Materials, *J. Electronic Materials* **29** (6), 809 – 817 (2000).
8. Itay Shtrichman, Daniel Aronov, Michael ben Ezra, et al., High Operating Temperature *Epi-InSb* and *XBn-InAsSb* Photodetectors, *Proceedings of SPIE* **8353**, Infrared Technology and Applications XXXVIII, 83532Y, May 1, 2012.
9. A. Piotrowski, J. Piotrowski, W. Gawron, J. Pawluczyk, and M. Pedzinska, Extension of Usable Spectral Range of Peltier Cooled Photodetectors, *ACTA Physica Polonica A* **116**, s-52 – s-55 (2009).
10. http://www.vigo.com.pl/
11. Michel Vuillermet, Philippe Tribolet, Operating Temperature: a Challenge for Cooled IR Technologies, *Proc. of SPIE* **7660** (2010).
12. Philip Klipstein, Olga Klin, Steve Grossman, Noam Snapi, et al., High Operating Temperature *XBn-InAsSb* Bariode Detectors, *Proc. of SPIE* **8268** (2012).
13. S. Tsao, H. Lim, W. Zhang, and M. Razeghi, High Operating Temperature 320×256 Middle-Wavelength Infrared Focal Plane Array Imaging Based on an *InAs*/*InGaAs*/*InAlAs*/*InP* Quantum Dot Infrared Photodetector, *Aplied Physics Letters* **90**, 201109-1 – 201109-3 (2007).
14. L.I. Anatychuk, L.N. Vikhor, Thermoelectricity, Vol. IV. Functionally-Graded Thermoelectric Materials (Chernivtsi: Institute of Thermoelectricity, 2012), 180 p.
15. L.I. Anatychuk, L.N. Vykhor, Optimal Functions of Magnetic Field for One- and Multi-Stage Peltier Coolers, *Journal of Thermoelectricity* **2**, 14 – 19 (1998).

Submitted 09.10.2013.

R.G. Cherkez, P.P. Fenyak, D.D. Demyanyuk

Institute of Thermoelectricity of the NAS and MES of Ukraine,
1, Nauky Str., Chernivtsi, 58029, Ukraine

COMPUTER SIMULATION OF PERMEABLE COOLING THERMOELEMENT

The results of computer research on a 3 D model of permeable thermoelement for cooling liquid and gas flows are presented. The physical model and design of permeable thermoelement is described, its mathematical description is given. A method for thermoelement calculation based on the Comsol Multiphysics package of applied computer programs has been created. The energy characteristics of thermoelement of Bi-Te-Se-Sb based materials have been calculated as a function of heat carrier pumping rate and supply voltage. The optimal values of hear carrier rate at thermoelement inlet whereby the values of cooling capacity and coefficient of performance will be maximum have been determined. Comparison of the energy characteristics of liquid and air cooling has shown their 30 to 50 % better values on water cooling.

Key words: permeable thermoelement, simulation, thermodynamic characteristics, semiconductors, cooling capacity, coefficient of performance.

Introduction

The widest application of thermoelectric power converters is based on the use of a thermocouple element [1, 2] whose energy conversion efficiency is determined by the figure of merit Z of used materials. Therefore, a search for materials with a maximum figure of merit value becomes the main challenge of thermoelectric material science. However, despite the active research pursued in this direction, there has been no essential figure of merit growth in recent 20 to 30 years [3, 4]. The maximum values of the dimensionless figure of merit parameter of industrial thermoelectric materials remain at a level of 1 to 1.2. So, to improve the figure of merit, one should use new, non-traditional approaches which consist in the use of unconventional variants of physical models of a thermoelement which is the main component of thermoelectric power converter.

One of them is the use of thermoelements with a developed internal heat exchange surface, i.e. permeable thermoelements. In such thermoelements, heat exchange with the source of heat and heat sink occurs not only on the junctions, but also in the bulk of the leg. Already the first theoretical [5] and experimental [6] investigations of thermoelements for cooling gas flows demonstrated their good prospects. They indicate the possibility of energy conversion efficiency improvement by a factor of 1.3 to 1.4.

However, such investigations were performed for a single-dimensional model that does not describe accurately enough the conjugate processes of heat exchange in solid-heat carrier system. Therefore, it is necessary to create and study a more real 3 D model of permeable thermoelement which is the objective of this work.

Physical model and its mathematical description

A physical model of permeable thermoelement where heat exchange between the source of heat and heat sink takes place not only through connecting plates, but also in the bulk of the leg, is given in Fig. 1. It

includes *n*- and *p*-type legs 1 made of materials based on *Bi-Te-Se-Sb* which together with openings in connecting plates 3 form a system of channels for pumping heat carrier, namely water. The model takes into account the presence of transient layer 2 due to a combination of connecting plates with thermoelement legs that has the properties of a solder. The legs material is homogeneous and isotropic with known temperature dependences of electric conductivity $\sigma(T)$, the Seebeck coefficient $\alpha(T)$, thermal conductivity $\kappa(T)$. The thermoelectric medium takes into account the bulk Thomson and Joule-Lenz effects and the near-contact Peltier effect. The temperature of heat carrier at thermoelement inlet was assumed equal to hot junction temperature.

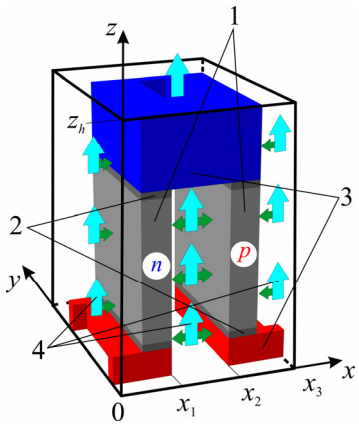

Fig. 1. Physical model of permeable thermoelement: 1 are n- and p-type legs; 2 is transient layer possessing the properties of a solder; 3 are connecting legs; 4 is heat carrier.

Heat exchange on the lateral surface of legs 1, connecting plates 3 and transient layer 2 that are in thermal contact with heat carrier 4 is described by the Newton-Richmann law:

$$q_0 = \alpha_T (t - T), \tag{1}$$

where α_T is heat exchange coefficient, T is thermoelement temperature, t is heat carrier temperature.

A system of equations describing the distribution of temperature and potential in thermoelectric medium is described by the fundamental laws of conservation of energy and current carriers [7]:

$$\nabla \vec{W} = 0, \tag{2}$$

$$\nabla \vec{i} = 0, \tag{3}$$

where $\vec{W} = \vec{q} + U\vec{i}$ is energy flux density.

Using the generalized Fourier's and Ohm's laws for the thermoelectric medium

$$\vec{q} = -\kappa \nabla T + \alpha \vec{i} T, \tag{4}$$

$$\vec{i} = -\sigma(\nabla U + \alpha \nabla T), \tag{5}$$

where U is potential, κ is thermal conductivity, α is the Seebeck coefficient, σ is electric conductivity, one can obtain a system of differential equations to find the distributions of temperatures and potentials:

$$\left.\begin{aligned} &\nabla \kappa \nabla T + \frac{i^2}{\sigma} - T\vec{i}\nabla\alpha = 0; \\ &\nabla(-\sigma(\nabla U + \alpha \nabla T)) = 0. \end{aligned}\right\} \tag{6}$$

The Navier-Stokes equation system and the continuity equation are used to describe heat carrier motion along a channel, and thermal conductivity equation is used to describe temperature distribution in heat carrier.

The Navier-Stokes equation and the continuity equation can be written as [8]:

$$\left.\begin{aligned} &\rho \frac{d\vec{\vartheta}}{dt} = \rho\vec{F} - \nabla P + \mu \nabla^2 \vec{\vartheta} + \frac{1}{3}\mu \nabla (div\,\vec{\vartheta}), \\ &div\ \rho\vec{\vartheta} = 0. \end{aligned}\right\} \tag{7}$$

The left side of the first equation (7) is the inertia force. The first term on the right side of this equation describes mass (volumetric) force, the second term – surface pressure forces (normal stresses), and the last two terms – tangential components of surface forces (internal friction forces).

Heat exchange in liquid is described by thermal conductivity equation [9]:

$$\rho C_p\left(\frac{\partial t}{\partial \tau}+(\vec{\vartheta}\nabla)t\right)=-(\nabla\vec{q})+\sum_{i,j}\Lambda_{ij}S_{ij}-\frac{t}{\rho}\frac{\partial\rho}{\partial t}\bigg|_P\left(\frac{\partial\rho}{\partial t}+(\vec{\vartheta}\nabla)P\right)+Q, \tag{8}$$

where ρ is liquid density, C_p is liquid specific heat, t is liquid temperature, $\vec{\vartheta}$ is liquid rate vector, $\vec{q}$ is heat flux density vector, P is pressure, Λ_{ij} is viscous stress tensor, $\vec{S}_{ij}$ is deformation rate tensor, Q are internal heat sources.

Of greatest practical interest is the problem of calculation of thermoelement energy characteristics in steady-state operating mode. In this case, time derivatives in (7) and (8) are set to zero. In the approximation of small influence of mass forces and insufficient liquid heating due to internal friction, its compression, as well as liquid heating at the cost of internal heat sources will be ignored in view of their small contribution as compared to thermoelectric thermal effects. In such approximations, the system of Navier-Stokes continuity and thermal conductivity equations will be written as:

$$\left.\begin{aligned}&-\nabla P+\mu\nabla^2\vec{\vartheta}+\frac{1}{3}\mu\nabla(div\vec{\vartheta})=0,\\&div\ \rho\vec{\vartheta}=0,\\&\rho C_p(\vec{\vartheta}\nabla)t+\nabla q=0.\end{aligned}\right\} \tag{9}$$

The boundary conditions for this problem (Fig. 1), are given below:

– for thermoelectric medium

$$T\big|_{z=0}=300\text{K},\ U\big|_{z=0}=0,\ U\big|_{x=x_3}=U_0,\ q\big|_{S_b}=\alpha_T(t-T),\ U\big|_{S_b}=0, \tag{10}$$

– for heat carrier

$$\vartheta\big|_{z=0}=\vartheta_0,\ P\big|_{z=z_h}=0,\ \vartheta\big|_{S_b}=0,\ t\big|_{z=0}=300\text{K},\ q\big|_{S_b}=\alpha_T(T-t), \tag{11}$$

where ϑ_0 is heat carrier initial rate, U_0 is given potential value, S_b is thermoelement lateral surface.

Realization of the formulated problem in the Comsol Multiphysics package of applied computer programs

To perform the calculation, the Comsol Multiphysics package of applied computer programs was selected [10]. The general view of the coefficient form of equation in partial derivatives is as follows:

$$e_a\frac{\partial^2\vec{u}}{\partial t^2}+d_a\frac{\partial\vec{u}}{\partial t}+\nabla(-c\nabla\vec{u}-\alpha\vec{u}+\gamma)+\beta\nabla u+a\vec{u}=f. \tag{12}$$

This equation is used for the thermoelectric medium and reduced to the form $\nabla(-c\nabla\vec{u})=0$. For this purpose, e_a, d_a, α, γ, β, a are set to zero, and the value c is written as a matrix:

$$c=\begin{pmatrix}\kappa+\alpha^2\sigma T+\sigma U\alpha & \alpha T\sigma+\sigma U\\ \alpha\sigma & \sigma\end{pmatrix}. \tag{13}$$

In this case, vector $\vec{u}$ has also the form of a matrix:

$$\vec{u} = \begin{pmatrix} T \\ U \end{pmatrix}. \tag{14}$$

To describe liquid motion and heat exchange, the Comsol Multiphysics-Non-Isothermal Flow is used [11]. The module includes the Navier-Stokes equation system, the continuity equation and liquid heat transfer equation in the steady-state mode.

The electric current value was calculated through the integral according to sectional area S_V:

$$I = \iint_{S_V} I_n \mathrm{d}S_V, \tag{15}$$

where $I_n = n_x I_x + n_y I_y + n_z I_z$ is electric current density vector. The values I_x, I_y, I_z, were determined by the relations:

$$I_x = -\sigma \frac{\partial U}{\partial x} - \sigma\alpha \frac{\partial T}{\partial x}, \tag{16}$$

$$I_y = -\sigma \frac{\partial U}{\partial y} - \sigma\alpha \frac{\partial T}{\partial y}, \tag{17}$$

$$I_z = -\sigma \frac{\partial U}{\partial z} - \sigma\alpha \frac{\partial T}{\partial z}. \tag{18}$$

Heat carrier flow rate was determined by integration of rate υ with respect to channel sectional area at liquid outlet S_{V1}:

$$G = \iint_{S_{V1}} \vartheta \mathrm{d}S_{V1}. \tag{19}$$

The thermoelement electric power $W = I \cdot U$, cooling capacity was determined through heat carrier flow rate as $Q_c = GC_p\Delta t$, coefficient of performance $\varepsilon = Q_c/W$.

Results of computer research on the energy characteristics of liquid and air permeable thermoelement of materials based on *Bi-Te-Se-Sb*

The calculation was performed for materials based on *Bi-Te-Se-Sb*. Functional temperature dependences of material parameters, namely the Seebeck coefficient α, thermal conductivity κ and electric conductivity σ were obtained by the least squares method from their experimental data.

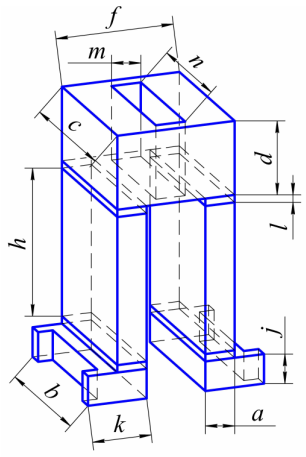

Fig. 2. Design of permeable thermoelement.

Simulation of permeable thermoelement was done for the following basic design (Fig. 2): height h = 10 mm, length b = 10 mm, width a = 2 mm. The dimensions of the lower connecting plates – height j = 2 mm, length b = 10 mm, width k = 4 mm; upper connecting plates – height d = 5 mm, length c = 10 mm, width f = 8 mm. Connecting material is copper. Connecting plates have cuts for heat carrier pumping of length n = 8 mm, width m = 2 mm, located in the plate centre. These cuts together with legs form a system of channels for heat carrier pumping. The design takes into account the presence of transient solder layer of thickness l = 0.5 mm.

Heat carrier flow rate at thermoelement inlet was assumed equal to 0.1 mm/s, 0.5 mm/s, 1 mm/s, 2 mm/s, 3 mm/s, 4 mm/s and 5 mm/s. With each rate value the supply voltage assumed the values: 0.02 V, 0.04 V, 0.06 V, 0.08 V, 0.10 V, 0.12 V, 0.14 V, 0.16 V and 0.18 V. Coefficient of heat exchange between water and thermoelement α_T in the Newton-Richmann law was assumed equal to 1000 W/(m^2·K).

For the above parameters the following thermoelement characteristics were determined: the values of electric current I, A; flow rate G, m^3/s; outlet liquid temperature t, °C; thermoelement cold junction temperatures T, °C; temperature difference of liquid Δt, °C and thermoelement ΔT, °C; power W, W; cooling capacity Q_c, W; coefficient of performance ε.

From the results of computer calculation the following energy characteristics were obtained: cooling capacity, coefficient of performance (Fig. 3 *a*) and temperature difference on the water and thermoelement (Fig. 3 *b*) depending on thermoelement voltage and different water flow rate.

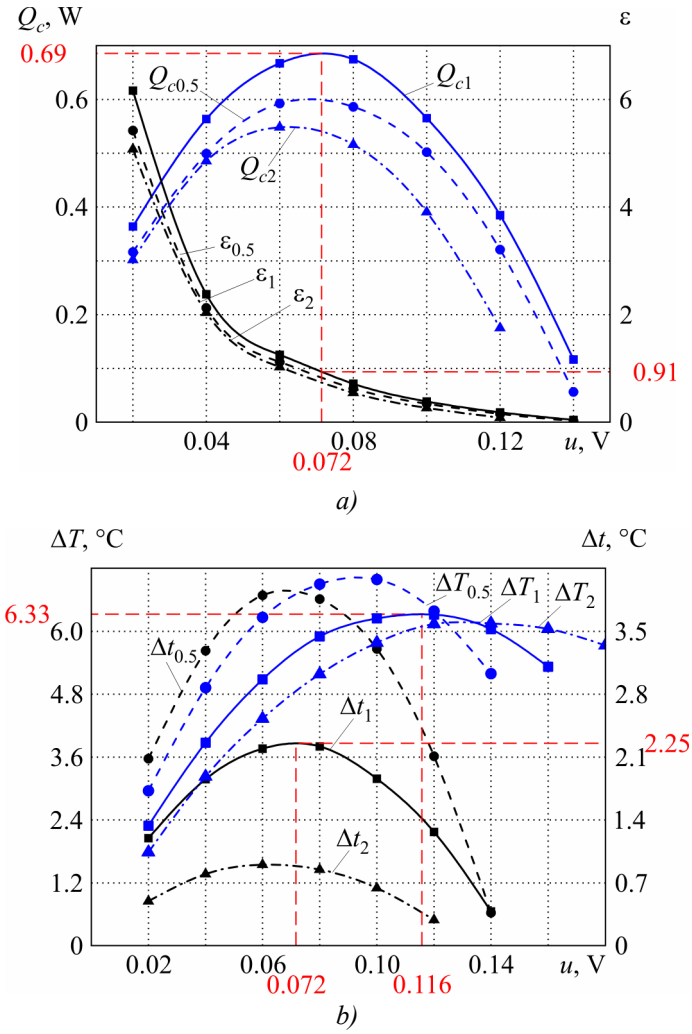

Fig. 3. Cooling capacity, coefficient of performance (a) and temperature difference of liquid and thermoelement (b) versus voltage for different rates: $Q_{c0.5}$, Q_{c1}, Q_{c2} is cooling capacity at liquid rate 0.5 mm/s, 1 mm/s, 2 mm/s, respectively; $\varepsilon_{0.5}$, ε_1, ε_2 is coefficient of performance at liquid rate 0.5 mm/s, 1 mm/s, 2 mm/s, respectively; $\Delta T_{0.5}$, ΔT_1, ΔT_2 is thermoelement temperature difference, $\Delta t_{0.5}$, Δt_1, Δt_2 is liquid temperature difference at the rate of 0.5 mm/s, 1 mm/s, 2 mm/s.

It is seen that maximum cooling capacity value falls on the rate $\upsilon = 1$ mm/s and makes $Q_c = 0.68$ W at the voltage of $u = 0.07$ V, and energy conversion at maximum cooling capacity occurs

with a thermodynamic efficiency $\varepsilon = 0.91$. Temperature difference on the thermoelement is $\Delta T = 6.3$ °C at the voltage of $u = 0.12$ V, and temperature difference on the liquid $\Delta t = 2.25$ °C.

To specify the value of optimal rate, the rate dependence of maximum cooling capacity with the optimal voltage has been constructed (Fig. 4). The same figure shows the dependence of temperature difference on the liquid obtained under these conditions.

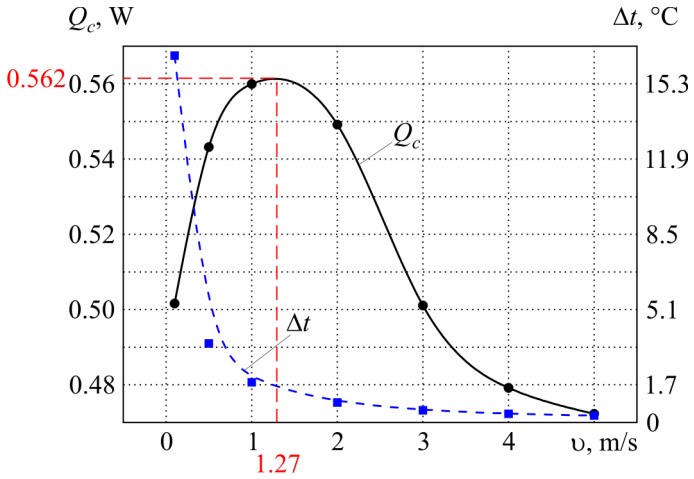

Fig. 4. Maximum cooling capacity and temperature difference of liquid versus the rate.

It is seen that maximum cooling capacity value is achieved at the rate of $\upsilon = 1.27$ mm/s. Temperature difference on the liquid increases with the rate decrease, which provides for a greater water cooling depth. A greater cooling depth calls for a lower water delivery rate, however, cooling capacity in this case is reduced. The existence of a rational range of water feed rate values determined by thermoelement operating mode is evident.

The distribution of temperature field in thermoelement and liquid at thermoelement voltage $u = 0.06$ V and optimal water rate at channel inlet $\upsilon = 1.27$ mm/s is given in Fig. 5 *a*. The distribution of rate field under these conditions is represented in Fig. 5 *b*.

In Fig. 5 *a* it is seen that the medium part of legs is overheated due to the Joule-Lenz heat release and heat input from the liquid. However, in the interconnect area the effect of Peltier heat is greater, which provides for water cooling. From Fig. 5 *b* it is seen that maximum rate is achieved with the lowest channel section.

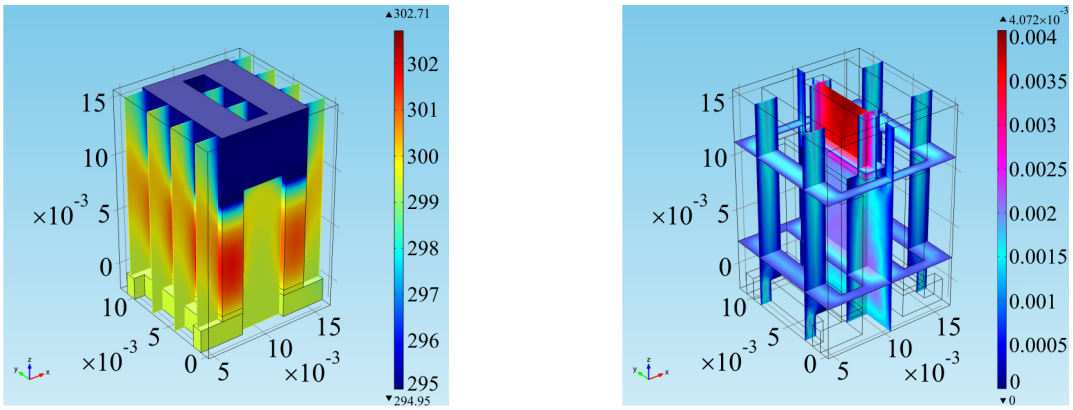

a) *b)*

Fig. 5. Temperature distributions in the thermoelement and liquid (a) and rate field distribution in the liquid (b).

Fig. 6 gives the dependences of the energy characteristics of liquid permeable thermoelement with the optimal liquid rate at channel inlet on thermoelement voltage.

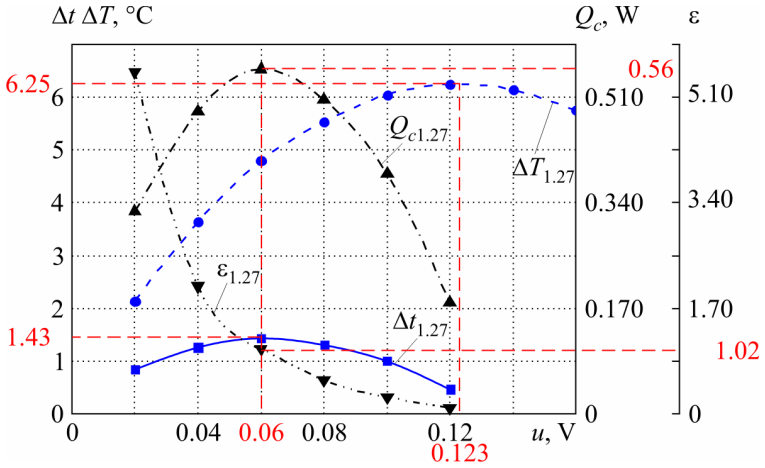

Fig. 6. Maximum cooling capacity Q_c, coefficient of performance ε, liquid temperature difference Δt, thermoelement ΔT versus voltage for the optimal rate.

It is evident from the figure that maximum value of cooling capacity $Q_c = 0.56$ W is achieved at the voltage of $u = 0.06$ V, and energy conversion in maximum cooling capacity mode occurs with thermodynamic efficiency ε = 1.023.

Maximum temperature difference value of thermoelement is equal to $\Delta T = 6.25$ °C at the voltage of $u = 0.12$ V, and of liquid – $\Delta t = 1.43$ °C at the voltage of $u = 0.06$ V.

A similar computer model for the air thermoelement in cooling mode was developed. The specific feature of this model of permeable air thermoelement is that heat carrier properties are replaced by gas-air thermophysical properties. The heat-exchange coefficient at the water-air interface in the Newton-Richmann law is at a level of 100 W/(m^2·K). The air rate at channel inlet was assumed equal to υ = 0.4 m/s. According to experimental investigations given in [6], this rate is optimal for the above geometry of thermoelement legs.

The distribution of temperature field in the thermoelement and in the air with the air rate at channel inlet υ = 0.4 m/s and thermoelement voltage $u = 0.08$ V is given in Fig. 7 *a*; the distribution of rate field in the air under these conditions is shown in Fig 7 *b*.

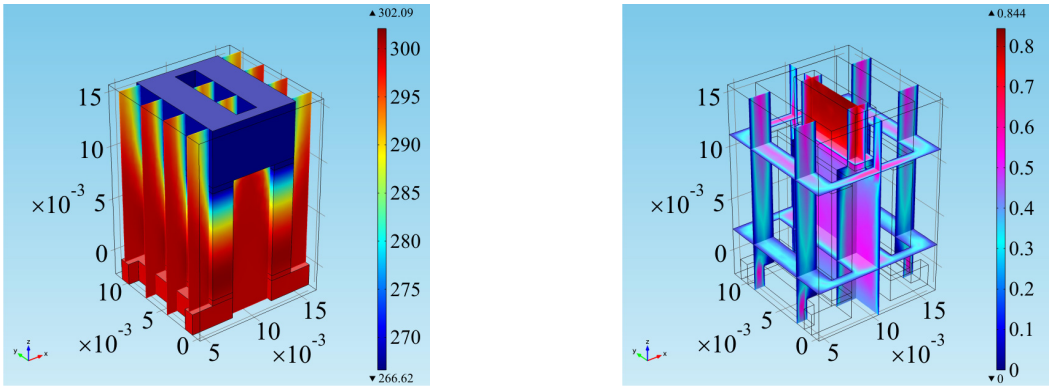

a) *b)*

Fig. 7. Temperature field distribution in the thermoelement and in the air (a) and rate field distribution in the air (b).

From Fig. 7 *a* it is seen that leg overheat due to the Joule-Lenz effect and thermal flux from the air is considerably less than in the liquid permeable thermoelement. Thus, one can make a conclusion

on the effect of thermophysical properties of liquid or gas heat carrier on the temperature field. The Peltier heat absorbed in the near-contact area prevails over heating and provides for cooling. From Fig. 7 *b* it is seen that the maximum rate is achieved with the smallest channel section which is similar to rate field distribution for water.

Fig. 8 shows voltage dependences of the energy parameters of the air thermoelement for the air rate at channel inlet $\upsilon = 0.4$ m/s.

From Fig. 8 it is seen that maximum cooling capacity value of the air permeable thermoelement $Q_c = 0.42$ W is achieved at the voltage of $u = 0.086$ V, and energy conversion with maximum cooling capacity occurs with the efficiency of $\varepsilon = 0.41$. Maximum temperature difference value of the air permeable thermoelement is equal to $\Delta T = 35.7$ °C at the voltage of $u = 0.11$ V, and of the liquid – $\Delta t = 11.44$ °C at the voltage of $u = 0.086$ V.

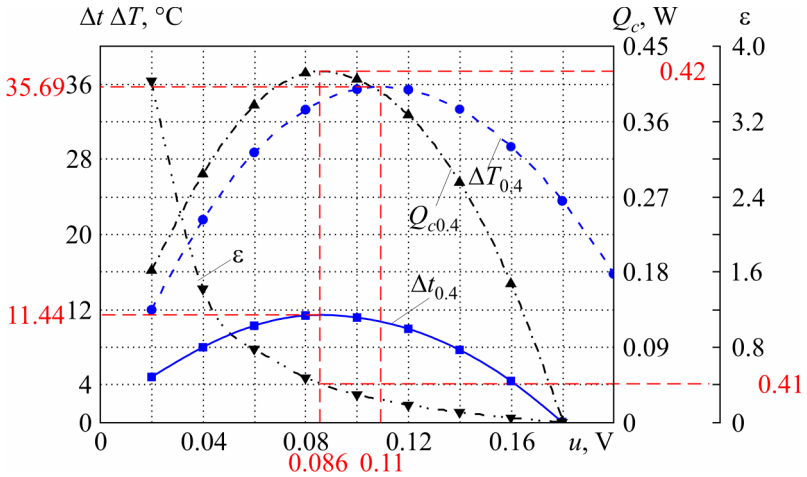

Fig. 8. Maximum cooling capacity Q_c, coefficient of performance ε, air temperature difference Δt, thermoelement temperature difference ΔT for the optimal rate versus voltage.

Based on the obtained results of calculation of permeable thermoelement for cooling liquid and gas flows in a three-dimensional case under optimal conditions, comparative dependences of cooling capacity and coefficient of performance have been constructed that are given in Fig. 9.

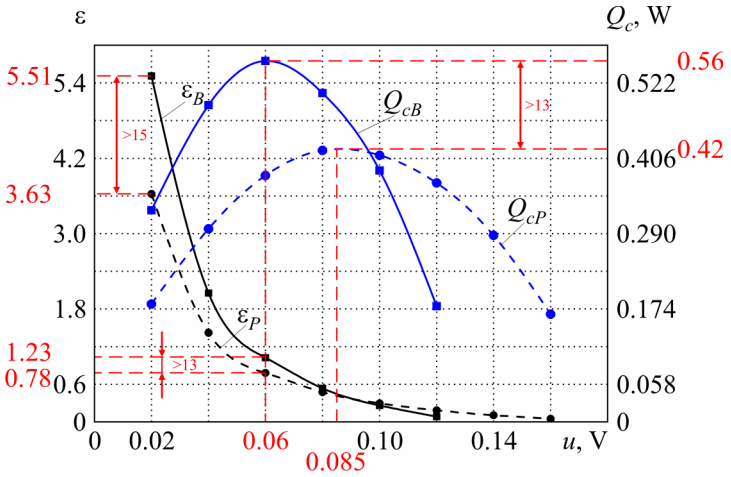

Fig. 9. Comparative dependence of cooling capacity Q_c, coefficient of performance ε for the liquid (index B) and the air (index P) on thermoelement voltage under optimal conditions.

From the above dependences it is seen that maximum cooling capacity value of the liquid permeable thermoelement $Q_{cB} = 0.56$ W is achieved at lower thermoelement voltage $u = 0.06$ V than

that of the air one – $Q_{cP} = 0.42$ W at a voltage of $u = 0.086$ V. In so doing, cooling capacity of the liquid thermoelement is higher than that of the air one by a factor of 1.3. Coefficient of performance of the liquid thermoelement at a voltage of $u = 0.02$ V exceeds that of the air thermoelement by a factor of 1.5, and at a voltage of $u = 0.06$ V – by a factor of 1.3.

Thus, there are optimal ranges of voltage values where the energy capabilities of permeable thermoelement for water cooling are superior to energy characteristics of thermoelement for air cooling. Therefore, there is a need in multi-parameter optimization of structural and thermophysical parameters of permeable thermoelement that will make it possible to determine maximum thermodynamic characteristics.

Conclusions

1. A 3*D* model of permeable thermoelement for cooling liquid and gas flows has been elaborated in the Comsol Multiphysics package of applied computer programs.
2. The distributions of temperatures in material of thermoelement legs and heat carrier, potentials in thermoelement, liquid rates and the energy characteristics of permeable thermoelement of materials based on *Bi-Te-Se-Sb* have been determined.
3. The effect of heat carrier pumping rate and thermoelement supply voltage on temperature difference and energy conversion characteristics has been investigated. The optimal values of water feed rate at channel inlets and potential difference on thermoelement whereby maximum cooling capacity is realized on liquid and air cooling have been determined.
4. Comparison of research results has shown the presence of such voltage range on thermoelement whereby the liquid permeable thermoelement outperforms the air one by a factor of 1.3 to 1.5.

References

1. L.I. Anatychuk, *Thermoelements and Thermoelectric Devices: Handbook* (Kyiv: Naukova Dumka, 1979), 768 p.
2. L.I. Anatychuk, *Physics of Thermoelectricity [Thermoelectricity, V. 1]* (Chernivtsi, 1998), 388 p.
3. G.J. Snyder, E.S. Toberer, Complex Thermoelectric Materials, *Nature Materials* **7**, 105 – 114 (2008).
4. L.I. Anatychuk, Current Status and Some Prospects of Thermoelectricity, *J. Thermoelectricity* **2,** 7 – 20 (2007).
5. L.I. Anatychuk, L.N. Vikhor, R.G. Cherkez, Optimal Control of the Inhomogeneity of Semiconductor Material for Permeable Cooling Thermoelements, *J. Thermoelectricity* **3**, 45 – 55 (2000).
6. L.I. Anatychuk, R.G. Cherkez, D.D. Demyanyuk, and N.R. Bukharayeva, Research on the Energy Characteristics of Permeable Plane Thermoelement, *J. Thermoelectricity* **2**, 84 – 88 (2012).
7. L.I. Anatychuk, V.A. Semenyuk, *Optimal Control of the Properties of Thermoelectric Materials and Devices* (Chernivtsi: Prut, 1992), 264 p.
8. I.M. Kadenko, O.M. Kharitovov, R.V. Yermolenko, *The Basics of Thermal Hydraulics of Nuclear Energy Installations* (Kyiv: Publishing and Printing Centre "Kyiv University", 2010), 320 p.
9. D.I. Okhrimenko, *The Use of COMSOL Multiphysics 3.4 Package for Solving Hydrodynamics and Heat Exchange Problems in Chemical Technology* [Yearly Project] (Donetsk, 2009), 64 p.
10. G.V. Biryullin, *Thermophysical Calculations in Finite-Element Package COMSOL/FEMLAB: Manual* (Saint-Petersburg: The National Research University ITMO, 2006), 78 p.
11. http://www.coml.com.

Submitted 09.10.2013.

L.I. Anatychuk, R.R. Kobylyanskii

L.I. Anatychuk

Institute of Thermoelectricity of the NAS
and MES of Ukraine, 1 Nauky Str.,
Chernivtsi, 58029, Ukraine

R.R. Kobylyanskii

ON THE ACCURACY OF TEMPERATURE MEASUREMENT BY ELECTRONIC MEDICAL THERMOMETER WITH THERMOELECTRIC POWER SUPPLY

The paper presents the results of computer studies on the impact of thermoelectric power supply of electronic medical thermometer on the accuracy of temperature measurement. Computer simulation was used to establish the dependence of the magnitude of temperature measurement error due to the impact of thermoelectric power supply on the distance between the sensor and thermoelectric power supply. An improved design of electronic medical thermometer with thermoelectric power supply was developed.

Key words: computer simulation, thermoelectric power supply, electronic medical thermometer, accuracy of temperature measurement.

Introduction

General characterization of the problem. At the present time, measurement of body temperature in medicine is one of the first and most common factors of the level of human health. For more than 300 years somatic temperature has been measured using mercury thermometers.

Until quite recently, nearly 45 million mercury thermometers have been produced in the world annually, with 45 tons of mercury spent on their production. Sooner or later, through negligent use of thermometers they were broken, and mercury was buried in the cracks of dwelling houses or hospitals, gradually poisoning the people there. So, in recent decades, due to advances in microelectronics, electronic medical thermometers have been developed that replace mercury ones little by little.

However, it does not solve environmental problems in full measure. As power supplies for electronic thermometers, chemical galvanic elements are used which contain poisonous substances, such as alkali, lead, cadmium, mercury, zinc and nickel. According to statistics, nearly 200 million electronic thermometers have been already fabricated, whereas to assure population with such thermometers they are needed in the amount about 1 milliard pieces. That is, such amount of chemical galvanic elements must be replaced in thermometers yearly, since their service life is not more than one year, and with intensive use of thermometer, for instance, in hospital, it is considerably less. However, recycling and processing of such galvanic elements is practically absent.

Chemical galvanic elements have another disadvantage, namely in the period of their expiry date the electronic thermometer readings become unreliable. This problem is important, since thermometer readings determine immediate actions that should be taken. The foregoing implies that replacement of chemical galvanic elements and development of thermoelectric power supply for electronic thermometer owing to which the thermometer will be operated on human body heat is a

problem of today [1-10]. However, no less important here is the accuracy of temperature measurement using electronic medical thermometer with thermoelectric power supply.

Therefore, the purpose of this work is to determine the impact of thermoelectric power supply of electronic medical thermometer on the accuracy of temperature measurement.

Computer simulation of the impact of thermoelectric power supply of electronic medical thermometer on the accuracy of temperature measurement

Electronic medical thermometer with thermoelectric power supply consists of three main functional units: temperature sensor, temperature recorder and thermoelectric power supply, operated on human body heat. It is common knowledge that the availability of heat sink, such as thermoelectric power supply, leads to a change in the temperature and thermal fields in the area of temperature measurement. This, in turn, reduces the accuracy of temperature measurement using such thermometer.

With a view to determine the impact of thermoelectric power supply of electronic medical thermometer on the accuracy of temperature measurement, a three-dimensional computer model of biological tissue was created, whose surface contacts the thermoelectric power supply of thermometer. The computer model was constructed with the use of Comsol Multiphysics package of applied programs [11], which allows simulating thermophysical processes in human body biological tissue with regard to blood circulation and metabolic processes. Calculation of temperature and thermal flux density distributions in the biological tissue and thermoelectric heat meter was done by finite-element method.

Computer simulation was used to determine the impact of thermoelectric power supply of electronic medical thermometer on the temperature of human skin surface under real operating conditions. Dependence of temperature measurement error on the distance between temperature sensor and thermoelectric power supply was established (Fig. 1 *a*, *b*).

It is established that to reduce the error of human body temperature measurement using such thermometer, the distance between temperature sensor and thermoelectric power supply must be such whereby a change in human body temperature caused by thermoelectric power supply would not change the temperature of the body where temperature sensor is located.

From Fig. 1 *a* it is evident that with arrangement of temperature sensor and thermoelectric power supply on the surface of human body at the distance of $L = 2$ cm, the deviation of measured temperature value from the true one is $\Delta T = 0.1$ °C. With the distance between temperature sensor and thermoelectric power supply $L = 5$ cm the deviation of temperature is $\Delta T = 0.01$ °C (Fig. 1 *b*). Thus, the accuracy of human body temperature measurement using electronic medical thermometer with thermoelectric power supply will depend on the selection of thermometer design, that is, on the distance between temperature sensor and thermoelectric power supply.

Hence it follows that, structurally, electronic medical thermometer with thermoelectric power supply must be made so that the distance between temperature sensor and thermoelectric power supply be equal to or greater than the value determined by the dependence of distance L on temperature deviation ΔT. The dependence $L(\Delta T)$ is a reciprocal function to that shown in Fig. 1 *a*. Using computer approximation of dependence $L(\Delta T)$, the following analytical form of such dependence was obtained:

$$L(\Delta T)=\left(a+c\cdot\Delta t^{0.5}+e\cdot\Delta t+g\cdot\Delta t^{1.5}+i\cdot\Delta t^{2}\right)/\left(1+b\cdot\Delta t^{0.5}+d\cdot\Delta t+f\cdot\Delta t^{1.5}+h\cdot\Delta t^{2}+j\cdot\Delta t^{2.5}\right), \quad (1)$$

where L is the distance between temperature sensor and thermoelectric power supply, ΔT is temperature measurement error, coefficients $a = 56.667757$, $b = 55.97536$, $c = 4504.9994$, $d = 5420.2644$, $e = 193369.08$, $f = 16196.544$, $g = -62445.826$, $h = -7992.4153$, $i = -8885.923$, $j = 4548.9939$.

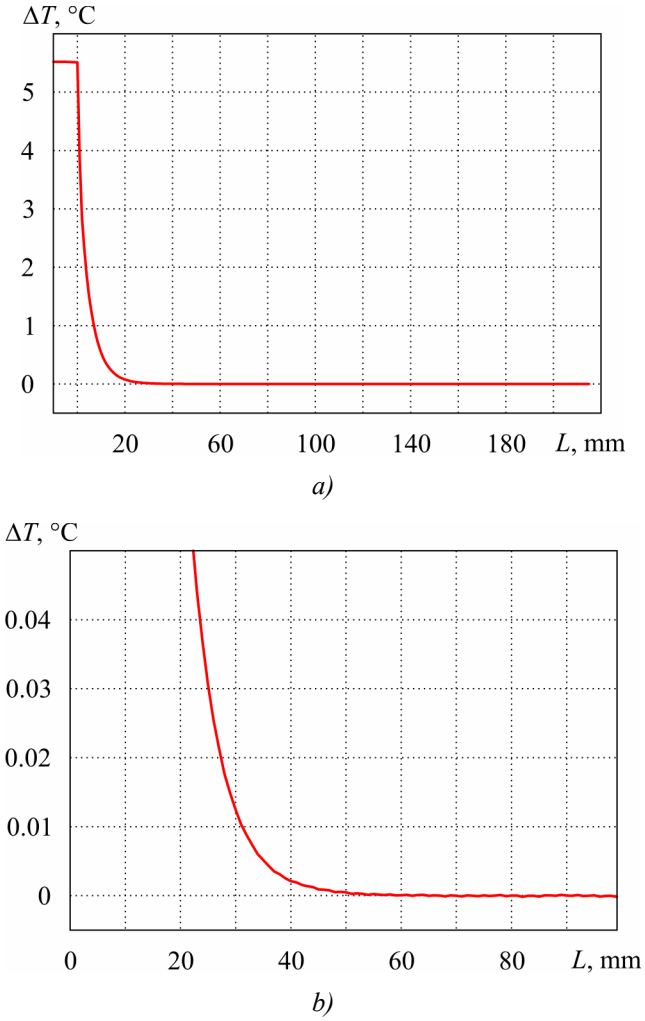

Fig. 1. Deviation of human body temperature in measurement area due to the impact of thermoelectric power supply of electronic medical thermometer a) in full range of change in temperature measurement error, b) in the range of optimal temperature measurement error (ΔT is temperature deviation (temperature measurement error), L is the distance from the edge of thermoelectric power supply of thermometer).

Design of electronic medical thermometer with thermoelectric power supply

Fig. 2 represents schematic design of electronic medical thermometer with thermoelectric power supply. Such thermometer comprises the electronic medical thermometer itself and thermoelectric power supply. In turn, the electronic medical thermometer comprises case 1, temperature sensor 2, analog-to-digital converter 3, voltage stabilizer 4, capacitor 5 and digital display 6. Thermoelectric power supply consists of two thermoelectric micromodules 7 and heat sink 8 that removes heat from the cold sides of thermoelectric micromodules 7 to the environment. Heat sink 8 is a case of material with high thermal conductivity. Temperature sensor 2 is arranged on the tip of thermally non-conductive element 9 connected to thermoelectric power supply. The length of thermally non-conductive element 9 was selected according to dependence (1) with regard to condition of non-exceeding prescribed temperature measurement error. Each thermoelectric micromodule 7 comprises a flat thermopile [1, 2] which is composed of a combination of semiconductor thermocouple elements connected into a series electric circuit, the intervals between which are filled with electrically isolating epoxy compound, and two ceramic plates closely contacting the upper and lower surfaces of

thermocouple elements, as well as two electric leads. Such micromodule is made on the basis of modern high-performance thermoelectric materials based on *Bi-Te*.

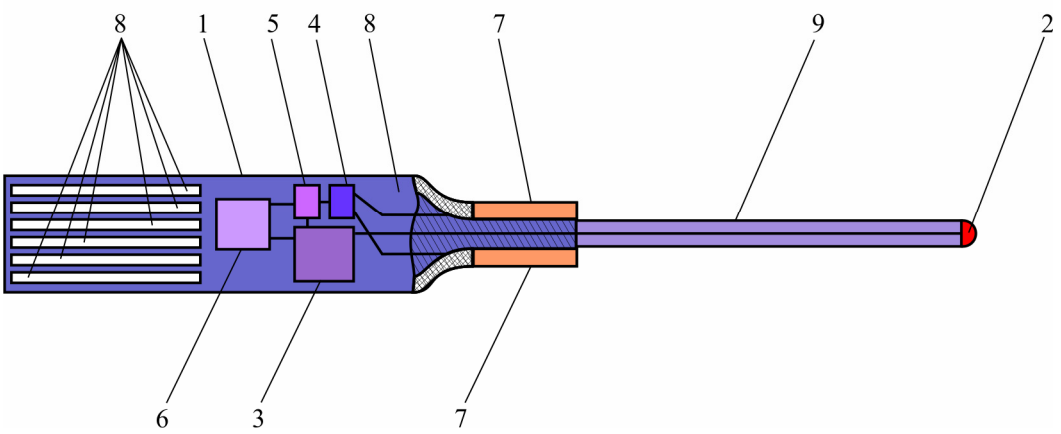

Fig. 2. Design of electronic medical thermometer with thermoelectric power supply [10]: 1 – case, 2 – temperature sensor, 3 – analog-to-digital converter, 4 – voltage stabilizer, 5 – capacitor, 6 – digital display, 7 – thermoelectric micromodules, 8 – heat sink, 9 – thermally non-conductive element.

Measurement of human body temperature using electronic medical thermometer is done by temperature sensor 2 in direct contact with human body, and electric power supply to such thermometer is assured by thermoelectric micromodules 7 due to human body heat. In order to obtain the required electric voltage and power using thermoelectric micromodules 7 for power supply to electronic medical thermometer, one should create temperature difference between the surfaces of micromodules. Application of electronic medical thermometer with thermoelectric power supply to human body (for instance, in the armpit) creates temperature gradient between the respective surfaces of thermoelectric micromodules 7 owing to which thermoelectromotive force (thermoEMF) will be generated on their leads, providing electric power supply to such device. The value of thermoEMF corresponds to the value of thermal flux passing through thermoelectric micromodules 7 whose cold sides contact heat sink 8 that removes heat to the environment. The device design also employs voltage stabilizer 4 of thermoelectric micromodules 7 to the level of 1.5 V and capacitor 5 for the accumulation of electric charge necessary for switching the electronic medical thermometer.

As compared to conventional electronic thermometer, such thermometer offers the advantage of ecological safety, as long as it comprises no chemical galvanic power supplies that require special recycling, as well as of ease of operation due to the absence of periodic replacement of power supplies. The suggested thermometer design assures increased accuracy of human body temperature measurement using electronic medical thermometer with thermoelectric power supply, the electric power supply to such thermometer being stable in time and requiring no maintenance expenses.

Conclusions

1. Using computer simulation, the impact of thermoelectric power supply of electronic medical thermometer on the accuracy of temperature measurement was determined. The dependence of the magnitude of temperature measurement error due to the impact of thermoelectric power supply on the distance between the sensor and thermoelectric power supply was established.
2. Design of electronic medical thermometer with thermoelectric power supply was developed which allows increasing the accuracy of human body temperature measurement using such thermometer.

References

1. L.I. Anatychuk, *Thermoelements and Thermoelectric Devices: Handbook* (Kyiv: Naukova Dumka, 1979), 768 p.
2. L.I. Anatychuk, *Thermoelectricity, Vol. 2, Thermoelectric Power Converters* (Kyiv-Chernivtsi: Institute of Thermoelectricity, 2003), 376 p.
3. L.I. Anatychuk, Rational areas of investigation and application of thermoelectricity, *J. Thermoelectricity* **4**, 3 – 15 (2000).
4. L.I. Anatychuk, Current Status And Some Prospects Of Thermoelectricity, *J. Thermoelectricity* **2**, 7 – 20 (2007).
5. L.T. Strutynska, Thermoelectric Microgenerators, Current Status and Prospects of Using, *Tekhnologiya i Konstruirovaniye v Elektronnoi Apparature* **4**, 5 – 13 (2008).
6. L.I. Anatychuk, R.R. Kobylyanskii, S.B. Romanyuk, Electronic Medical Thermometer with a Thermoelectric Power Supply, *Poster report to XV International Forum on Thermoelectricity* (Tallinn, Estonia, 2013).
7. L.I. Anatychuk, R.R. Kobylyanskii, S.B. Romanyuk, *Application № u201308794 of 15.07.13*. Electronic Medical Thermometer with a Thermoelectric Power Supply.
8. L.I. Anatychuk, R.R. Kobylyanskii, S.B. Romanyuk, *Application № u201308855 of 15.07.13*. Electronic Medical Thermometer with a Photoelectric Power Supply.
9. L.I. Anatychuk, R.R. Kobylyanskii, S.B. Romanyuk, *Application № u201308793 of 15.07.13*. Electronic Medicxal Thermometer with a Combined Power Supply.
10. L.I. Anatychuk, *Application № u201312570 of 28.10.13.* Electronic Medical Thermometer with a Thermoelectric Power Supply, 2013.
11. *COMSOL Multiphysics User's Guide* (COMSOLAB, 2010), 804 p.

Submitted 29.10.2013.

T.A. Ismailov, O.V. Yevdulov, D.V. Yevdulov

Federal State Budget Educational Institution of Higher Professional Education
"Dagestan State Technical University", 70, Imam Shamil Ave.,
Makhachkala, 367015, Russia

RESULTS OF FULL-SCALE TEST OF A PROTOTYPE SYSTEM FOR NON-UNIFORM COOLING OF ELECTRONIC BOARDS

This paper is concerned with a description of a prototype system for non-uniform cooling of electronic boards and a test bench for conducting its full-scale test. The respective results of experimental research are given. Based on the full-scale test it has been determined that non-uniform cooling of electronic boards is superior to uniform one in the energy and mass-dimensional parameters. It has been established that practical use of the elaborated system requires optimizing between thermopile supply current and the amount of working agent used.
Key words: prototype, test bench, full-scale test, electronic board, thermoelectric module, non-uniform heat removal, melting agent.

Introduction

Electronic boards belong to the most popular components of modern electronic equipment. Depending on the arrangement of conductive pattern, they can be classified as single-sided, double-sided and multilayer. Irrespective of electronic board type, their basic feature is distribution along the area of heat-emitting elements. At the present time, heat removal from heat-emitting elements is based on air, liquid, evaporative and thermoelectric cooling. The list of some manufacturers of this equipment is given in Table 1. When analyzing their products as applied to heat removal from electronic boards characterized by non-uniform heat release, it should be noted that electronic equipment cooling systems based on liquid and conductive methods are little efficient owing to low intensity of heat removal and the accuracy of temperature maintenance on the required level. Liquid and evaporative heat removal systems are difficult to implement, they call for bulky and structurally complicated equipment. Thermoelectric coolers mainly realize uniform heat removal from all electronic board components and are not efficient in this application aspect either.

Therefore, based on the strongly marked temperature field non-uniformity of electronic board, the authors have proposed a cooling system for its components [20] that takes this factor into account.

The device schematic is shown in Fig. 1, and its appearance – in Fig. 2.

The device comprises a metal container filled with the working agent having high value of melting heat and melting temperature in the range of 35 to 65 °C (for instance, paraffin, wax, nickel nitrate, etc). A container accommodating an electronic board with respective heat-emitting elements has a profiled surface, with recesses formed at places of arrangement of electronic equipment components most critical to temperature operation mode or requiring considerable temperature reduction. In said recesses, thermopiles powered from DC source are placed. The recess dimensions are selected so as to match the thermopile size.

Table 1

№	Companies	Type of manufactured products	Reference
1	2	3	4
1.	AAVID Thermalloy (USA)	Liquid coolers and air heat sinks	[1]
2.	Ligra (Russia)	Pin and plate heat sinks	[2]
3.	Proton-Electrotex (Russia)	Pin and plate heat sinks	[3]
4.	Summit Heat Sinks Metal co. (Taiwan)	Pin and plate heat sinks	[4]
5.	Alutronik (Germany)	Pin and plate heat sinks, electronic equipment packages	[5]
6.	ThermoFlow (USA)	Heat sinks of all types	[6]
7.	Melcor (USA)	Thermoelectric cooling systems	[7]
8.	Marlow Inc. (USA)	Thermoelectric cooling systems	[8]
9.	FerroTec. (USA)	Thermoelectric cooling systems	[9]
10.	Fandis (Italy)	Thermoelectric cooling systems	[10]
11.	Komatsu Electronics (Japan)	Thermoelectric cooling systems	[11]
12.	Kryotherm (Russia)	Thermoelectric cooling systems	[12]
13.	Osterm (Russia)	Thermoelectric cooling systems	[13]
14.	RMT (Russia)	Thermoelectric cooling systems	[14]
15.	Evercool (Taiwan)	Fan units, liquid systems	[15]
16.	Titan (Taiwan)	Fan units, liquid systems	[16]
17.	Zalman (South Korea)	Fan units, liquid systems	[17]
18.	Sunon (Taiwan)	Fan units, liquid systems	[18]
19.	Thermaltake (Taiwan)	Fan units, liquid and evaporative systems	[19]

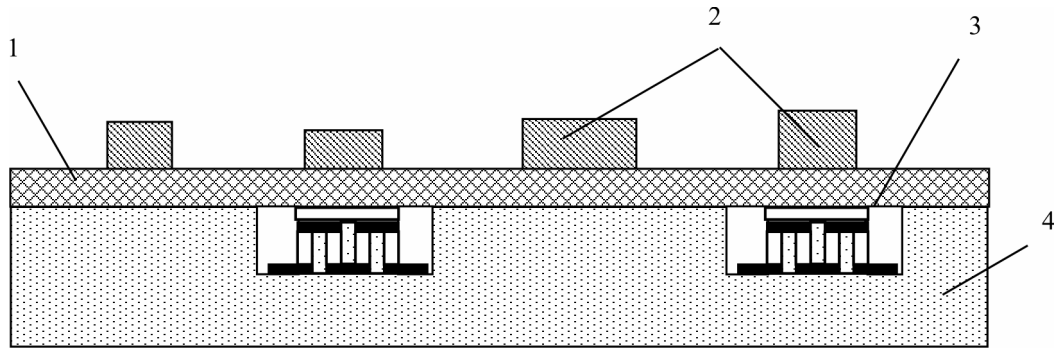

Fig. 1. Schematic of electronic board cooling with a joint use of melting working agent and thermopile (1 – electronic board, 2 – radio elements, 3 – thermopile, 4 – melting working agent container).

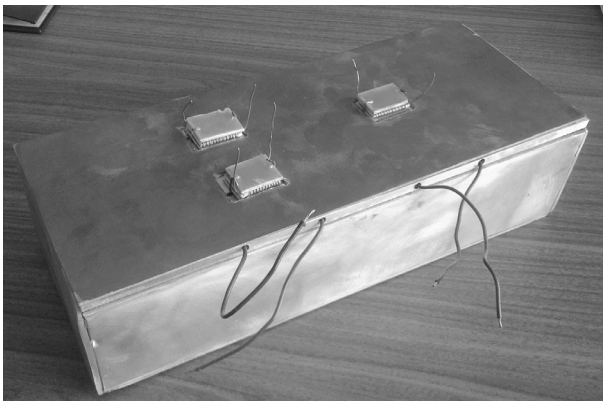

Fig. 2. Outside view of cooling device with electronic board simulator.

In device operation, heat coming from electronic equipment components placed on the electronic board is transferred to metal container and through the contact surface to the working agent. Then the working agent is heated to melting temperature, and melting process accompanied by the absorption of heat spent for change of state occurs. Heat removal due to change of state of the working agent is fundamental and can be used to assure the necessary temperature operation mode of electronic equipment components that do not require essential temperature reduction or are not critical to considerable overheat with respect to environment. For cooling electronic equipment components particularly critical to overheat or requiring essential temperature reduction, use is made of thermopiles that assure additional heat pickup, the cooling capacity value of each thermopile being determined in conformity with the heat release level of specific electronic equipment component. In so doing, heat from thermopile hot junctions is also removed to the working agent in the container the amount of which is calculated from the durability of electronic equipment components, their heat release power, thermopile heat production, as well as the operating conditions.

For device characterization an experimental bench was assembled, schematically shown in Fig. 3.

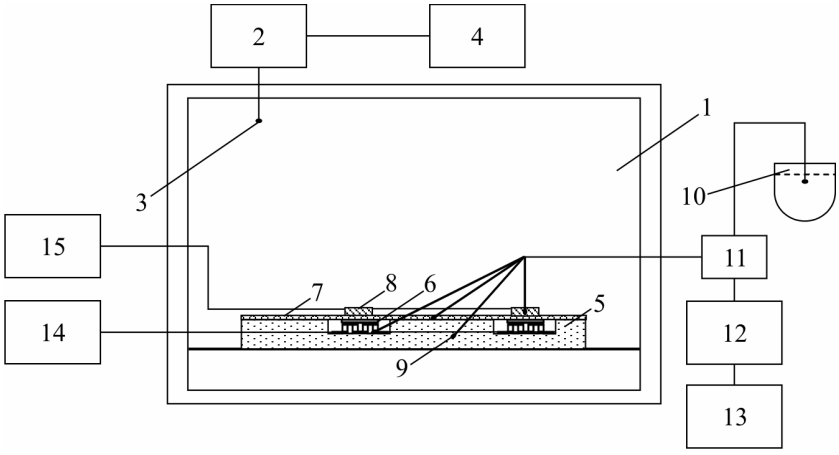

Fig. 3. Schematic of experimental bench.

Investigations were performed in thermally insulated climatic chamber 1 with thermostated working volume 120 liters. The chamber assures maintenance of temperature in the range from 283 to 343 K to an accuracy of 0.2 °C and relative humidity from 30 % to 98 %. Given temperature and relative humidity in the chamber are controlled by control unit 2 related to temperature and humidity sensor 3 whose readings are recorded by digital display 4.

The object for experimental research was a prototype cooling system in the form of a container 5 filled with the working agent, namely paraffin. The upper surface of the container is profiled, with two grooves accommodating standard TEM 6 of the type DRIFT-08. The location of the grooves corresponds to location on electron board simulator 7 of heat-emitting elements 8 represented by flat nichrome electric heaters. The topology of arrangement of heat-emitting elements on electronic board simulator is shown in Fig. 4. The simulator corresponds to electronic board of high-frequency power amplifier designed by Open JSC "P.S.Pleshakov Radio Factory" (Russia, Republic Dagestan, Izberbash city).

To determine the basic parameters of prototype under test, the following values were measured: voltage and current on TEM; their junction temperatures; voltage and current on the heaters, the temperatures at control points of electron board simulator, including the heaters, and the cover temperature of the working agent container.

The hot and cold side temperatures of TEM, as well as at control points of electron board simulator were measured by copper-constantan thermocouples 9 whose reference junctions were in Dewar vessel 10. Output signals from the thermocouples through multi-channel switch 11 came to measuring complex IRTM 12 with personal computer 13 connected to its output to register measured temperature readings at preset time intervals. TEM was powered by controlled DC source 14. Current passing through TEM and its voltage were controlled by devices embedded in power supply unit. A similar DC source 15 was used to power thermal load simulators (electric heaters).

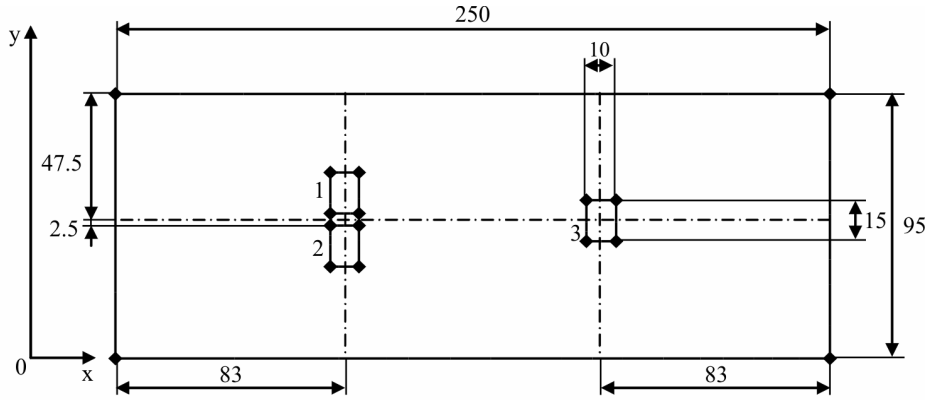

Fig. 4. Topology of electronic board simulator.

The basic task when conducting experimental investigations was to determine the temperature dependences of electronic board simulator heat-emitting elements, when non-uniformly cooled, on the TEM and working agent parameters, as well as time variation of the cover temperature of the working agent container. It was important to compare the experimental data to theoretical ones.

Figs. 5 – 6 represent the experimental dependences of temperature variation at control points of electronic board simulator in time without cooling system at different powers. For comparison, the same figures show theoretical plots obtained on the basis of elaborated mathematical model [21]. According to the data presented, the temperature of heat-emitting elements is increased considerably. Thus, for the source of heat 1 (see Fig. 2) in the steady-state mode the temperature value is 428 K with heat release power 120 W and 410 with heat release power 100 W (the temperature values for heat-emitting element 2 are the same), and for the source of heat 3 – 396 K and 382 K, respectively. In so doing, the temperature in the electronic board areas adjacent to heat sources is of the same value. In Figs. 5 and 6 its value is 415 K and 403 K, which testifies to the presence of considerable temperature background that may have an adverse effect on the operation of electron board components, namely cause their failure.

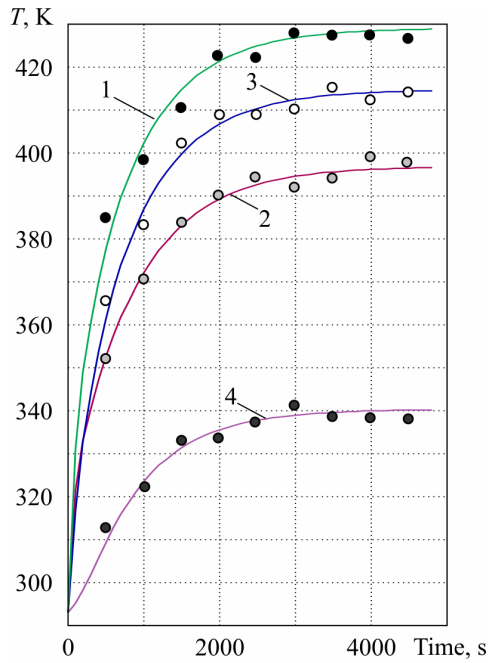

Fig. 5. Temperature variation at different points of electronic board versus time with the power of heat-emitting elements 120 W. 1 – temperature of heat source 1; 2 – temperature of heat source 3; 3 – temperature at x = 125 mm, y = 47.5 mm; 4 – temperature at x = 17 mm, y = 14 mm.

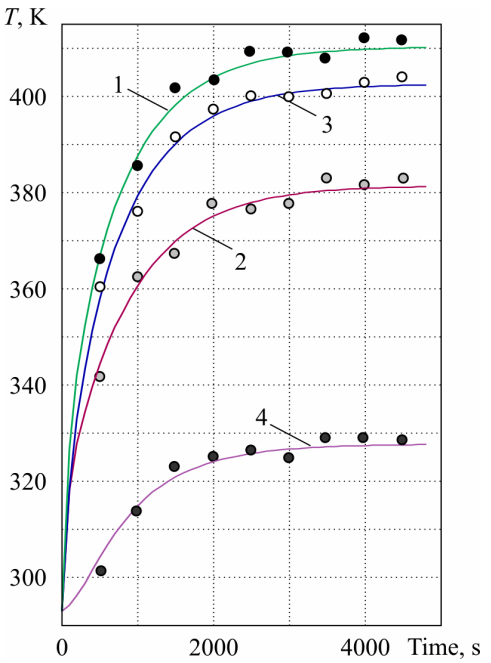

Fig. 6. Temperature variation at different points of electronic board versus time with the power of heat-emitting elements 100 W. 1 – temperature of heat source 1; 2 – temperature of heat source 3; 3 – temperature at x = 125 mm, y = 47.5 mm; 4 – temperature at x = 17 mm, y = 14 mm.

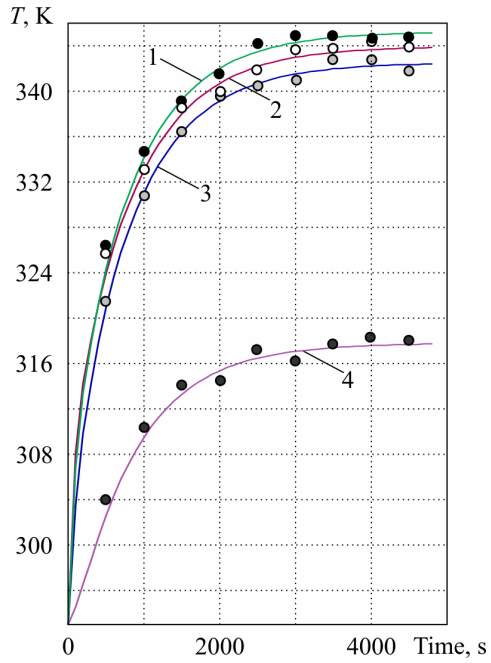

Fig. 7. Temperature variation at different points of electronic board versus time with the power of heat-emitting elements 120 W and thermopile supply 10 A. 1 – temperature of heat source 1; 2 – temperature of heat source 3; 3 – temperature at x = 125 mm, y = 47.5 mm ; 4 – temperature at x = 17 mm, y = 14mm.

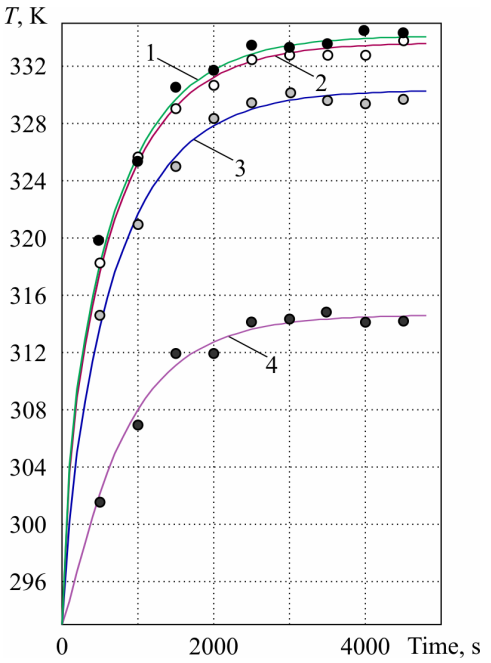

Fig. 8. Temperature variation at different points of electronic board versus time with the power of heat-emitting elements 100 W and thermopile supply current 10 A. 1 – temperature of heat source 1; 2 – temperature of heat source 3; 3 – temperature at x = 125 mm, y = 47.5mm; 4 – temperature at x = 17 mm, y = 14mm.

Figs. 7 and 8 show the plots of temperature variation at control points of electronic board simulator versus time with the use of prototype cooling system. According to the data presented, the use of cooling system reduces the temperature of heat-emitting elements to acceptable values. For the case in Fig. 7 the temperature of heat sources is reduced to 345 K and 344 K, and for Fig. 8 – to 334 K and 333 K. In so doing, temperature background created by heat-emitting elements in the near-by areas of electron board simulator is also reduced.

For the analysis of the energy characteristics of cooling system Figs. 9 and 10 represent temperature variations at control points of electron board simulator versus thermopile supply current and electric energy consumption. According to the data obtained, with increase in current flowing through thermopile, the temperature at all control points is reduced. In so doing, its lowest value for this case at the power of sources of heat 120 W is 344 K, which corresponds to thermopile supply current 9 A. It is obvious that further electric current increase up to the optimal value for this type of TEM (11.3 A) will yield further temperature reduction at control points.

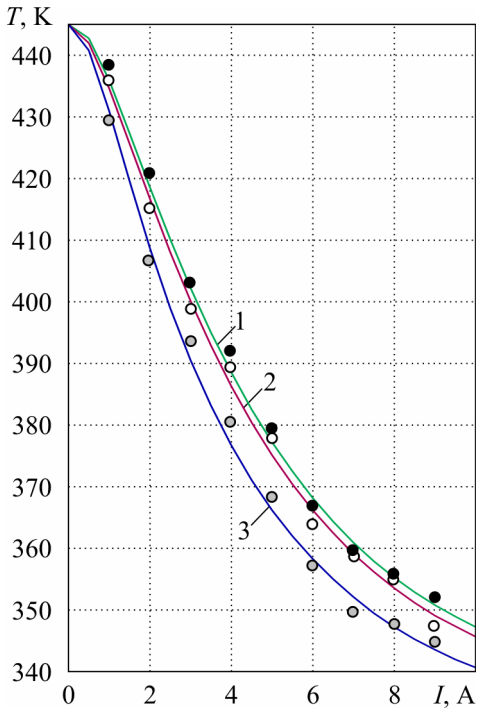

Fig. 9. Temperature variation at different points of electronic board versus thermopile supply current in steady-state mode with the power of heat-emitting elements 120 W. 1 – temperature of heat source 1; 2 – temperature of heat source 3; 3 – temperature at x = 125 mm, y = 47.5 mm.

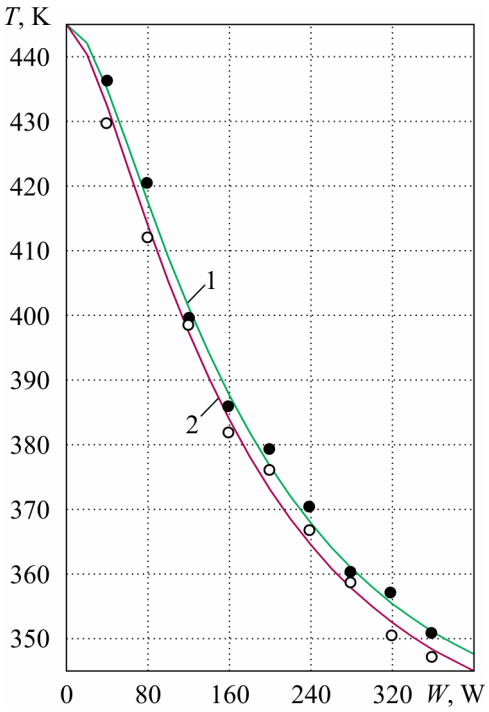

Fig. 10. Temperature variation at different points of electronic board versus thermopile power consumption in steady-state mode with the power of heat-emitting elements 120 W. 1 – temperature of heat source 1; 2 – temperature of heat source 3.

With thermopile current increase, its electric power consumption is increased respectively. For the case represented in Fig. 10 current 9 A is matched by consumed power 360 W.

Fig. 11 gives the data on temperature variation at control points of electronic board simulator with heat removal to the working agent without the use of a thermopile. According to the results, such kind of cooling does not assure the necessary temperature mode of electronic board simulator components. Thus, the temperature of heat-emitting elements is reduced only to the values of 383 K and 385 K, which is insufficient for provision of their temperature working mode.

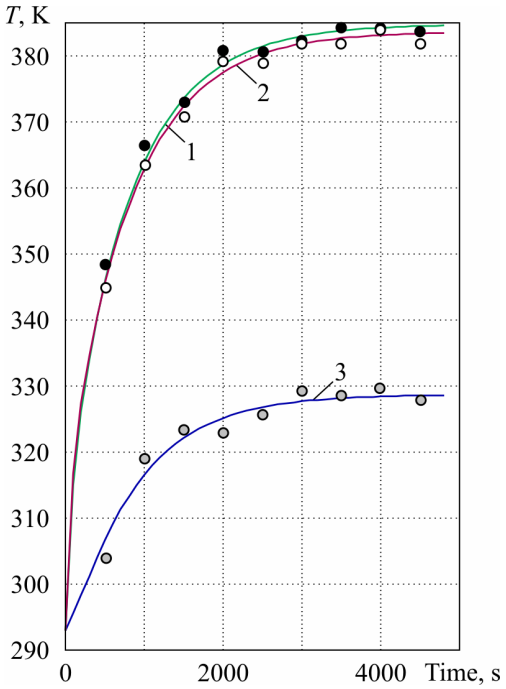

Fig. 11. Temperature variation at different points of electronic board versus time with the power of heat-emitting elements 120 W and heat removal to melting working agent without thermopile. 1 – temperature of heat source 1; 2 – temperature of heat source 3; 3 – temperature at x = 17 mm, y = 14 mm.

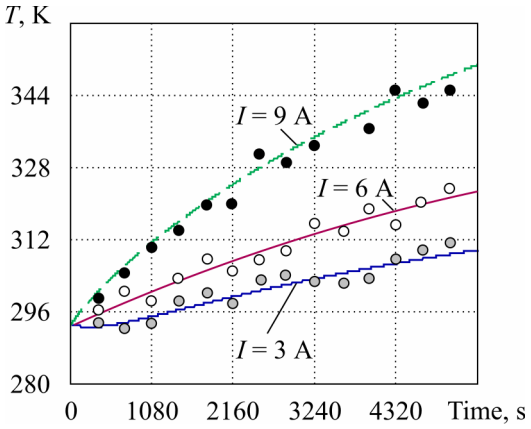

Fig. 12. Time dependence of the cover temperature of working agent container at different thermopile supply currents.

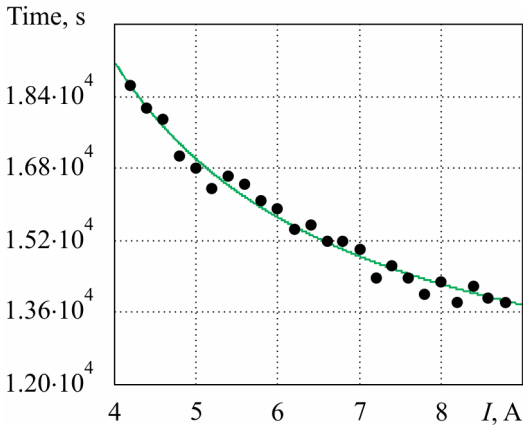

Fig. 13. The time of full melting of the working agent versus thermopile supply current.

Fig. 12 represents experimental time dependences of the cover temperature at working agent melting for different values of thermopile supply current. According to the plots, with a rise in supply current, the amount of heat supplied to the surface of container per unit time (thermal power) is increased, raising the cover temperature. Thus, with the use of paraffin as the working agent, increase in thermopile supply current from 3 to 9 A increases cover temperature by about 40 K in 1.5 h. The agent melting rate is increased respectively. According to Fig. 13 presenting the data on the duration of full melting of agents with different values of thermopile current, increase in electrical current from 4 to 9 A reduces the time of full melting of agents from 5.1 h. to 3.3 h. As a result, it can violate the normal operating mode of

electronic board components under respective thermal loads. So, this fact should be taken into account in the design of cooling system.

Based on the above investigations the following conclusions can be made:

1. For efficient cooling of electronic board components, owing to non-uniform distribution of thermal flux on its area, it is advisable to use adequate cooling characterized by non-uniformity of heat pick up along the electronic board area.
2. The above cooling method offers advantages over the usual one, uniform in the energy parameters. According to experimental investigations, the value of power consumption can be reduced by a factor of 1.35 – 1.5. Moreover, the number of thermoelements, heat sink mass, and, respectively, the mass of the entire cooling device can be reduced.
3. With increasing power of electronic board components, the power of thermopiles used for its cooling is increased, which affects the amount of working agent used and must be taken into account in the design of cooling system.

References

1. http://www.aavidthermalloy.com
2. http://www.ligra.narod.ru
3. http://www.eletex.ru
4. http://www.heat_sink.com.tw
5. http://www.alutronic.de
6. http://www.thermaflo.com
7. http://www.melcor.com
8. http://www.marlow.com
9. http://www.ferrotec.com
10. http://www.fandis_tm.com
11. http://www.komatsu_electronics.co.jp
12. http://www.kryotherm.ru
13. http://www.osterm.ru
14. http://www.rmtltd.ru
15. http://www.evercool.com.tw
16. http://www.titan_cd.com
17. http://www.zalman.co.kr
18. http://www.sunon.com.tw
19. http://www.thermaltake.com
20. T.A. Ismailov, O.V. Yevdulov, M.U. Agayev, Patent of Russian Federation № 2365072, 2009, Bul. № 23.
21. T.A. Ismailov, O.V. Yevdulov, M.U. Agayev, Mathematical Simulation of a System of Non-Uniform Cooling of Electronic Boards with a Joint Use of Melting Working Agents and Thermoelectric Energy Conversion Method, *Izvestia Vuzov. Radioelectronics* **6**, 51 – 58 (2010).

Submitted 12.07.2013.

NEWS

INTERNATIONAL THERMOELECTRIC ACADEMY

YURIY GENRIKHOVICH GUREVICH

(DEDICATED TO 70-TH BIRTHDAY)

This 1st of November is the date of 70th anniversary of Yuriy Genrikhovich Gurevich, a well-known physicist, Doctor of Science in Physics and Mathematics, Vice-President of the International Thermoelectric Academy, professor of Physics Department of Center for Research and Advanced Studies of the National Polytechnic Institute in Mexico (CINVESTAV – I.P.N).

The range of his research interests covers the nonlinear theory of electromagnetic waves propagation in semiconductors and plasma; theory of transport phenomena of confined semiconductors in strong temperature and electric fields; new mechanisms of thermo- and photogalvanics generation in semiconductors; electric instability in semiconductors; creation of thermoelectric and ecologically pure photoelectric converters; electric and photon thermal waves in semiconductors.

Yu. Gurevich is the author of three monographs, twelve chapters in the scientific publications, five manuals for universities, nearly two hundred journal publications, over four hundred reports to scientific conferences, and two certificates of authorship. Under the scientist's supervision, three doctors and nineteen candidates of science have been trained.

Yuriy Genrikhovich Gurevich is an academician of the International Thermoelectric Academy, a member of scientific board "Thermoelectric materials and their application" of the National Academy of Sciences of Ukraine, an expert of governmental scientific and technical programs "Ukraine-2002", a corresponding member of the Academy of Engineering Science of Ukraine (1996), a permanent member of the Mexican Academy of Sciences, an honorary member of the Advisory Council of Research (American Biographical Institute, USA), since 1995 – an honorary member of the Advisory Council of the International Biographical Center (Cambridge, England), a member of Committee for awarding prizes of the Mexican Society of Science for Surfaces and Vacuum for the best PhD thesis. Yu. Gurevich was a researcher and head of many projects of California Institute of Mexico and USA (UC MEXUC) and the Mexican National Council of Science and Technology (CONACYT) from 1994 till 2012.

Professor Gurevich was elected a member of "Physics and Chemistry of Solid State" and "Journal of Thermoelectricity" editorial boards.

For his fruitful research and organizational activity Yu. Gurevich has been awarded with a Diploma of the International Thermoelectric Academy, honoured with a title "National Researcher Level II, The National System of Researchers, Mexico, 1995" and "National Researcher Level III, the National System of Researchers, Mexico, 1998", and Francisco Mejia Lira Award, Mexican Society of Science and Technology of Surfaces and Materials (2003), as well as commended for participation in the project ETI@home and study on the data of search for extra-terrestrial civilizations pursued by California University in Berkeley and sponsored by the Planetary Society (USA, 2000).

International Thermoelectric Academy, Institute of Thermoelectricity of the NAS and MES of Ukraine, "Journal of Thermoelectricity" Publishers sincerely greet the esteemed Yuriy Genrikhovich Gurevich on his 70-th jubilee, wishing him sound health, inexhaustible energy, happiness and new achievements.

ARTICLE PREPARATION RULES

The article shall conform to the journal profile. The article content shall be legible, concise and have no repetitions.

The article shall be submitted to the editorial board in electronic version.

The text shall be typed in text editor not lower than MS Word 6.0/7.0.

Page setup: "mirror margins"- top margin – 2.5 cm, bottom margin – 2.0 cm, inside – 2.0 cm, outside– 3.0 cm, from the edge to page header – 1.27 cm, page footer – 1.27 cm.

Graphic materials, pictures shall be submitted in color or, as an exception, black and white, in .opj or .cdr formats, .jpg or .tif formats being also permissible. According to author's choice, the tables and partially the text can be also in color.

The article shall be submitted in English on A4 paper sheets; the number of pages shall not exceed 12. By agreement with the editorial board, the number of pages can be increased.

To accelerate publication of the article, please adhere to the following rules:

- the authors' initials and names are arranged in the centre of the first page at the distance of 1 cm from the page header, font Times New Roman, size 12 pt, line spacing 1.2;
- the name of organization, address (street, city, postal code, country) – indent 1 cm below the authors' initials and names, font Times New Roman, size 11 pt, line spacing 1.2, center alignment;
- the title of the article is arranged 1 cm below the name of organization, in capital letters, semi-bold, font New Roman, size 12 pt, line spacing 1.2, center alignment. The title of the article shall be concrete and possibly concise;
- the abstract is arranged 1 cm below the title of the article, font Times New Roman, size 10 pt, in italics, line spacing 1.2 ,center alignment;
- key words are arranged below the abstract, font Times New Roman, size 10 pt, line spacing 1.2, justified alignment. The title "Key words" – font Times New Roman, size 10 pt, semi-bold;
- the main text of the article is arranged 1 cm below the abstract, indent 1 cm, font Times New Roman. size 11 pt, line spacing 1.2, justified alignment;
- formulae are typed in formula editor, fonts Symbol, Times New Roman. Font size is "normal" – 12 pt, "large index" – 7 pt, "small index" – 5 pt, "large symbol" – 18 pt, "small symbol" – 12 pt). The formula is arranged in the text, centre aligned and shall not occupy more than 5/6 of the line width, formulae are numbered in round brackets right;
- dimensions of all quantities used in the article are represented in the International System of Units (SI) with the explication of the symbols employed;
- figures are arranged in the text. The figures and pictures shall be clear and contrast; the plot axes – parallel to sheet edges, thus eliminating possible displacement of angles in scaling;
- tables are arranged in the text. The width of the table shall be 1 cm less than the line width. Above the table its ordinary number is indicated, right alignment. Continuous table numbering throughout the text. The title of the table is arranged below its number, center alignment;
- references should appear at the end of the manuscript. References within the text should be enclosed in square brackets. References should be numbered in order of first appearance in the text. Examples of various reference types are given below.

– L.I. Anatychuk, *Thermoelements and Thermoelectric Devices: Handbook* (Kyiv: Naukova Dumka, 1979), p.766. (Book)
– T.M. Tritt, Thermoelectric Phenomena, Materials, and Applications, *Annual Review of Materials Research* **41**, 433 (2011). (Journal paper)
– U. Ghoshal, *Proceedings of the XXI International Conference on Thermoelectrics* (N.Y., USA, 2002), p. 540. (Proceedings Conference)

The article should be supplemented by:

• letter from the organization where the work was performed or from the authors of the work applying for the publication of the article;

• information on the author (authors): last name and initials; full name and postal address of the institution where the author works; academic degree; position; telephone number; E-mail;

• author's (authors') photo in color or, as an exception, in black and white. With the number of authors more than two their photos are not given;

• author's application to the following effect:

We, the undersigned authors, … transfer to the founders and editors of "Journal of Thermoelectricity" the right to publish the article…in Ukrainian, Russian and English. This is to confirm that the present publication does not violate the copyright of other persons or organizations.

Date Signatures

Below is given an example of article preparation.

Author's photo 3 × 4 cm

A.I. Casian[1], B.M. Gorelov[2]

[1]Technical University of Moldova,
168, Stefan cel Mare Ave.,
Chisinau, MD-2004, Moldova;
[2]Institute of Surface Chemistry of National Academy
of Sciences of Ukraine, 17, Gen. Naumov Str.,
Kyiv, 03164, Ukraine

Author's photo 3 × 4 cm

STATE OF THE ART AND PROSPECTS OF THERMOELECTRICITY ON ORGANIC MATERIALS

The aim of the paper is to analyze the expected thermoelectric opportunities of organic materials, including some highly conducting quasi-one-dimensional crystals. It is shown that interest of investigators in these materials has been growing recently. Quasi-one-dimensional organic crystals have high prospects for thermoelectric applications. These materials combine the properties of multi-component systems with more diverse internal interactions and of quasi-one-dimensional quantum wires with increased density of electronic states. It is shown that the values of the thermoelectric figure of merit ZT ~ 1.3 – 1.6 at room temperature are expected in really existing organic crystals of tetrathiotetracene-iodide, TTT_2I_3, if the crystal parameters are approaching the optimal ones.

Key words: thermoelectricity, tetrathiotetracene-iodide, polarizability.

Introduction

It is known that conducting organic materials usually have much lower thermal conductivity than the inorganic materials. Moreover, the organic materials can be fabricated by simpler chemical methods, and it is expected that such materials will be less expensive in comparison with the inorganic ones. Exactly these properties attracted attention to such materials for the use in thermoelectric (TE) applications long time ago [1, 2]. In spite of relatively high value of the thermoelectric figure of merit $ZT = 0.15$ at room temperature observed in polycopper phthalocyanine [2] as early as 1980, the thermoelectric properties of organic materials are still weakly investigated. This situation has the only explanation that thermoelectricians are still weakly interested in organic materials, and organic chemists are also weakly interested in thermoelectric materials. Moreover, in order to seek good organic thermoelectrics, it is necessary to organize multidisciplinary consortiums of physicists, organic chemists and engineers in the field of thermoelectricity. …

The aim of this paper is to present briefly the state-of-the-art of investigations in the area of new organic thermoelectric materials and to describe the nearest expected results for really existing quasi-one-dimensional organic crystals of tetrathiotetracene-iodide, TTT_2I_3.

Quasi-one-dimensional organic crystals of TTT_2I_3

The structure of quasi-one-dimensional organic crystals of tetrathiotetracene-iodide, TTT_2I_3, has been briefly described in [34]. These needle-like crystals are formed of segregate chains or stacks of planar molecules of tetrathiotetracene *TTT*, and iodine ions. The chemical compound TTT_2I_3 is of mixed-valence: two molecules of *TTT* give one electron to the iodine chain which is formed from I_3^- ions. The

conductivity of iodine chains is negligibly small, so that only *TTT* chains are electrically conductive and holes serve as carriers. The electrical conductivity σ along *TTT* chains at room temperature varies between 10^3 and $10^4\ \Omega^{-1}\text{cm}^{-1}$ for crystals grown by gas phase method [35], and between 800 and $1800\ \Omega^{-1}\text{cm}^{-1}$ for crystals grown from solution [36]. Thus, the conductivity is very sensitive to crystal impurity and perfection which depends on growth method. In the direction perpendicular to chains σ is by three orders of magnitude smaller than in the longitudinal direction and is neglected. …

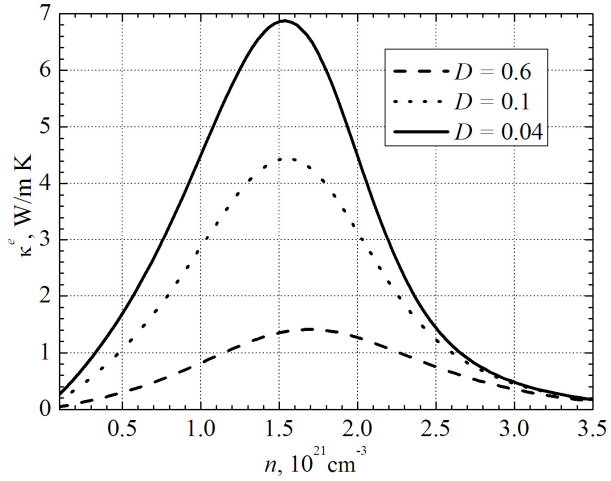

Fig. 1. Dependences of electron thermal conductivity κ^e on n.

$$\sigma = R_0,\ S = R_1 / eTR_0,\ \kappa^e = \left(e^2T\right)^{-1}\left(R_2 - R_1^2 / R_0\right), \tag{1}$$

Thermoelectric properties

Expressions (2) – (3) have been calculated in order to determine the thermoelectric properties of quasi-one-dimensional organic crystals of TTT_2I_3 with different degrees of purity….

Conclusions

The state-of-the-art of research on new organic materials for thermoelectric applications is analyzed. It is shown that the interest of investigators in these materials has been growing in recent years. The highest value of $ZT \sim 0.38$ at room temperature has been measured in doped acetylene, with the only problem that this material is not stable. Accurate control of the oxidation level in poly (3, 4-ethylenedioxythiophene) (PEDOT) gave the power factor $324\ \mu\text{W}\cdot\text{m}^{-1}\text{K}^{-2}$ and in combination with its low intrinsic thermal conductivity ($\kappa = 0.37\ \text{W}\cdot\text{m}^{-1}\text{K}^{-1}$) yielded $ZT = 0.25$ at room temperature, and this material is air-stable….

References

1. Ali Shakouri, Recent Developments in Semiconductor Thermoelectric Physics and Materials, *Annu.Rev.Mater.Res*.**41**, 399-431 (2011).
2. L.I. Anatychuk, *Thermoelectricity, Vol.2, Thermoelectric Power Converters* (Kyiv, Chernivtsi: Institute of Thermoelectricity, 2003), 376p.
3. M.E. Bengen, *German Patent Appl*. OZ 123, 438, 1940; *German Patent* 869,070, 1953, Tech. Oil Mission Reel, 143,135, 1946.

ISSN 1607 - 8829. Journal of Thermoelectricity. 2013. № 5. 1-88